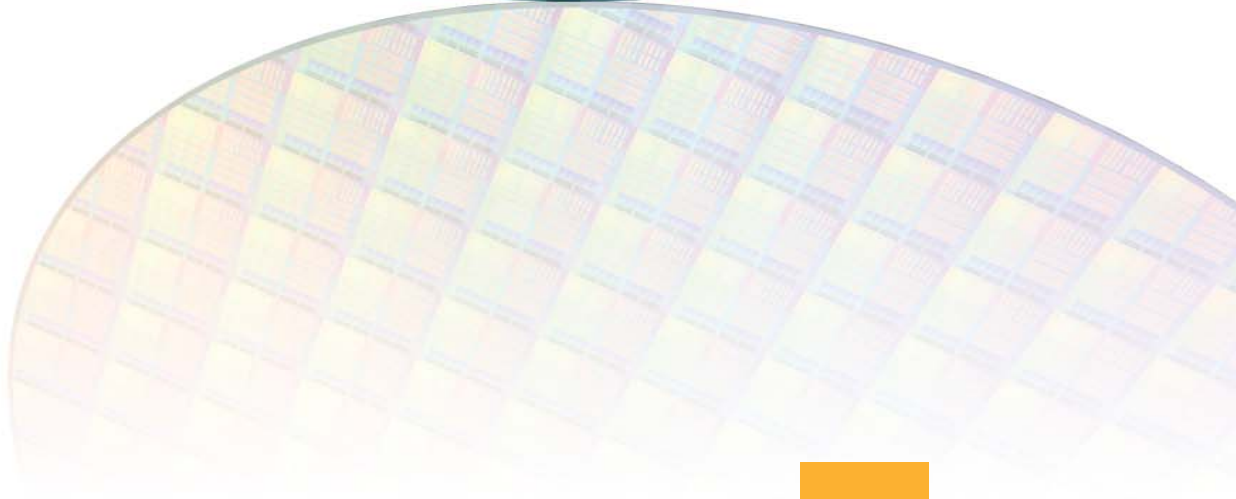
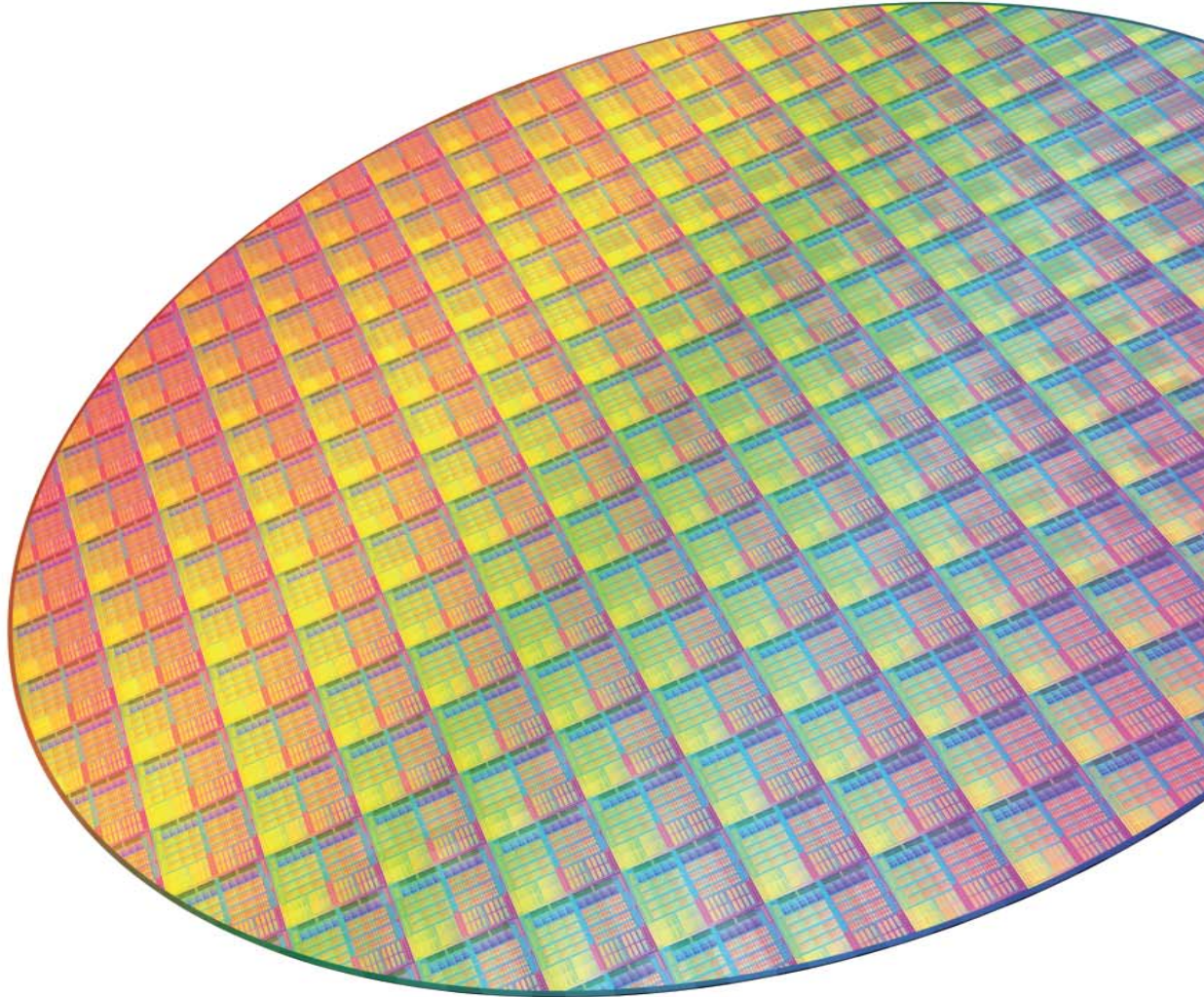




# sussreport<sub>+</sub>

THE CUSTOMER MAGAZINE OF SUSS MICROTEC ISSUE 2015



---

## EDITORIAL

- 03 *Per-Ove Hansson*  
CEO, SÜSS MicroTec AG
- 

## IN THE SPOTLIGHT

- |    |  |    |   |
|----|--|----|---|
| 04 | SUSS MicroTec's Unique DSC300 Gen2 Platform – Combined Projection Lithography Performance with Advantages of Full-field Exposure<br><i>Ralph Zoberbier</i>     | 46 | Excimer Laser Ablation – A Novel Patterning Solution for Advanced Packaging<br><i>Ralph Zoberbier</i>                       |
| 14 | Ruthenium Capping Layer Preservation for 100X Clean Through pH Driven Effects<br><i>Davide Dattilo</i>   | 54 | Auto-Alignment Insights<br><i>Marc Hennemeyer</i>   |
| 24 | Ultra-Small Via-Technology of Thinfilm Polymers Using Advanced Scanning Laser Ablation<br><i>Michael Töpfer</i>  | 58 | Auto-Alignment Insights – Part 2: Case Studies<br><i>Marc Hennemeyer</i>  |
| 32 | Evaluation of a Novel Exposure Concept to Enhance the Capabilities of Mask Aligner Lithography at Large Proximity Gaps<br><i>Frank Windrich</i>                | 64 | Excimer Laser Debonder for 2.5 and 3D Integration<br><i>Tim Griesbach</i>   |
| 40 | Low-Temperature Hermetic Seal Bonding for Wafer-Level MEMS Packaging Using Submicron Gold Particles with Stencil Printing Patterning<br><i>Hiroyuki Ishida</i> | 70 | SUSS Smile Technology – Large Area Imprint. A Solution for Patterning of Micro and Nano Features<br><i>Eleonora Storace</i> |

## + EDITORIAL



*Dr. Per-Ove Hansson, CEO, SÜSS MicroTec AG*

Valued Customers, Partners, and Friends  
of SÜSS MicroTec,

It is a great pleasure for me to greet our readers of the SÜSS Report for the first time as CEO of SÜSS MicroTec. It has been a very intense time since I started in May 2015. I have spent quite some time getting to know the company, our customers, products and employees. My impressions are very positive in terms of the great technology and product potential we have. We have to continue and build on our technology leadership position and deliver high quality innovations to help enable our customers' roadmaps. There are of course areas identified where we have to do much better. We have to improve our responsiveness to customer requirements and speed up our time to market for new products and retrofits. We need to demonstrate accountability and make sure we follow up on our commitments according to plan. We want to earn the trust of our customers and become the partner of choice through consistent delivery according to or above expectations.

I am also very happy to report progress in our core segments, Advanced Packaging, MEMS, 2.5 and 3D Integration, and Photomask Equipment. We were able to report very positive news regarding sales of our Lithography Scanner product, DSC300, which combines the advantages of projection lithography with full field exposure, enabling industry leading cost of ownership performance for wafer-level fan-out applications in advanced packaging. Further, we are very pleased to announce our re-entry into the Permanent Bonding market with our new XB8 product, specifically developed for the high end MEMS market.

Our solutions for Ru-based capping layer mask cleaning are showing very promising results and we have completed EUV clean compatibility for our mask cleaning products. Our core coater and mask aligner products have been upgraded with a new suite of technical solutions, which have enabled us to gain market share in advanced packaging and MEMS. Laser ablation technology for next generation back-end lithography, enabling direct etch of features in non-photo sensitive materials, such as polymers, is another technology of great potential.

You will be able to read more about these and many more advancements in this issue of the SÜSS Report, which in fact is the most comprehensive volume we have published to date.

Finally, I would like to thank all our readers for your interest. Don't hesitate to contact us with your suggestions and feedback. We are here to serve the semiconductor and optics industry with enabling solutions that will extend Moore's Law and make More than Moore integration reality. We intend to stay close to our readers and collaborate closely in order to deliver the enabling solutions you require.

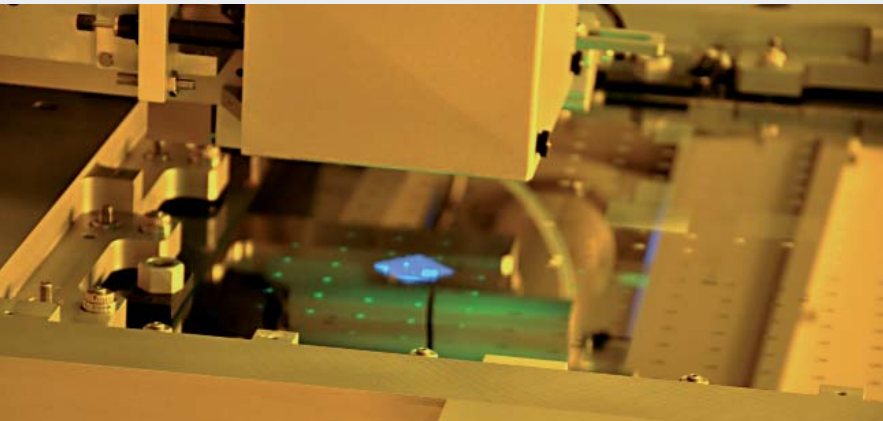
A handwritten signature in black ink, appearing to read 'Per-Ove Hansson'. The signature is fluid and stylized, with a long horizontal stroke extending to the right.

Per-Ove Hansson

# SUSS MICROTEC'S UNIQUE DSC300 GEN2 PLATFORM – COMBINED PROJECTION LITHOGRAPHY PERFORMANCE WITH ADVANTAGES OF FULL-FIELD EXPOSURE

Ralph Zoberbier SUSS MicroTec Lithography GmbH, Schleissheimer Str. 90, 85748 Garching, Germany

Markus Arendt, Habib Hichri, Jeff Hansen SUSS MicroTec Photonic Systems Inc. 220 Klug Circle, Corona, CA 92880-5409, USA



The DSC300 Gen2 lithography system of SUSS MicroTec represents the latest generation of its projection scanner technology that is tailored to deliver high imaging performance at lowest cost of ownership. The system is designed to meet key requirements for advanced packaging applications both technically and economically. Its unique scanning exposure technology allows the use of large area photo masks that contain the full pattern image of the substrate which allows the production of non-repeatable features like edge exposure or test die structures. At the same time, a 1:1 projection lens provides high resolution patterning performance combined with a large depth of focus that is required to ensure high pattern fidelity when working with thick resists that are commonly used in advanced packaging or MEMS applications. The system is designed to automatically process 200 and/or 300mm wafers and is based on a less complex system design compared to traditional step and repeat projection lithography systems that directly translates into lower cost of ownership.

## INTRODUCTION

For decades, photolithography is a fundamental process used in the fabrication and packaging of microelectronic devices. A key component of any photolithography process is the exposure tool, which uses light in the ultraviolet wavelength range to pattern a photosensitive resist or polymer. The exposure tool must be able to precisely create the desired feature in the photo resist and place it to previously fabricated structures in underlying layers. Several types of exposure technologies exist today: proximity or contact printing, laser direct imaging and projection lithography. These technologies and the equipment toolsets mainly differ in terms of technical capability like optical resolution, overlay performance and effective throughput but also heavily impact the costs related to the exposure process. Looking at the main drivers and trends in the semiconductor industry, it clearly shows that on the one hand innovation and performance improvements of microelectronic devices are required to meet future end user trends. For example, consumer electronic devices like tablets and smartphones getting thinner and thinner and at the same time have to have higher computing power with increasing data storage and communication capabilities. On the other hand manufacturing costs become more and more important for companies to maintain or improve their market position in a global and highly competitive environment.

As photolithography is a key manufacturing process and cost contributor, the careful selection of the right exposure solution is mandatory to achieve the best possible cost structure in today's industrial lithography applications. SUSS Mask Aligner technology is by far the lowest cost exposure solution in the market that provides excellent patterning capability coupled with leading edge throughput. However, emerging applications in the semiconductor industry require increasing resolution and overlay performances that are beyond the physical capabilities of a mask aligner. Up to now the industry had the only selection to switch to expensive stepper technology. With the DSC300 Gen2 and its scanning lithography technology, engineers have an alternative choice of an exposure technology that uses the advantages of full-field lithography, well-known from mask aligners, but extends the capabilities as it provides projection lithography performance at a lower cost point. However, the right selection of the exposure technology requires a deep understanding of the pros and cons of each technology plus a good understanding of the application requirements.

### TRENDS AND REQUIREMENTS IN ADVANCED PACKAGING APPLICATIONS

Today a wide variety of advanced packaging technologies exist to meet the different requirements of the semiconductor industry. The leading advanced packages, including chip-on-chip, wafer-level packages, chip-on-chip stacking, embedded IC, all have a need to structure thin substrates, redistribution layers and other package components like high resolution interconnects. The consumer's constant push for higher functionality on smaller and thinner end devices – like smart phones or tablets – drives the need for next generation packages with finer features at increasing reliability of the package. In addition, cost considerations become more and more important to survive in

the competitive landscape for all parties within the supply chain, from chip manufacturer, foundry, assembly and test suppliers to the device manufacturer. Therefore, the industry desperately strives for innovative approaches to lower manufacturing costs coupled with enabling technologies that meet the challenging technical requirements.

A very good example of this trend is the flip chip technology. While solder bumping and single RDL layer technology were mainstream several years back, Cu pillar interconnects and multilayer RDL are considered as one of the main growing application segments for the upcoming years. Cu pillar technology enables fine pitch interconnects needed for the adoption of wafer-level packaging technology for leading edge devices with high I/O count. Figure 1 shows a typical example of the Cu pillar process integration flow. However, the high number of interconnects limited to the chip scale area requires photo lithography of thick resist with almost vertical sidewalls and very good overlay of the pillar, opening to underlying metal pads.

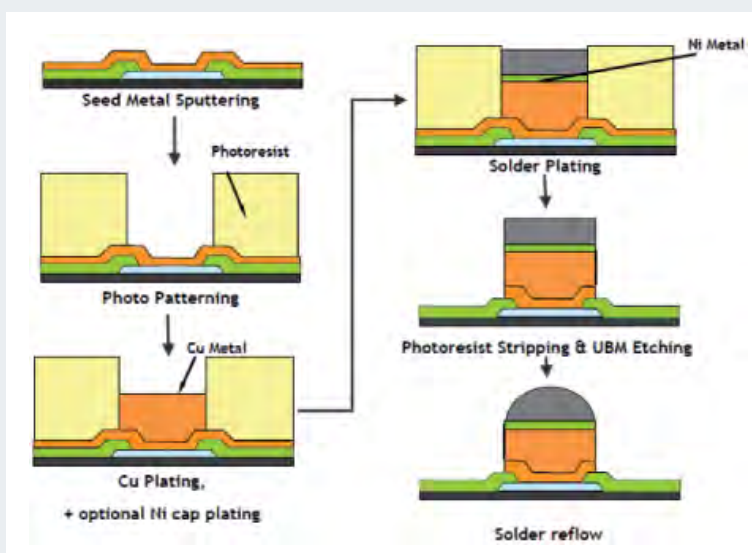


Figure 1 Typical Cu pillar process flow (Source: Yole Development, Courtesy ASE)

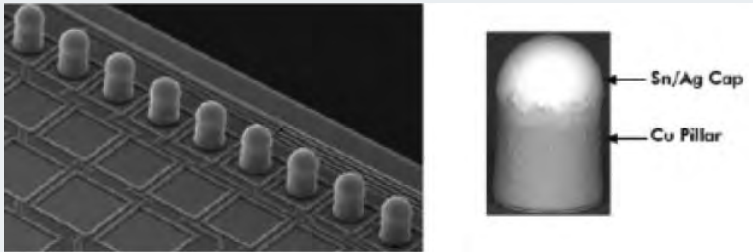


Figure 2 Cu pillar example (Courtesy Amkor)

The technical requirements of the lithography process define the best available exposure technology to meet the performance but also to provide lowest possible manufacturing costs. Figure 18 shows a typical example of a cost of ownership comparison in a wafer bump application.

### EXPOSURE TECHNOLOGIES IN TODAY'S PHOTOLITHOGRAPHY APPLICATIONS

Full-field proximity printing and step and repeat projection lithography are the traditional exposure technologies of the electronic industry in applications fields such as wafer-level packaging, MEMS, LED and displays.

**Mask Aligners** (also known as proximity or contact printers) are used for transferring a geometric pattern of microstructures from a full-field photomask to a light-sensitive photoresist coated on a wafer or substrate by exposing with collimated ultraviolet light. The mask and the wafer are aligned to each other and are in close contact or proximity. A mask aligner typically includes an illumination system, a mask stage for aligning the mask and a wafer stage for aligning the wafer.

Contact lithography in theory offers the highest resolution down to the sub-micron range, in the order of the wavelength of the illumination light. However, practical problems such as mask con-

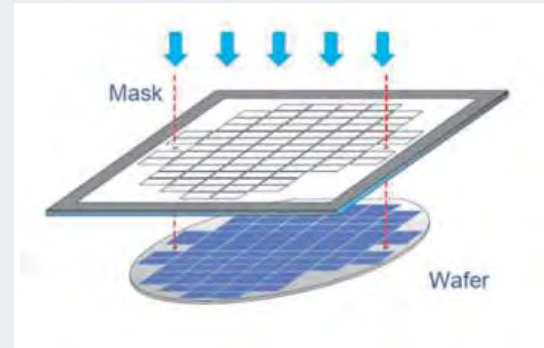


Figure 3 Mask aligner alignment technology

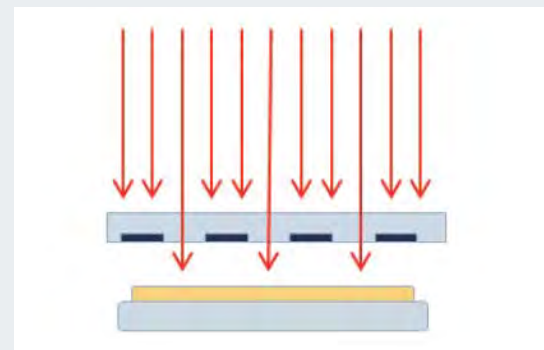


Figure 4 Full-field exposure in a proximity distance between mask and wafer

tamination make this process difficult to use for mass production. Proximity lithography, as shown in figure 4, where the photomask and the wafer are physically separated by a typical proximity gap of 20 to 50 microns, is well suited for mass production and achieves resolution down to  $3\mu\text{m}$  on a 300mm wafer.

The mask aligner is by far the exposure technology with highest throughput available on the market, since one wafer is exposed in a single shot. At the same time these exposure systems are available at lowest capex due to lower equipment complexity compared to projection lithography and UV stepper tools which results in the lowest cost of ownership.

Latest developments in innovative and unique illumination systems for mask aligners allow the optimization of exposure results. As an example, the SUSS MO Exposure Optics, illustrated in figure 5, allows the use of front-end like lithography techniques as illumination shaping, and the use of assistant features on the photo mask, to provide the best possible result.

However, limitations can still arise in cases when thick resist processes require very straight resist sidewalls and when practical overlay requirements reach a level of 1-2 microns or below on 300mm wafers.

**Step and Repeat Projection Systems**, also known in the industry as UV Stepper, have been selected by users whenever they reached the process limitations of mask aligners. The type of a UV stepper is typically defined by the optical layout used. In semiconductor back-end applications today, steppers are either build with 1X or 2X demagnification coupled with a corresponding stepping stage. Depending on the available field size of the optics, the system exposes a certain area of the wafer at a time and performs a step and repeat process to cover the whole wafer area. The main advantages of using a stepper lie in its overlay capability and, when 2X demagnification systems are used, in its enhanced resolution. A 2µm resolution capability with 0.5µm overlay performance is state-of-the-art technology. However, this performance is usually not required for the main applications in wafer-level packaging applications and comes together with higher capex which is typically a factor of 3-4x compared to 300mm mask aligner systems.

Another limitation of a step and repeat system is the limitation of the field size. The maximum die or package size that can be exposed is limited by the lens design itself. The larger the lens design the higher the costs of the lens and the more complex is the optical design to correct for optical aberrations.



Figure 5 Conceptual drawing of SUSS MO Exposure Optics with exchangeable illumination filter plates

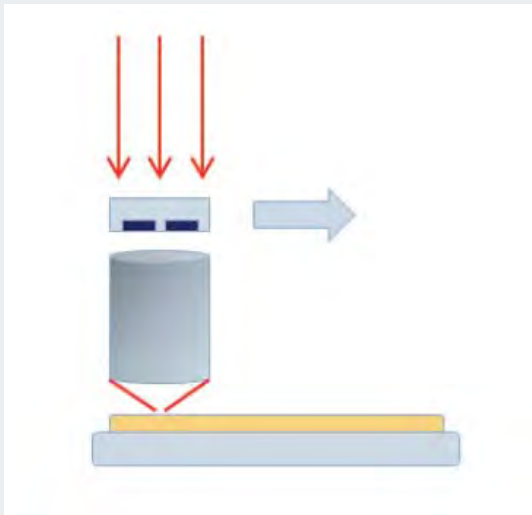


Figure 6 Step and repeat exposure in a UV Stepper

The field size that is usable, is limited to be a multiple of a die size, to allow for step and repeat. With the limited usable field size these systems typically require 80 or more exposure steps to pattern a complete 300mm wafer with the corresponding sacrifice in throughput. Furthermore a step and repeat systems cannot expose non-repeated features on a wafer or substrate. For example, flip chip or RDL layers require the exposure of the wafer edge to enable electrical connection of electrodes for the sub-subsequent plating processes as shown in figure 7.

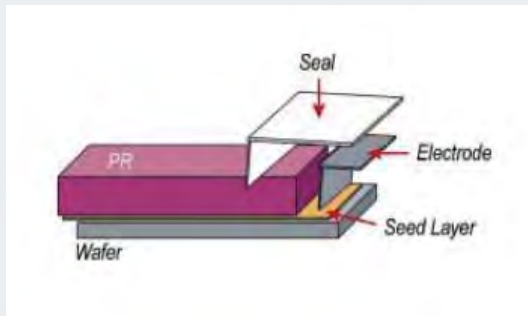


Figure 7 Edge exposed substrate for plating electrode connection

To overcome this limitation, UV steppers use either an edge exposure function on the pre-alignment station that further reduces the effective throughput of the exposure tool itself or require additional edge exposure equipment that adds capex and complexity to the manufacturing line.

The DSC300 Gen2 with its **Full-Field Projection Scanning** technology promises to be the missing piece that offers projection lithography performance, coupled with the advantages of a full-field exposure tool at a lower cost point compared to a traditional UV stepper. This unique exposure concept meets the majority of process requirements and is built on a less complex projection lens design without the requirement of a highly sophisticated step and repeat stage. Figure 8 shows a full field scan exposure setting for the DSC300 Gen2.

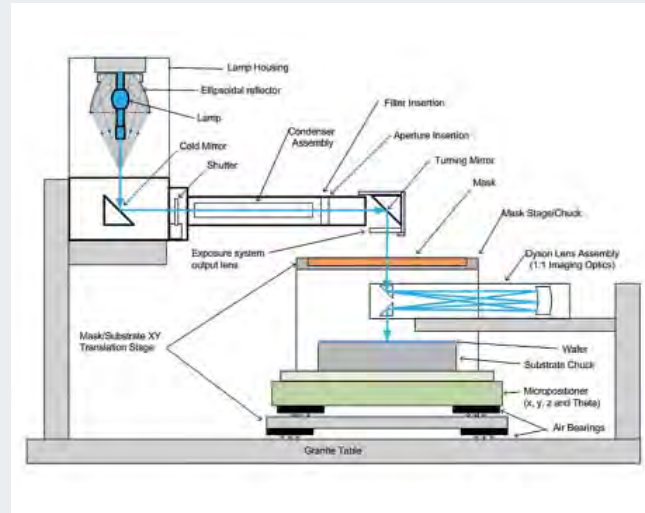


Figure 8 Full-field scan exposure setup

The projection scanner uses a 1X catadioptric lens design with a field size of approx. 30x30mm. This area is used to image the features from a full-field mask onto the wafer in a continuous scan process.

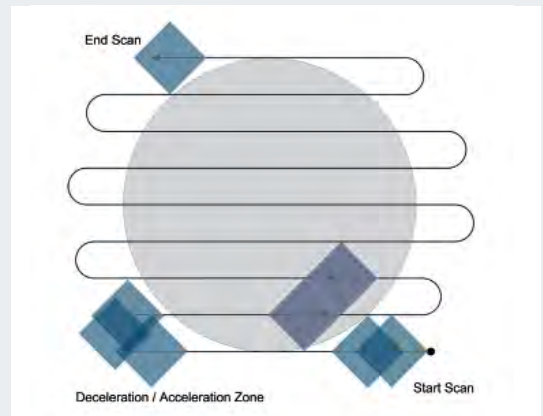


Figure 9 Continuous scan operation for the exposure of an entire 300mm wafer

The complete wafer layout, including non-repeated features like the edge exposure ring can be implemented into the mask design. The alignment of the mask to wafer is performed either through on-axis or TTL (through the lens) alignment or by off-axis

alignment, depending on the process conditions. Thermal management of the mask itself has to be considered when operating a 14" soda lime mask to process 300mm wafers.

It is important to understand that mask contamination or intensive mask cleaning is not a requirement or limitation for this full-field exposure technology as mask and wafer are operated with a large separation of about 200mm, shown in figure 10.

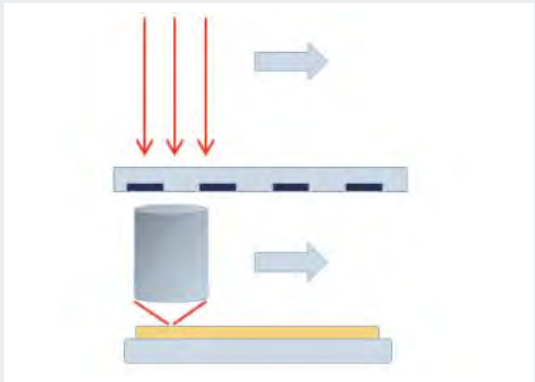


Figure 10 Full-field scan exposure setup

**DSC300 GEN2 KEY FEATURES**

The processing of thick resists is very common in Advanced Packaging applications. As mentioned, today's emerging bump applications require often straight sidewalls to enable a high pin count. However, this requires a high depth of focus (DOF) of the projection exposure tool. The projection scanner technology from SUSS MicroTec provides the optimal combination of high DOF and resolution performance at a reasonable cost level. A flexible and interchangeable NA setting of the system allows the selection of the ideal combination of resolution and DOF. The correlation between NA, DOF and resolution capability of the DSC300 Gen2 is shown in figure 11. In addition, focus adjustments as one of the key process parameters can be used to adjust sidewall performance to the application requirements.

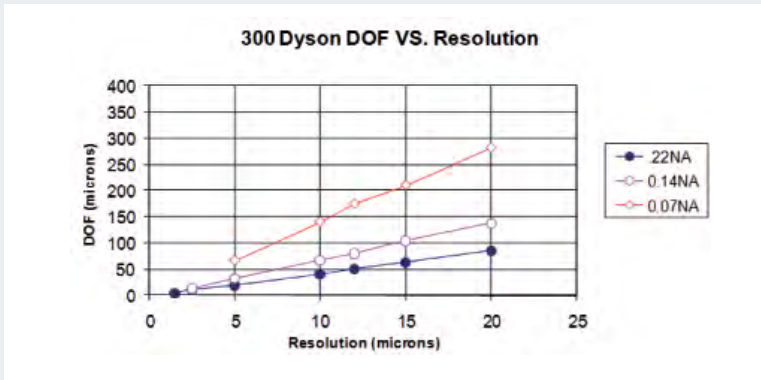


Figure 11 Selectable DOF through interchangeable numeric apertures

The DOF of the exposure tool also defines the process window when processing highly warped substrates. Wafer bow and warpage becomes more and more an issue when the substrate contains different types of materials with various CTE. New packaging concepts like Fan-Out Wafer-Level Packaging (FO-WLP) use artificial wafer substrates based on compound materials. The trend to thinner packages and wafer can result in significant warpages up to several mm. The effective exposure of these substrates now requires pulling the substrate as flat as possible to stay inside the DOF

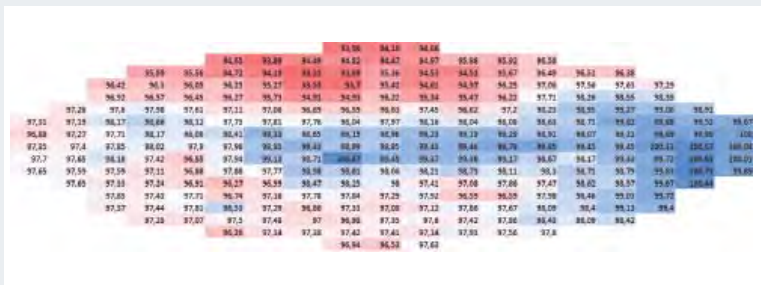
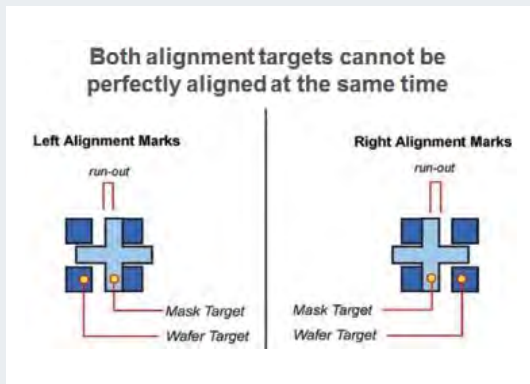


Figure 12 Typical wafer plot of high-low variation after wafer chucking

of the systems. Only then acceptable resolution and CD uniformity of the exposure process can be expected.

Latest developments and improvements show that i.e. eWLB (FOWLP) wafers with initial 5mm bow can be pulled flat down to a remaining high-low variation of <math><20\mu\text{m}</math> on the exposure station which is well inside the DOF for targeted feature sizes.

Finally, thermal control of the exposure mask during the process is a key requirement for full-field exposure systems. The exposure of a 300mm wafer requires a 14" photo mask that is typically made of soda lime to maintain reasonable pricing while UV steppers use 6" reticles made of Quartz. As soda lime has a much different CTE compared to the typical Silicon substrate, temperature changes result in a run-out effect between mask and wafer. Run-out is a magnification mismatch between the mask and the wafer which would lead to overlay inaccuracies, illustrated in figure 13. Adjustments and tight control of the mask temperature is needed to maintain a minimum runout and high overlay performance.



**Figure 13** Thermal runout (magnification mismatch) between mask and wafer identified during alignment process

The DSC300 Gen2 utilizes very effective measures to either cool or heat the mask. This ensures that the system adjusts the level of mask magnification before the first exposure and maintains this level even though high exposure dose processes are performed on the exposure tool (Figure 14).

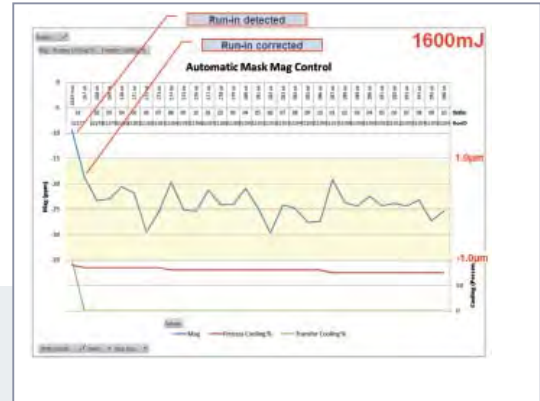


**Figure 14** Data plot of magnification control at a 1600mJ/cm<sup>2</sup> process condition

The final overlay performance on the DSC300 Gen2 for a typical lithography process that requires 300 - 1000 mJ/cm<sup>2</sup> is in the range of 1 - 2 μm which meets the application requirements (Figure 15-17).

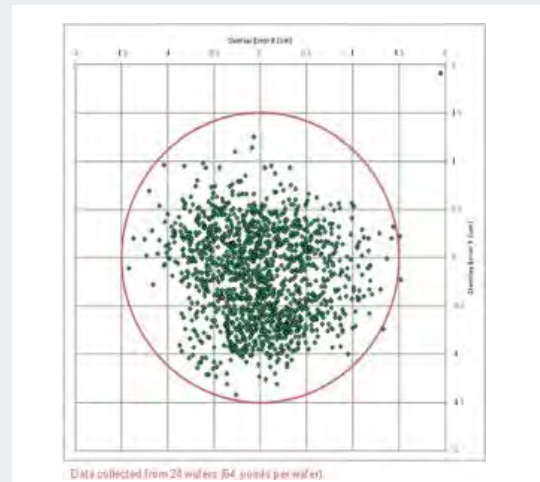


**Figure 15** Thin resist (~1 μm, 300 mJ/cm<sup>2</sup> dose) overlay performance; data from 10 wafers

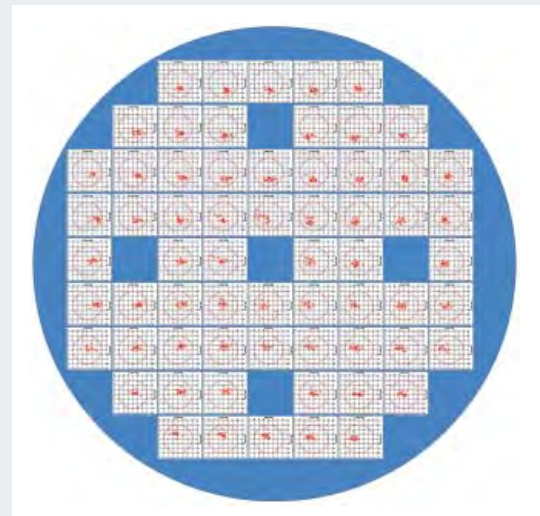


**Figure 16** Thin resist (~1 μm, 300 mJ/cm<sup>2</sup> dose) overlay performance within wafer at each measurement site; data from 10 wafers

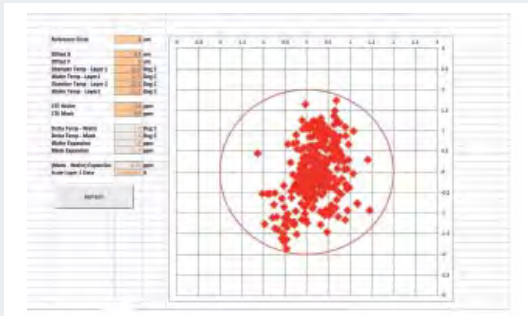


Figure 17 Thick resist (60µm, 300mJ/cm<sup>2</sup> dose) overlay performance; data from 10 wafers

Cost per wafer	Mask Aligner	UV Scanner	UV Stepper
<b>CAPEX</b>	<b>\$1.3M</b>	<b>\$1.8M</b>	<b>\$3.0M</b>
<b>Throughput (WPH)</b>	<b>65</b>	<b>39</b>	<b>35</b>
<b>Depreciation</b>	<b>\$0.87</b>	<b>\$1.47</b>	<b>\$2.75</b>
<b>Mask costs</b>	<b>\$0.96</b>	<b>\$0.42</b>	<b>\$0.19</b>
<b>Service and maintenance</b>	<b>\$0.22</b>	<b>\$0.37</b>	<b>\$0.69</b>
<b>Consumables</b>	<b>\$0.16</b>	<b>\$0.70</b>	<b>\$0.84</b>
<b>Labor</b>	<b>\$0.02</b>	<b>\$0.03</b>	<b>\$0.04</b>
<b>Cost per exposure:</b>	<b>\$2.23</b>	<b>\$2.98</b>	<b>\$4.51</b>
<b>CoO comparison</b>	<b>75%</b>	<b>100%</b>	<b>150%</b>

Figure 18 Cost of Ownership comparison of exposure technologies based on a typical WLP process (1500mJ/cm<sup>2</sup> dose)

The features of the DSC300Gen2 can also be applied to achieve overlay targets for Fan-Out-Wafers, where dies may be shifted due to runout effects during the molding process or die position variations occur due to pick-and-place-robot accuracy. The closed-loop mask heating and cooling allows compensating for up to 30ppm runout (this corresponds to ~5µm die shift on a 300mm wafer). In addition, an averaging algorithm applied to multi-point alignment data allows the system to perform best fit overlay of the full-field mask to the wafer. A third method to achieve good overlay results for Fan-Out-Wafers, that is only applicable for full-field masks, is the use of a biased mask, which is an efficient way in case the placement pattern on the wafer is repeatable and known.

### COST OF OWNERSHIP CONSIDERATIONS

The reduction of manufacturing costs and optimization of the equipment park is a key topic in every modern fab for semiconductor devices and packaging services. Therefore cost effective equipment that meets the technical requirements but is not over engineered is a key to maintain profit margins and to grow market share. Depending on the process requirements a careful selection of the exposure technology helps improve the cost structure. A cost of ownership comparison between the different selections should help to demonstrate the

cost impact that come along with each of the technologies (industry example shown in Figure 18).

Obviously the mask aligner technology provides the best CoO due to the low capex required and high throughput. The SUSS DSC300 Gen2 with its superior technical properties still offers a ~50% cost advantage over a traditional UV Stepper. This additional alternative helps users to lower their manufacturing costs for the majority of today's processes and ensures availability of existing UV steppers for more critical layers.

### SUMMARY

With the DSC300 Gen2 projection scanner, SUSS MicroTec offers an alternative exposure solution to UV steppers that provides projection lithography performance coupled with the advantages of a full-field exposure system. The system is designed to extend the mask aligner capabilities and to address the unique challenges of emerging packaging applications at lowest cost of ownership within the projection lithography equipment market.

The projection scanning technology is available in two different equipment models to address different substrate sizes. The SUSS DSC300 Gen2 is capable to run up to 300mm wafers while the SUSS DSC500 is designed to process substrates or panels up to 450x500mm.

Typical Exposure Results:

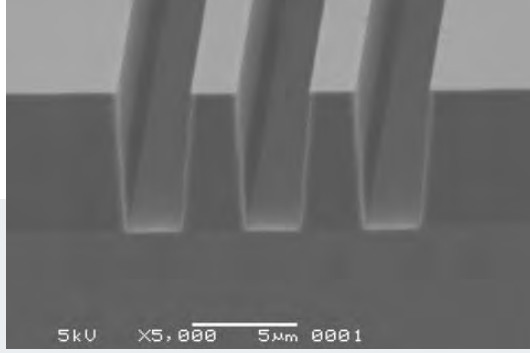


Figure 19 DSC300 performance using TOK TMMR P-W1000T, 3µm L/S, 7µm thick

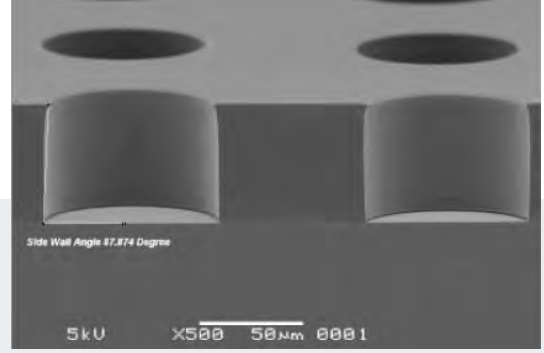


Figure 20 DSC300 performance using TOK-PMER-CR4000, 80µm via with side wall angle ~87°

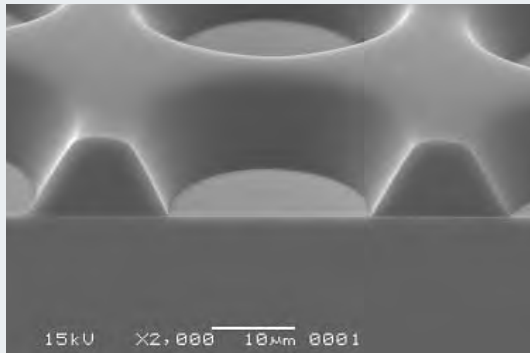


Figure 21 DSC300 performance using HD PBO 8820, 20µm via, 10µm thick

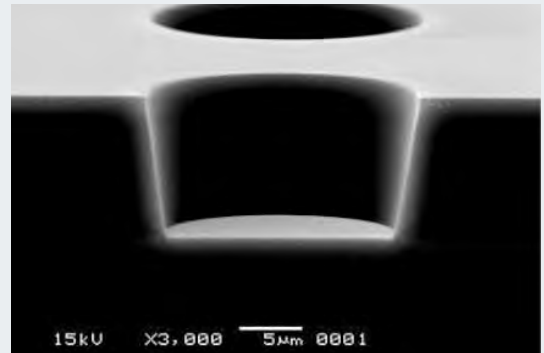


Figure 22 DSC300 performance using AZ4620, 20µm via, 10µm thick

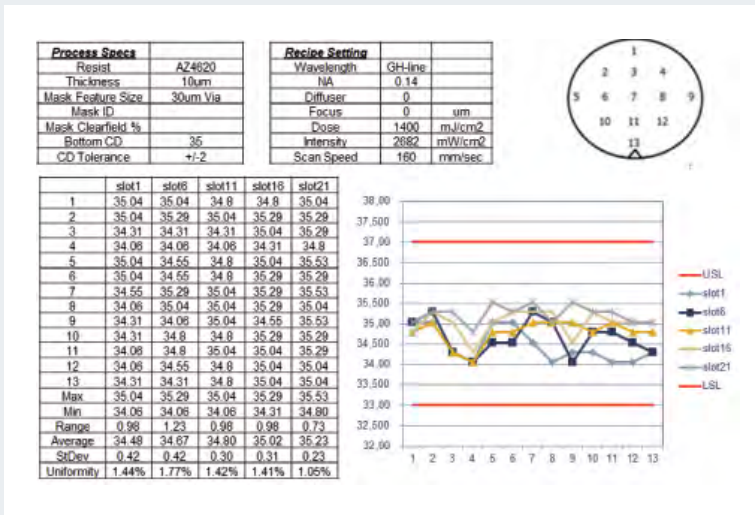
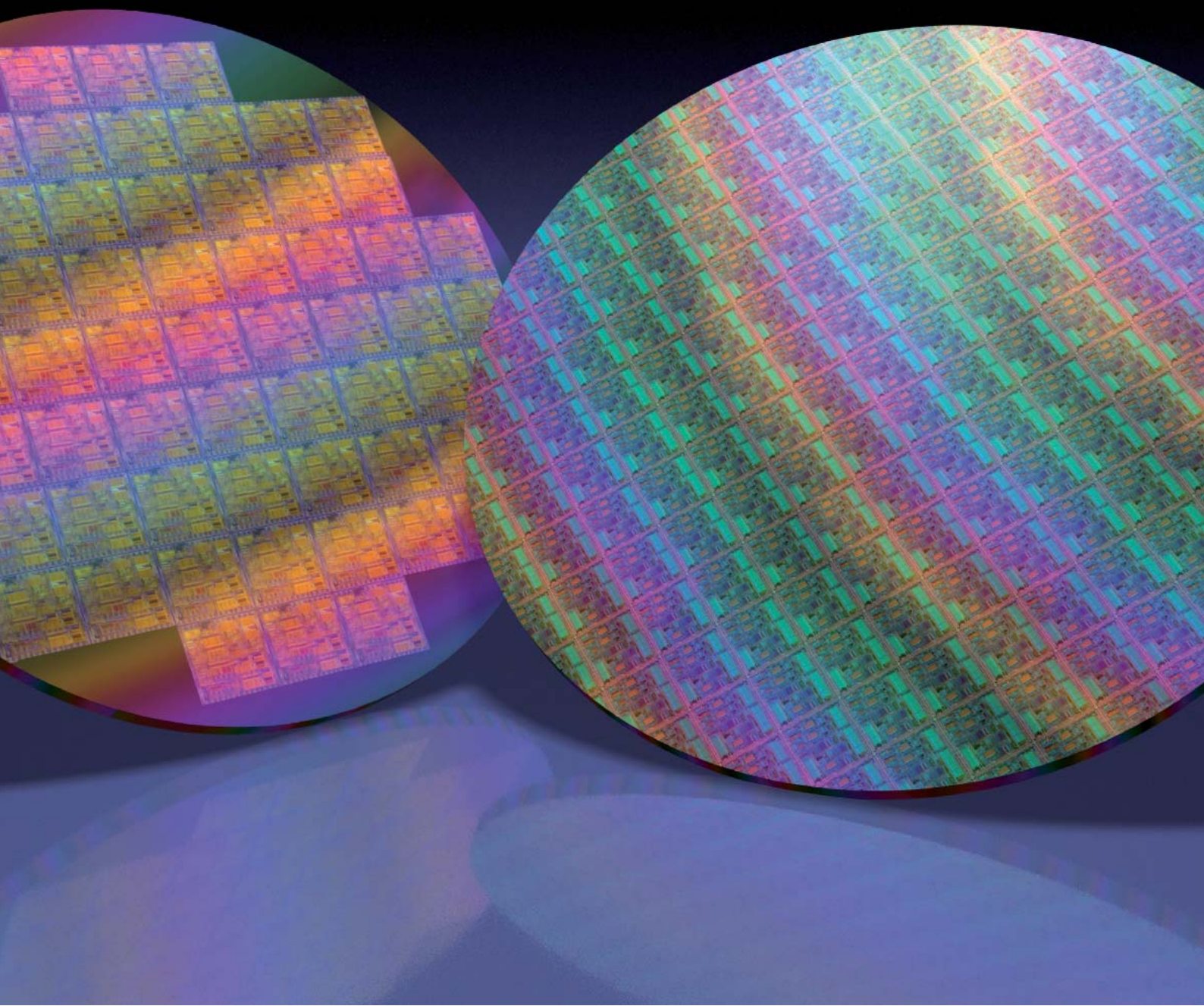


Figure 23 DSC300 performance using AZ4620, 20µm via and wafer-to-wafer/within wafer uniformity

Ralph Zoberbier graduated in Precision Engineering and Microsystems Technology from the University of Applied Sciences in Nuremberg. He joined SUSS MicroTec in 2001 as R&D Project Manager. In 2005 he became International Product Manager Aligner. From 2010 – 2014, he led the Aligner Product Management team as Director Product Management. With the acquisition of Tamarack Scientific Inc. his responsibility was extended by complementary projection lithography and laser process technology. In 2014 he was appointed to General Manager Exposure and Laser Processing. Ralph gained his MBA degree in Entrepreneurship at Louisville University, Kentucky.





# RUTHENIUM CAPPING LAYER PRESERVATION FOR 100X CLEAN THROUGH PH DRIVEN EFFECTS

**Davide Dattilo** SUSS MicroTec Photomask Equipment, Ferdinand-von-Steinbeis-Ring 10, 75447 Sternefeld, Germany  
**Uwe Dietze** SUSS MicroTec Photomask Equipment, Ferdinand-von-Steinbeis-Ring 10, 75447 Sternefeld, Germany  
**Jyh-Wei Hsu** SUSS MicroTec (Taiwan) Co., 8F-11, No. 81, Shui-Lee Rd., HsinChu, 300, Taiwan

In the absence of pellicle a EUVL reticle is expected to withstand up to 100x cleaning cycles. Surface damage upon wet and dry cleaning methods has been investigated and reported in recent years [1]. Thermal stress, direct photochemical oxidation and underlying Silicon layer oxidation are reported as the most relevant root-causes for metal damage and peeling off [2,3]. An investigation of final clean performance is here reported as a function of operating pH; the results show increased Ruthenium durability in moderately alkaline environment. The electrochemical rationale and the dependency of the reducing strength of the media with the pH will be presented as possible explanations for reduced damage.

## INTRODUCTION

EUV technology uses light reflected from the photomask surface rather than light transmitted through the substrate, which changes the photomask nature for the imaging process onto the wafer-level from transmissive to reflective. So far, the best EUV reflector design known for lithographic purposes at 13.5nm is based on the stacking multilayer concept. Schematic representation of the EUV reflector scheme and the TEM image are shown in Figure 1 [4].

Silicon is easily oxidized into silicon dioxide, thus, the EUV reticle required a protective capping layer. This is currently accomplished by a 2-3nm layer of metallic Ruthenium; this is chosen because of its high transmission in the extreme ultra violet wavelength range and quite high resistance toward corrosive conditions [5,6].

Presently, no pellicles are available for EUV masks to protect the pattern side from contamination during storage, use or transport. This implies that EUV masks are more exposed to contamination than optical masks and thus it is expected that EUVL masks need to undergo more cleaning cycles during their useful life in order to maintain high device production yields. With increasing cleaning cycles mask defectivity remains one of the obstacles to commercial viability [7,8]. Key to overcome this is the development of a mask clean process that is effective for defect removal and preserves the integrity of the mask surface. Damage to the Ru capping surface degrades EUV reflectivity which can lead to critical dimension (CD) shift and non-uniformity [9].

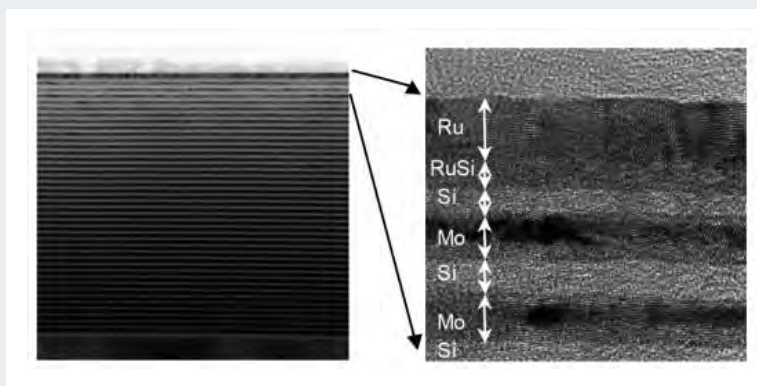


**Figure 1** EUV reticle schematic: Molybdenum and Silicon layers alternate to form the reflector. Ideal reflectivity is found at 40 pairs of Mo/Si layers. 2-3 nm layer of Ruthenium is required to protect Silicon from oxidation and damage

Therefore, it is very crucial to understand the effect of cleaning and exposure processes on EUV mask quality and printing performance.

A full cleaning cycle includes a surface preparation step followed by photoresist removal, particle and ion removal, and final clean. It has been shown that Ruthenium damage occurs mostly during the final clean step, where the metal layer is directly exposed to cleaning chemistry [10].

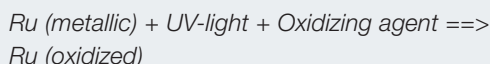
In this paper we report a new chemical approach for final clean which preserves the Ruthenium durability up to more than 100 cleaning cycles. Possible chemical explanations for metal preservation will be proposed.

## BACKGROUND

Previously, SUSS MicroTec demonstrated techniques for organic removal, surface preparation, residual ion removal and final clean without surface damage on the 193i masks [11,12,13]. These new techniques are based on POU UV exposure of the wet cleaning chemistry and the mask surface simultaneously. Recently, the major root-causes for Ruthenium capping layer damage have been extensively reviewed and several mechanisms for metal damage have been proposed; two major root causes for capping layer degradation have been individuated:

- 1) Direct or in-direct metal oxidation [10]
- 2) Silicon dioxide formation underneath the Ruthenium layer, leading to metal peeling off the surface [3]

Ruthenium oxidation can occur during exposure of the metal layer to UV-light and oxidizing agents:



Commonly used UV-light source are the two main mercury emissions at 185 and 254 nm; oxidizing agents are formed in-situ through the photolysis of absorbing media such as molecular Oxygen, Ozone or Hydrogen Peroxide.

Recently, an additional mechanism for Ruthenium peeling off has been proposed; Oxygen, in the form of molecule or atom (as radical) can inter-diffuse into the capping layer, as shown in Figure 2.

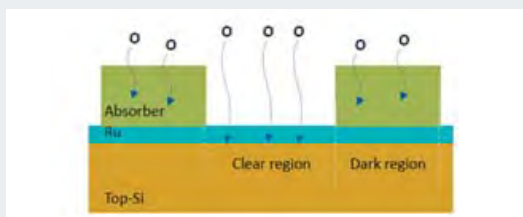


**Figure 2** Oxygen inter-diffusion through Ruthenium layer into the under-laying Silicon layer [3]

Under the absorber features Oxygen inter diffusion is quite difficult to occur; however, in clear regions, Oxygen can diffuse through the 2 nm thick metal layer and get in contact with the first Silicon layer. This, in turn, leads to oxidation as this is very favorable thermodynamic process for elemental silicon. Amorphous silicon dioxide has a higher volume than elemental Silicon, thus, the expansion of the underling Silicon layer leads to Ruthenium peeling off (Figure 3).



**Figure 3** Silicon dioxide formation with resulting volume increase and Ruthenium peeling-off

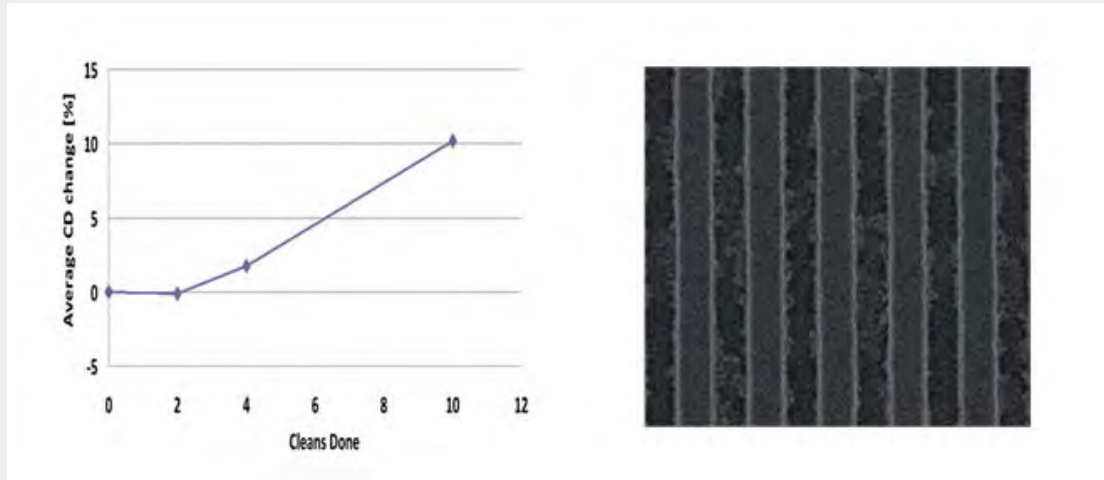


**Figure 4** Average relative CD change in printed CD on wafer-level after cleaning the mask in total for 10 times; a majority of these changes occurs between 4th and 10th cleaning process of the EUV mask (left); evidence of Ruthenium peeling at the interface between absorber and capping layer (right) <sup>[15]</sup>

Previous reports showed how EUV reticles can undergo capping layer damage after only a few cleaning cycles; Figure 4 shows a published result from 2011, where SEM surface image documents the Ruthenium damage in the form of massive peeling around the absorber features.

The damage becomes even more evident at the interface between absorber and Ruthenium capping layer. This suggested that thermal stress could also contribute to the damage. High pressure Mercury lamps used during in-situ UV process have residual emission in the infrared spectrum, which could in turn heat the mask materials leading to stress and peeling off <sup>[2]</sup>.

Furthermore, it has been observed that the damage depends on mask vendor origin. This indicates a strong influence of the mask manufacturing process on surface durability.

Especially the absorber etch process has been reported to play a major role in the stability of the Ru layer during cleaning <sup>[14]</sup>.

## EXPERIMENTAL

### Process parameters

All the tests were performed using the SUSS SMT PE MaskTrackPRO (MTPRO) mask cleaning tool. The process parameters were automatically monitored and controlled with a standard recipe programmed on the MTPRO tool. DI water used for the tests was de-gassed before it was supplied to the cleaning chemical distribution system. Chemicals and gases were added into the de-gassed water to prepare the respective cleaning media. The cleaning media tested are: Chemical A ( $4 \leq \text{pH} \leq 6$ ), Chemical B ( $6 \leq \text{pH} \leq 8$ ) and Chemical C ( $10 \leq \text{pH} \leq 12$ ).

### Characterization

To evaluate Ruthenium damage SEM pictures were taken at specific mask locations. TEM was used to assess Ruthenium integrity after 100 cleaning cycles.



**Figure 5** SEM image of Chemical A treated EUV test pattern: Ruthenium capping layer peeling-off was observed in the top and bottom mask corners (left and right images). No damage was observed for the central region of the EUV mask

## EXPERIMENTS PERFORMED, RESULTS AND DISCUSSION

Repeated final clean cycles, up to 100 times, have been performed by using in-situ UV technology. A water solution at pH comprised between 4 and 6 was used as baseline (Chemical A). The organic removal mechanism has been reported as direct Carbon activation through absorption of light followed by reaction with molecular Oxygen leading to consecutive oxidation steps; the final decomposition products of this photochemical reaction are  $\text{CO}_2$  and water [2]. Ozone formation through media absorption at 185nm, followed by photolysis into Hydroxyl radicals, also contributes to hydrocarbon decomposition. Figure 5 shows SEM image at different surface locations of Chemical A ( $4 \leq \text{pH} \leq 6$ ) treated EUV test reticle after 100 cleaning cycles.

Massive peeling off was observed for Ruthenium at the top and bottom areas of the test EUV mask. Only the central area of the mask resulted in undamaged capping layer; this observation demonstrates once more that the absorber etching parameters play a major role in the surface integrity upon repetitive cleaning cycles [15].

### Electrochemical motivation

As explained, one major root-cause for Ruthenium damage is direct metal oxidation [10]. The 100X clean experiment was conducted in water solution of Chemical A, which had a measured pH comprised between 4 and 6. A review of the electrochemical behavior of possible Ruthenium states (metallic ruthenium or ruthenium oxides) is required to individuate the best media environment for reduction or elimination of the damage. Figure 6 shows the Pourbaix diagram for Ruthenium.

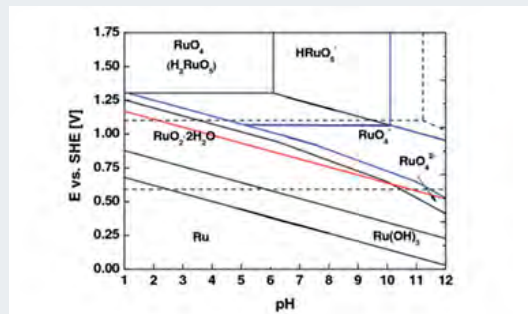
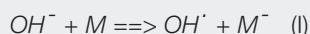


**Figure 6** Pourbaix diagram for Ruthenium. Electrochemical potential for ruthenium and ruthenium oxides is decreasing with increasing pH [16]

Pourbaix diagrams are a schematic representation of the electrochemical potential (i.e., the amount of energy needed to get oxidation) respect to pH. These diagrams are strictly holding in solution phase, but can provide a fair estimation of the oxidation behavior of the possible involved ruthenium oxides (and metallic ruthenium). At higher electrochemical potentials, i.e., in highly oxidizing conditions,  $\text{RuO}_4$  is expected to be formed. This oxide is extremely volatile (boiling point  $40^\circ\text{C}$ ), thus leading to surface etching upon its formation. The Pourbaix diagram shows how at more alkaline pH values the system is in a reducing environment, with more stable lower oxidation state oxides or hydroxides such as  $\text{RuO}_2$  or  $\text{Ru}(\text{OH})_3$  [16]. Based on this scenario we decided to investigate the Ruthenium damage as a function of operating pH. A shift at more alkaline pH was then decided to check if direct metal oxidation has a major role in the damage mechanism. To further motivate the choice of shifting the pH at more alkaline pH we reviewed the electrochemical behavior of different Ruthenium oxides at alkaline pH values along with electrochemical properties of aqueous alkaline media. Literature reports the ability of Hydroxide ion to be a good one electron reducing agent [17]:



Equation (I) shows the one electron transfer to a generic metal center, with production of reduced  $\text{M}^-$  and  $\text{OH}^\cdot$ . As confirmation of the reducing power of Hydroxyl ions, the literature reports how  $\text{RuO}_4$  is reduced into more stable  $\text{RuO}_4^-$  and  $\text{RuO}_4^{2-}$  at alkaline pH [18]:

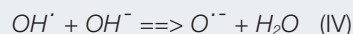


Equation (II) shows Ruthenium tetra oxide reduction by means of two mono-electron reducing events.

With emitting light sources at 185nm Hydroxyl radicals can be formed (by light absorption from water and Oxygen, leading to atomic oxygen which in turn reacts with water to lead to  $\text{OH}^\cdot$ ); also, equations (I) and (II) show as the reaction byproduct of metal reduction in alkaline media is Hydroxyl radical; however, literature reports that Hydroxyl radical is partially converted into  $\text{O}^{\cdot-}$  radicals in alkaline media:



This can be written as a simple reaction between  $\text{OH}^\cdot$  and  $\text{OH}^-$ :



This conversion is quantitative for  $\text{pH} > 12$  and partial at  $\text{pH} = 10 \div 12$ .  $\text{O}^{\cdot-}$  can be exposed to the same reactions as  $\text{OH}^\cdot$ , however its negative charge reduce its electrophilic character, i.e., in the presence of a metal center the one electron oxidation process is less favorable respect to  $\text{OH}^\cdot$  [19]. As for organic removal, where the mechanism is mostly by Hydrogen abstraction, their behavior is very similar [20]. This shows how conversion of  $\text{OH}^\cdot$  radicals into  $\text{O}^{\cdot-}$  radicals prevents metal oxidation. In presence of light source emitting below 200nm, Ozone is likely to be formed, due to UV-light absorption from dissolved molecular Oxygen; Ozone will be readily converted into Hydroxyl radicals, however, if the conversion is not quantitative, some un-decomposed Ozone could still be in solution. Molecular Ozone is reported to be cause of surface oxidation for EUV mask cleaning [21]. In alkaline conditions, however, Ozone is readily converted to Hydroxyl radicals [22]:



This may further minimize the risk of direct surface oxidation.

Our literature overview of the electrochemical properties leads to the following conclusions:

- 1) Alkaline pH values represent a reducing condition (lower electrochemical potentials for Ru oxides; Figure 6) <sup>[17]</sup>
- 2)  $\text{OH}^-$  as such, can act as reducing agent;  $\text{RuO}_4$  that could arise from direct metal oxidation can be efficiently reduced back to  $\text{RuO}_4^{2-}$  (equations I and II) <sup>[18]</sup>
- 3) Hydroxyl radicals (arising from 185 nm exposure or by-product of reduction with  $\text{OH}^-$  shown in equations I and II) are partially converted into less oxidizing  $\text{O}^{\cdot -}$  species.  $\text{O}^{\cdot -}$  are less aggressive toward metal centers, and equally efficient toward organic degradation <sup>[19,20]</sup>
- 4) Any generated Ozone is readily converted into Hydroxyl radicals and then into less oxidizing  $\text{O}^{\cdot -}$  ions, thus minimizing risk of surface damage <sup>[21]</sup>

The above described four conclusions, in combination with experimental results from Chemical A treatment during final clean, which were conducted at acid pH (between 4 and 6), directed us to decide to run extensive (up to 100 cleaning cycles) at increased pH. We planned to run experiments at two different pH values, such as:

- a) Chemical B,  $6 \leq \text{pH} \leq 8$
- b) Dissolved strong base at high dilution, Chemical C,  $10 \leq \text{pH} \leq 12$

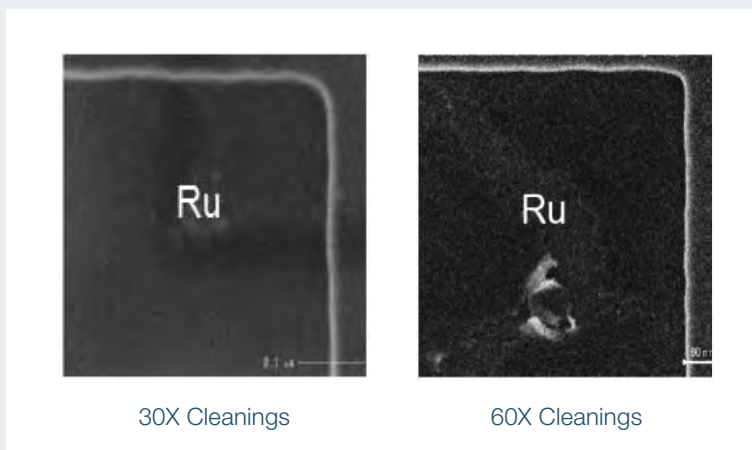


**Figure 7** SEM images taken at different mask locations after cleaning of EUV test reticle at pH comprised between 6 and 7 (Chemical B) Left: after 30X cleaning cycles no Ruthenium damage is found. Right image: after 60X cleaning cycles, peeling off of metal layer was observed

#### **Chemical B, pH comprised between 6 and 8. Results.**

Given the results collected by using Chemical A as cleaning media, we thought to use Chemical B at pH comprised between 6 and 8 as intermediate experiment to check if a slight increase in pH would have led to any improvement in surface integrity. A test pattern EUV mask was cleaned multiple times in Chemical B and AFM inspection followed every 30 cleaning cycles. Figure 7 shows SEM images collected after 30 and 60 cleaning cycles:

After 30 cleaning cycles in Chemical B no Ruthenium damage was found, whereas at 60 cleaning cycles peeling off of the metal layer was observed. The experiment was not brought up to 100 cleaning cycles because a visible damage was already present after 60 cycles.

### Chemical C; molecular motivation.

In section “*Electrochemical motivation*” we have provided motivations for choosing alkaline chemistry during final clean of EUV mask.

After having performed experiments at pH comprised between 6 and 7 we wanted to bring the pH to more alkaline values, such as between 10 and 12. Higher pH values (>12), although favorable in terms of oxidation chemistry, would have high risk of metal dissolution through the formation of soluble hydroxides. pH driven effects could not be the only ones playing a role in surface preservation. In section “*Background*” we have reported the current root-causes for Ruthenium peeling, and mentioned a direct oxidation and Oxygen inter-diffusion as most relevant root-causes. The alkaline pH could cover the direct oxidation root-cause; however, Oxygen inter-diffusion has little to do with pH. To address this equally relevant root-cause for Ruthenium damage we have made molecular and reactivity considerations on choosing the appropriate base. As a matter of fact, the molecular structure of the used base could play an important role in surface integrity.

Literature reports a strong molecular size dependent effect happening during alkaline silicon and silicon dioxide etching; the bigger is the positive counter-ion used, the slower is the etch rate into the silicon, because bigger positive ions electrostatically bond on the silicon surface and prevent further diffusion into the bulk silicon (blocking effect)<sup>[23]</sup>. Ammonia is very often used as a base during semiconductor cleaning; however the small size of the  $\text{NH}_4^+$  cation represent a high risk for oxygen inter-diffusion through the Ruthenium capping layer. For this reason, Chemical C was chosen to be:

- A strong base
- A base with molecular structure such that the positive counter ion is much bigger comparing to  $\text{NH}_4^+$  ion

Both Ammonia and Chemical C bases give in solution Hydroxide ions, thus both bases could be used for pH adjustment. However, the (positive) counter ion dimensions are quite different, with the  $\text{B}^+$  ion being substantially bigger than  $\text{NH}_4^+$  ion.

For these explained reasons we have chosen to conduct our experiment at pH comprised between 10 and 12 by using as a base such BOH. BOH was also chosen to be a non-coordinating agent. Coordinating agents (i.e., compounds capable to establish a direct bond with metal center through available external electrons) can in fact promote metal dissolution through the formation of soluble complexes; Ammonia is a good coordinating agent, whereas BOH is not.

To avoid possible interaction with cleaning UV mechanism (i.e., direct absorption of Hydrocarbons at 254nm) we verified that absorption at 254nm of chemical A, Chemical B and chemical C was very low. Negligible absorption at 254nm is measured for the three used media, thus direct absorption of Hydrocarbons at 254nm is not influenced by media absorption. Residual absorption of BOH at 185nm could be expected, however massive photolysis can be excluded due to the very low BOH concentration in solution.

### Chemical C, pH comprised between 10 and 12. Results.

Extremely diluted BOH solutions ( $10 \leq \text{pH} \leq 12$ ) were used to run cleaning cycles and evaluate surface integrity afterward. Figure 8 shows SEM images of EUV test pattern after 30, 60 and 100 cleaning cycles.

AFM images revealed that after 30, 60, and 100 cleaning cycles Ruthenium peeling off was not observed; only in a single spot, an increase in surface roughness was observed.

SEM IMAGES AFTER 30 CLEANING CYCLES



SEM IMAGES AFTER 60 CLEANING CYCLES



SEM IMAGES AFTER 100 CLEANING CYCLES

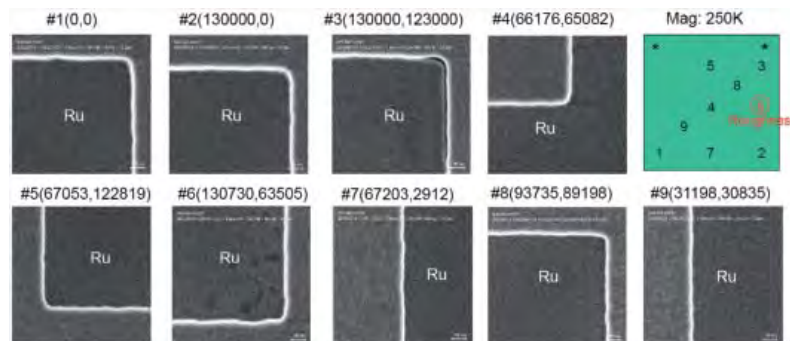


**Figure 8**

Top image: SEM pictures at different mask locations taken after 30 cleaning cycles in Chemical C; no Ruthenium damage was observed.

Middle image: SEM pictures with same chemistry and in the same mask locations taken after 60 cleaning cycles; no Ruthenium damage was observed.

Bottom image: SEM pictures with same chemistry and in the same mask locations taken after 100 cleaning cycles; no Ruthenium damage was observed; one single mask location showed increased roughness, without evident surface damage.

To assess Ruthenium integrity, TEM analysis was performed on Ruthenium capping layer; Figure 9 shows TEM results.

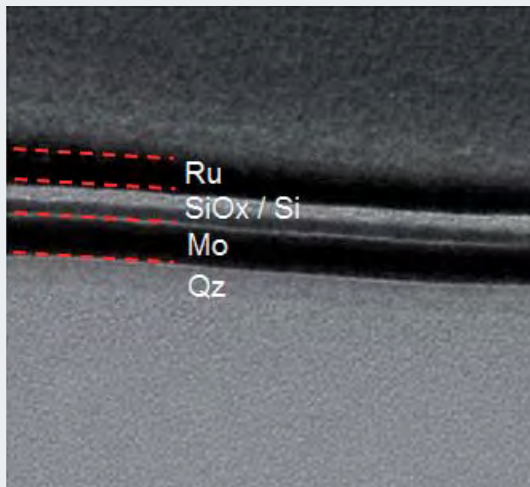


**Figure 9** TEM image of Ruthenium capping layer of EUV test pattern reticle exposed to in-situ UV final clean for 100 cleaning cycles with alkaline ( $10 \leq \text{pH} \leq 12$ ) chemistry. The image shows uniform Ruthenium layer without damage; this is on top of a single Si/Mo layer; also the underlying silicon does not increase its volume, ruling out massive Silicon oxidation

The SEM image shows preserved Ruthenium integrity; the metal layer looks uniform and without damage. A mono-layer of Si/Mo has been used for this test EUV mask; the Silicon layer appears undamaged and uniform through the whole scanned area. Massive Silicon oxidation can be excluded because no increased volume has been observed.

## CONCLUSIONS

EUV masks are more likely to be cleaned due to the lack of pellicle respect to traditional 193nm Mask. Particle deposition and carbon contamination can occur in several points in time of the mask lifetime, like during handling and exposure steps; along with these degrading effects Ruthenium damage is often observed in the form of volatile  $\text{RuO}_4$  formation. In this paper, the latest proposed root-causes for Ruthenium damage have been recalled; direct metal layer oxidation, and underlying silicon dioxide formation are presented as major root-causes for capping layer peeling. A review of the electrochemical properties of Ruthenium oxides shows how alkaline pH place the metal layer into reducing conditions, thus optimal to decrease risk of direct Ruthenium oxidation. The ability of Hydroxyl ions to act as reducing agent is also recalled; furthermore, hydroxyl radicals convert into less oxidizing  $\text{O}^{\cdot -}$  species in alkaline media. Any undissociated molecular Ozone is also rapidly converted into Hydroxyl radicals. These theoretical considerations were tested by running sequential cleaning experiments at increasing pH (Chemical A,  $4 \leq \text{pH} \leq 6$ ; Chemical B,  $6 \leq \text{pH} \leq 8$ ; Chemical C,  $10 \leq \text{pH} \leq 12$ ). Results show decreasing damage with increasing pH, and Ruthenium capping layer preservation after 100 cleaning cycles when operating at pH comprised between 10 and 12. Molecular effects (such as blocking effect) cannot be ruled out; thus, the choice of base for alkaline conditions may be of crucial importance. For an extensive understanding of surface integrity mechanism, further experiments are conducted by varying the base molecular structure, to separate pH from molecular symmetry driven effects. Weak vs strong bases, coordinating vs non-coordinating bases as well as small vs big molecular sized bases are being tested.

*"This paper has been originally published as SPIE Vol. 9635-47 (2015)"*

## References

- [1] Shimomura, Liang T. "Chemical durability studies of Ru-capped EUV mask blanks" SPIE Proc. Vol. 7122, pp. 712226 (2008)
- [2] S. Singh, D. Dattilo, U. Dietze, A. JohnKadaksham, Il-Yong Jang, F. Goodwin "Investigation of EUVL Reticle Capping Layer Peeling under Wet Cleaning", SPIE Vol. 8880-36, (2013)
- [3] Y. Jang, A. John, F. Goodwin, S. Y. Lee, S. S. Kim "Understanding the mechanism of capping layer damage and development of a robust capping material for 16 nm HP EUV mask", International Symposium on Extreme Ultraviolet Lithography, Toyama, Japan 6-10 October 2013
- [4] L. Belau, J. Y. Park, T. Liang, H. Seo, and G. A. Somorjai "Chemical Effect of Dry and Wet Cleaning of the Ru Protective Layer of the Extreme Ultraviolet (EUV) Lithography Reflector", J. Vac. Sci. Technol. B, 2009, 27 (4), 1919
- [5] H. Over, Y.B. He, A. Farkas, G. Mellau, C. Korte, M. Knapp, M. Chandhok, M. Fang "Journal of Vacuum Science & Technology B", 25, (2007) 1123-1138
- [6] T.E. Madey, N.S. Faradzhev, B.V. Yakshinskiy, N.V. Edwards "Applied Surface Science", 253 (2006) 1691-1708
- [7] Liang T., Zhang G., Naulleau P., Myers A., Park S. J., Stivers A., Vandentop G. "EUV Mask Pattern Defect Printability," BACUS News, 22 (10), pp. 1-11(2006)
- [8] R. M. Jonckheere, F. Iwamoto, A. Myers, J. van der Donck, T. Liang, Intel Corp.; J. D. Zimmerman, G. F. Lorusso, A. Goethals "Investigation of EUV Mask Defectivity via Full-Field Printing and Inspection on Wafer" SPIE Proc. Vol. 7379-26 (2009)
- [9] R. M. Jonckheere, F. Iwamoto, A. Myers, J. van der Donck, T. Liang, Intel Corp.; J. D. Zimmerman, G. F. Lorusso, A. Goethals "Investigation of mask defectivity in full field EUV lithography" SPIE Proc. Vol. 6730-37 (2008)
- [10] D. Dattilo, U. Dietze "Efficient ozone, sulfate and ammonium free resist stripping process" Proc. SPIE 9256, Photomask and Next-Generation Lithography Mask Technology XXI, 925604 (July 28, 2014)
- [11] S. Singh, P. Dress, S. Helbig, U. Dietze "Study on surface integrity in photomask resist strip and final cleaning processes" SPIE Proc. Vol. 7379-12 (2009)
- [12] S. Singh, S. Chena, K. Selinidis, B. Fletcher, I. McMackin, E. Thompson, D. J. Resnick, P. Dress, U. Dietze "Automated imprint mask cleaning for Step-and-Flash Imprint Lithography" SPIE Proc. Vol. 7271-88 (2009)
- [13] S. Singh, S. Helbig, P. Dress, U. Dietze "An advanced method to condition and clean photomask surfaces without damage" Sematech – 6th Annual Mask Cleaning Workshop, Monterey, CA (2009)
- [14] T. Wähler, S. Singh, U. Dietze, R. Jonckheere, K. Ronse, B. Baudemprez "Preserving Printed Wafer CD Stability in High-Frequency EUVL Mask Cleaning" International Symposium on Extreme Ultraviolet Lithography and Lithography Extensions, Miami, USA, Oct. 2011
- [15] D. W. Lee, S. J. Jo, S.K. Sung Hyun Oh, T. Joong Ha, S. P. Kim, D. G. Yim "Analysis of EUV mask durability under various absorber etch conditions" SPIE Proceeding Vol. 8880-73 (2013)
- [16] H. Cui, J.H. Park, J. Park "Effect of Oxidizers on Chemical Mechanical Planarization of Ruthenium with Colloidal Silica Based Slurry" ECS Journal of Solid State Science and Technology, 2013, 2 (1), 26
- [17] D. T. Sawyer, J. Robert "Hydroxide Ion: An Effective One-Electron Reducing Agent?" Acc. Chem. Res. 1988, 21, 469-476
- [18] J. A. Rard "Thermodynamic Data bases for Multivalent Elements: an example for Ruthenium" International Conference of Thermodynamics of Aqueous Systems with Industrial Applications Airlie House, Warrenton, Virginia, May 10-14, 1987
- [19] G. Duca "Homogeneous Catalysis with Metal Complexes: Fundamentals and Applications", Ed. Springer, 2012
- [20] I. G. Draganic "The radiation chemistry of water", Ed. Academic Press, 1971
- [21] S. H Lee, B. K. Kang a, H. M. Kim , M. S. Kim , H. K. Cho, C. Jeon, H. Ko, H. S. Lee, J. Ahn, J. G. Park "Damage/organic free ozonated DI water cleaning on EUVL Ru capping layer" Proc. of SPIE Vol. 7823 7823Z-1 (2010)
- [22] C. S. Chiou, K. J. Chuang, Y. F. Lin, H.W. Chen, C. M. Ma "Application of Ozone Related Processes to Mineralize Tetramethyl Ammonium Hydroxide in Aqueous Solution" International Journal of Photoenergy Volume 2013, Article ID 191742, 2013
- [23] I. Zubel, I. Barycka, K. Kotowska, M. Kramkowska "Silicon anisotropic etching in alkaline solutions IV: The effect of organic and inorganic agents on silicon anisotropic etching process" Sensors and Actuators A 2001, 87, 163



Davide Dattilo receives the third best poster award at SPIE Photomask Technology 2015 conference, held in Monterey (CA) in September 2015. On the left, Mr. Naoya Hayashi, Research Fellow Dai Nippon Printing Co Ltd, Fellow Member. Co-authors are Uwe Dietze and Jhy-Wei Hsu.

Since September 15th 2012 Davide Dattilo is working as Process Scientist in the Surface Technology Innovations department at SUSS MicroTec. He is leading chemistry related projects in Photomask cleaning. Davide graduated in Chemistry in 2000 at the University of Calabria (Italy) where he attended a three years Ph.D. program, with final graduation in 2004, in Molecular Materials. His main focus was non-linear optical materials and their application in photonic systems. He moved to University of Padova for three years getting a post-doctoral position in Surface Chemistry (2007). Before joining SUSS MicroTec Davide worked for five years as Staff Scientist in a bio-technology company dealing with the developing of MEMS, DNA microarrays and biosensors.

# ULTRA-SMALL VIA-TECHNOLOGY OF THINFILM POLYMERS USING ADVANCED SCANNING LASER ABLATION

Michael Töpper, Martin Wilke, Klaus-Dieter Lang Fraunhofer Research Institution for Reliability and Microintegration IZM, Berlin, Germany

**In this paper a new process technology will be discussed which uses a laser scanning ablation process. Laser ablation of polymers is in principle not a new technology. Low speed and high cost was the major barrier for further developments twenty years ago. But the combination of a scanning technology together with a quartz mask has opened this technology to overcome the limitation of the current photo-polymer process. The new technology is described in details and the results of structuring BCB down to less than 4µm via diameter in a 4µm thick film has been demonstrated. The via-side wall can be controlled by the fluence of the laser pulse.**

## INTRODUCTION

There is a strong demand to increase the routing density of substrates, interposers and on-chip routing to match the requirements for future micro-electronic systems which are mainly driven by miniaturization and performance. Photo-resists for structuring the metallization or acting as a mold for electroplating are common for very fine lines and spaces supported by the developments in the front-end processing. For example chemical amplified photo-resists are now moving in the back-end and wafer-level packaging process. The results are mainly governed by the performance of the equipment i.e. the photo-tool. The major difference between photo-resists and dielectric photo-polymer are the unequal functions of the material systems. Photo-resists are only temporary masks for subsequent process steps like etching and plating.

This is different for the photo-polymers which are a permanent part of the future systems. Therefore it has a strong influence on the reliability but also on the performance of the system. Properties like high thermal stability, excellent mechanical properties, low water up-take, low dielectric constant and low loss have to be achieved together by the chemical synthesis of the polymer and are therefore limiting the optical resolution.

Depending on the application the importance of the polymer properties may be different. Highly important are also the following properties:

- Cu-Compatability
- Low temperature cure
- High Breakdown V
- Low cost by alternative processes

Mainly photo-polymers are used for electronic packaging and MEMS applications today. Mask aligners and steppers with UV light are used. For most of the thinfilm polymers like PI (Polyimide), PBO (Polybenzoxazole) and BCB (Benzocyclobutene) limits of the via sizes are in a range of 20-30µm in production. The lithography tools have a much higher resolution but the photo-sensitivity of the thinfilm polymers are limited which is not more compatible for the roadmap of 4µm lines and space of the metallization in the near future. Vias must have similar sizes as the metal lines to achieve a dense routing.

## LASER ABLATION TECHNOLOGY

Pulsed-laser ablation is a process when material is removed by a short high-intensity laser pulse. This ablation takes place far from equilibrium. Therefore the excitation energy can be suppressed beyond the volume that is ablated during the ablation.

In general a single- or multiphoton excitation is essential for the process. This energy can be transformed instantaneously into heat which will raise the temperature of the material and vaporization will follow (or thermal induces stress if the energy was too low).

Each material has a threshold for the laser ablation. If the fluence is below this threshold the energy of the laser will be absorbed and transferred into heat. The threshold value for laser ablation is in the range of 10-100mJ/cm<sup>2</sup> for polymers. The bonding energies of C-C and C-H are between 3.6eV and 4.3eV. If the fluence of the laser is higher as this threshold the laser ablation process starts immediately. The chemical bonds will break and gaseous products will be formed. The enormous change in volume changing from the solid state to the gaseous state leads to an explosive-like ablation process.

## PROCESS DESCRIPTION OF LASER ABLATION TECHNOLOGY COMPARED TP PHOTO-POLYMERS

The process for structuring photo-sensitive polymers consists of multiple steps. First the polymer (in the pre-cursor state) has to be coated on the substrate mainly using spin-coating technique for WLP applications. Emphasis has to be taken into account that these polymers are temperature-sensitive. The shelf-life of some of the materials is limited to one week at room temperature. Therefore a sophisticated material support has to be established from the polymer supplier to the pump of the spin-coater module at the wafer production site. After the coating most of the solvent has to be removed from the coated polymer layer by heating

the wafer on hotplates. This process has a high influence on the whole process and has to be optimized for each polymer type. If the temperature (or time) of the process is too high (or too long) the photo-sensitive components will be damaged which will heavily limit the resolution of the via. If the temperature (or time) is too low (or too short) the vias in the polymer will be not formed well. It may even lead to a dissolving effect in the later developing step. After the baking process the photo-polymers are exposed to UV light using either mask aligner or steppers. Some of the photo-polymers then need a post-exposure bake to improve the UV-induced chemical reaction in the polymer. Then the polymers have to be developed i.e. the polymers have to be washed out of the vias. There is a difference in the process for positive- or negative-acting polymers which is shown in Figure 1:

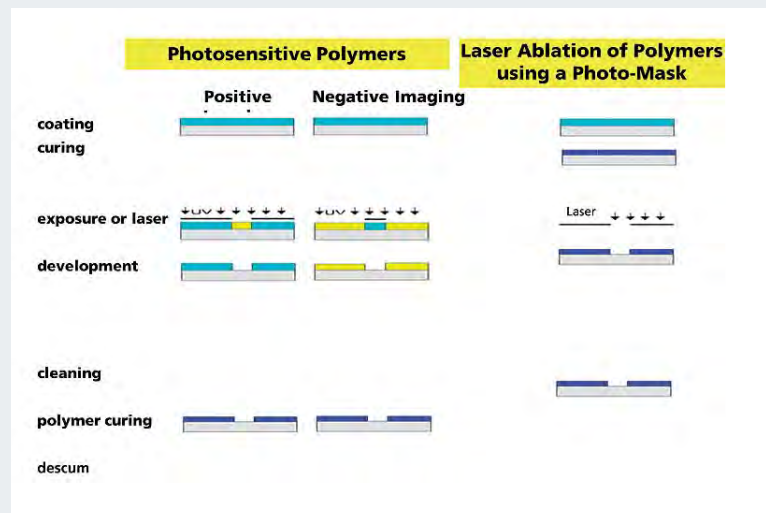


Figure 1 Comparison of process of the photo-sensitive polymers vs. laser ablation process

The developing step is also very sensitive to the duration of the process. The developing solvent may swell the polymer and may lead to a strong film loss (i.e. reduction of film thickness) or even a complete delamination. The next step is then the polymerization process (i.e. called cure) which

gives the mechanical properties for the later application. Some of the polymers will shrink to close to 50% of the film thickness which also has an influence on the via shape. For some of the polymers a descum process is necessary to remove any residues in the via to ensure a low electrical contact resistivity for the next metallization layer. In summary the photo-process is a quite complex process which has multiple time- and temperature-sensitive process steps.

This is totally different for the laser ablation process of non-photo-sensitive polymers. All these sensitive process steps are not necessary. The thin film polymer is coated on the wafer similar to the photopolymer step but the cure will be done as the next step. Final process is the laser ablation process described in details in the next chapter. The process can be also used for photo-sensitive polymers if the cure is done directly after the coating.

#### LASER SCANNING ABLATION PROCESS USING A MASK

The wavelength of the system used for this investigation is 248nm which is excellent to pattern a wide variety of dielectrics. The excimer is a powerful, pulsed, ultraviolet laser that is well-proven in microlithography.

The laser ablation process can be simply described by as the removal of the polymer without damaging the surrounding areas. No cracks or any other heat affected zone should limit the high density applications.

When a high-energy UV-Laser pulse is focused onto a material so that the intensity (which is measured as the fluence) is above a material-dependent threshold value, then the high energy ultraviolet photons directly excite electrons and break interatomic bonds. This threshold is quite important because it can be used to structure polymers on top of inorganic materials without destroying the metal underneath for example because the threshold of metals is mostly very different to the threshold of dielectric materials.

Along with the subsequent shock wave, this causes material to be ejected at high velocity in the form of a fine powder. Each pulse lasts a few nanoseconds and removes a thin layer of the polymer. It is assumed that the process is relatively cold.

Unlike most other laser types, the excimer produces a large area beam that is usually rectangular in cross-section. This has the advantage to be highly compatible with the use of photomasks. Main requirement for the mask is the transmission of the glass material to the wavelength of the laser. Therefore quartz has to be used. For the light blocking metal Al is most suitable due to a very high threshold level which makes the mask stable for a long production cycle time. The UV laser beam path of the equipment of SUSS MicroTec is shown in Figure 2:

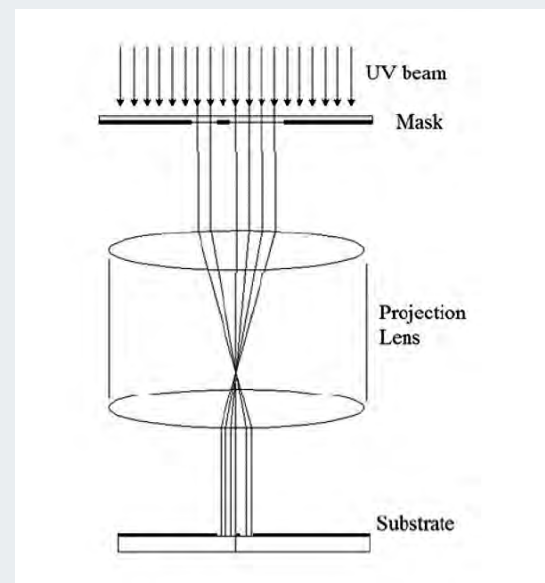


Figure 2 Eximer UV Laser Beam Path

The aluminum is patterned as the inverse of the pattern to be structured on the actual polymer layer. The openings in the metal on the mask define the pattern that will be laser ablated.

The photomask output is then reduced through a reduction lens (2.5x) onto the target – the targeted

area depends on the laser power and the ablation threshold of the target material. In this work a laser ablation system from SUSS MicroTec (ELP 300) has been used. The laser was a Coherent LXPpro 305 with a power of 40W. The laser characteristics are summarized below:

- Wave length: 248 nm (KrF)
- Shoot repetition rate: 50 Hz
- Puls length: ~ 30 ns
- Beam spot size: 6,5x6,5 mm<sup>2</sup>
- Fluence range: 70 - 650 mJ/cm<sup>2</sup>

Therefore the throughput is very high (i.e., multiple vias per second) and at higher pitches, the number of vias per second actually increases. The reason is that the amount of material removed with each laser pulse, i.e., the depth of any hole or trench, is dependent only on the pulse intensity and the specific materials to be ablated.

So only the stepping of the mask is the limiting factor for the process besides the nature of the polymer and the thickness of the layer (Figure 3).

The maximum scan speed is therefore  $50/s \times 6.5\text{mm} = 325\text{mm/s}$ .

Because ablation directly breaks the interatomic bonds with minimal thermal effects, it results in excellent surface quality, no micro-cracking and no recast (melted) debris. The only postlaser process is a cleaning step.

The smallest feature (x-y axes) that can be ablated with the laser depends on the laser wavelength, the optical resolution of the projection lens and the photomask.

The precision depth control in z-axis is controlled mainly by the number of pulses. The high pulse-to-pulse energy stability of the latest excimer lasers means that every pulse will remove an identical depth of material. So depth control is easily provided simply by programming a fixed number of pulses at each stepper site location. In addition, excimer laser ablation even allows control of side-wall angle, by adjusting the laser intensity (fluence)

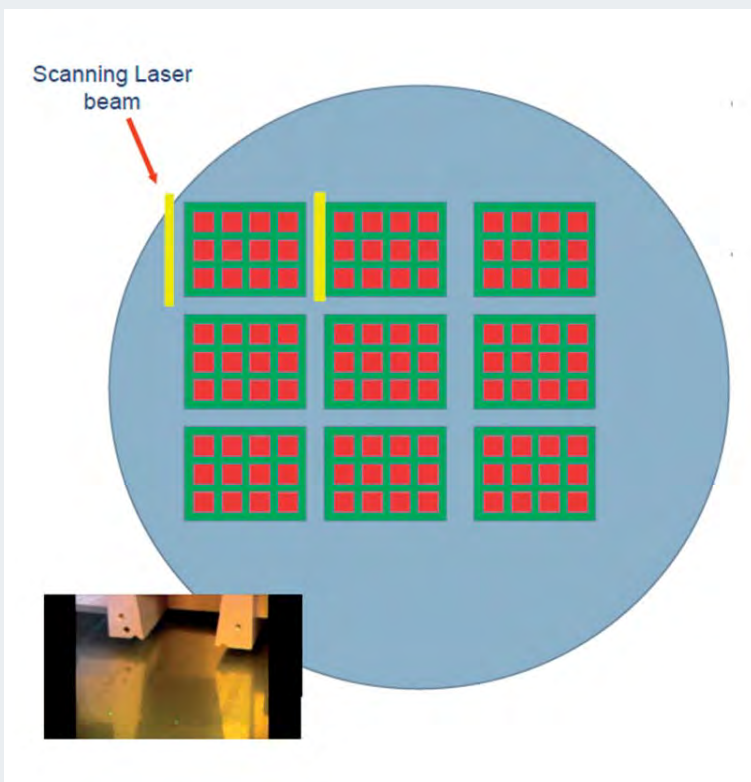


Figure 3 Scanning laser ablation process

and other means. A higher fluence produces a via or trench with steeper sidewalls, whereas a lower fluence results in a shallower side wall which has been proven using BCB (Figure 4):

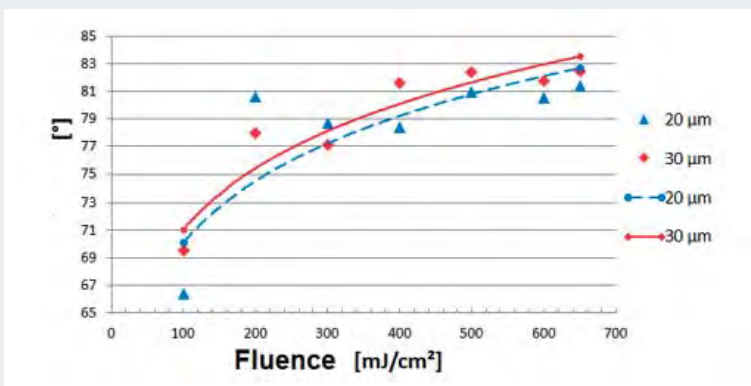


Figure 4 Sidewall angel of dry-etch BCB structured by laser ablation for different via sizes

Dry-etch BCB has been used for this investigation with a thickness of around 8µm on 200mm wafers using a test mask with via sizes between 20µm and 30µm. With a low fluence the sidewall is in a range between 67° to 71° influenced by the via dimension on the mask. The angel can be as high as 83° if the fluence is increased to 650mJ/cm<sup>2</sup>. This is different to the photo-sensitive polymers.

### LASER ABLATION PROCESS OF BCB

The main requirement for a successful ablation process is the absorption of the polymer to be ablated to the UV light of the laser system. This has been already tested for BCB in the past.

For the evaluation of the laser ablation process BCB has been coated on 200mm oxidized Si-wafers. The BCB was the so-called dry-etch BCB (Cyclotene 3000 series, trade-mark from The Dow chemical Company). The BCB-process was done according previous published results using an adhesion promoter before BCB coating. The BCB was fully cured at 250 °C for 90 min.

Each pulse removes a certain amount of material. The etch rate of the process is the amount of material removed by each pulse. The ablation rate is higher for larger fluence which is also shown in Figure 5:

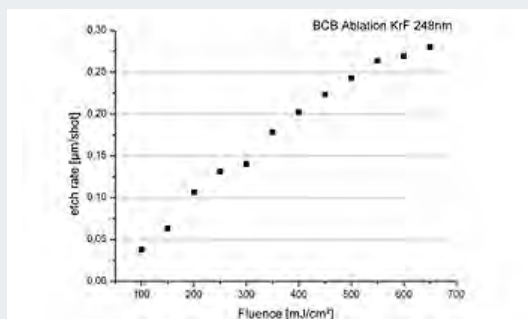


Figure 5 Etch rate of BCB vs. fluence

The etch rate is less than 50 nm for low fluence of 100mJ/cm<sup>2</sup> and can reach over 250nm per pulse for the high.

### CLEANING PROCESS OF LASER ABLATED BCB

One of the few disadvantages of laser ablation processes is the fact that some of the ablated material will condense as a kind of dust on the layer. Therefore a cleaning process is essential to avoid any interference with the subsequent process steps. No changes to this for the laser scanning process introduced here.

One approach has been evaluated which is also common in laser ablation technology: The usage of a protection layer (Figure 6):



Figure 6 Principle of a protection layer for laser ablation

In this case a very thin layer of an addition thinfilm polymer is deposited on the BCB or other polymer after the cure. It acts as a sacrificial layer. Any residues which will fall as a debris on the polymer not being ablated will be removed after the process using a simple stripping process. The advantage of the process is that very mild stripping solvents can be used for this process. An example is given in Figure 7:

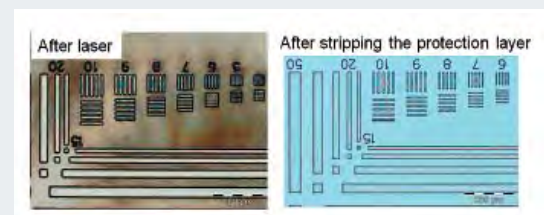


Figure 7 Cleaning process: After laser ablation (left) and after stripping the protection layer (right)

The debris is well visible on the BCB on the left hand side of Figure 7. No residues are in the opening which are here small lines. The stripping

process is then removing the protection layer together with all debris (right hand side in Figure 7). The main advantage is the usage of very mild stripper which will not affect the surface chemistry of the polymer layer. Even water-soluble protection layers are under investigation by the authors. The disadvantage is the additional process step which implies a coating process of polymeric layer after the cure of the polymer being ablated. This might require an additional coater module in production. Therefore a trade-off has to be made between the process line and the impact on the surface chemistry by the stripping solvents which may vary for different polymer.

### TEST LAYOUT FOR LASER ABLATION PROCESS EVALUATION

The prime property to judge the quality of a new via formation process is the electrical contact resistance between the metallic layers. Therefore a test mask has been designed to give feedback from electrical point of view. A classical two-layer metalization has been designed which gives information about single via resistance using 4-Point Kelvin structures. The metal layers are structured using full-field mask aligner technology. 200mm wafer size was chosen for this evaluation. The equipment is fully compatible to 300mm wafer technology but 200mm was chosen to save cost.

There was no issue to adjust the alignment marks generated by the mask aligner to the mask of the laser ablation tool. The optical resolution of the tools is correlated to a precise alignment system for an accurate layer-to-layer registration. This is done by an automated alignment system – global and site-on-site with autopattern recognition. Front side alignment precision is much below  $\pm 1\mu\text{m}$ . Details of the test structure are shown in Figure 8:

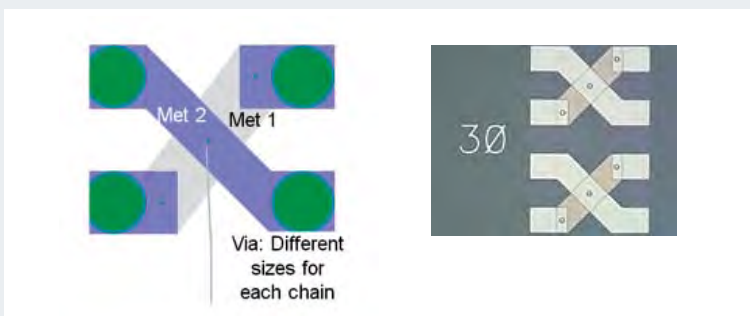


Figure 8 Kelvin test structure for the electrical validation of the process (left: design, right: example for Al/BCB/Al)

The via sizes have been varied on the laser mask between  $2\mu\text{m}$  and  $30\mu\text{m}$  to see the limits of the process. A via with a mask dimension of  $10\mu\text{m}$  in  $4\mu\text{m}$  thick BCB is shown in Figure 9:

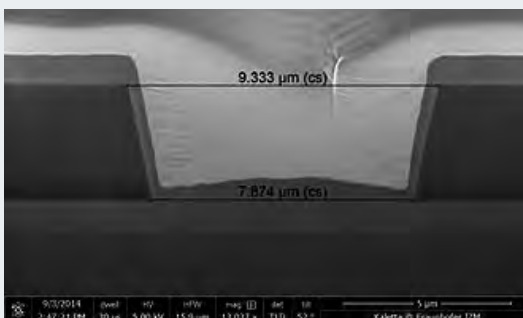


Figure 9 Laser-ablated BCB via ( $10\mu\text{m}$  mask,  $650\text{mJ}/\text{cm}^2$ )

The opening is around  $9.3\mu\text{m}$  at the top and  $7.9\mu\text{m}$  on the bottom. The result for the  $7\mu\text{m}$  mask dimension is shown in Figure 10:

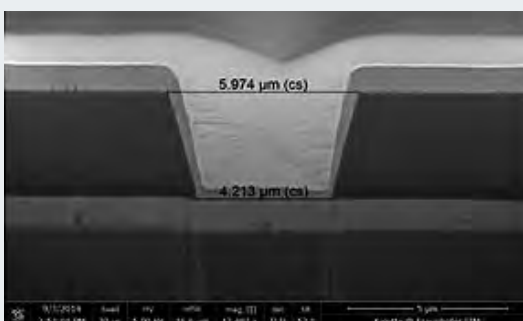
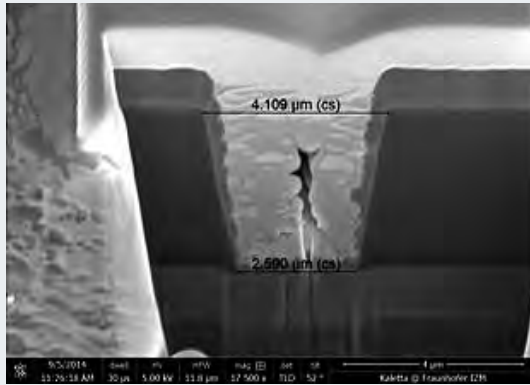


Figure 10 Laser-ablated BCB via ( $7\mu\text{m}$  mask,  $650\text{mJ}/\text{cm}^2$ )



**Figure 11** Laser-ablated BCB via ( $5\mu\text{m}$  mask,  $650\text{mJ}/\text{cm}^2$ ). Platinum (necessary for FIB) is visible in the middle of the via

For this mask the via size is less than  $6\mu\text{m}$  on the top. A via with  $4\mu\text{m}$  opening on the top and less than  $3\mu\text{m}$  on the bottom can be achieved with the  $5\mu\text{m}$  mask. Such small vias have never been published for BCB using mask aligner or stepper technology.

The threshold of different sputtered metals has been compared. Values of  $1000\text{mJ}/\text{cm}^2$  threshold

for sputtered Cu and Al have been published. To verify this data for this new process and expand them to plated metal the following three metallization schemes for the first metal layer have been tested in this evaluation:  $1\mu\text{m}$  AISi,  $1\mu\text{m}$  sputtered Cu ( $200\text{nm}$  TiW underneath) and  $1\mu\text{m}$  plated Cu on  $300\mu\text{m}$  Cu with a  $200\text{nm}$  TiW layer as an adhesion layer. All test were done on  $200\text{mm}$  Si wafer with an  $100\text{nm}$  Oxide layer.

A comparison of these metals for metal 1 in the laser ablation process is shown in Figure 12:

The FIB (focus ion beam) cuts show the clean interface between the metal 1 and metal 2. No metal was damaged by the laser process.

This indicates the large difference in the threshold between polymers like the BCB and the metal like Al or Cu. No difference haven been found between sputtered Cu and plated Cu. All sample had an protection layer for the removal of the debris. No descum-like process was used after the removal of the protection layer. Standard back-sputtering of Ar was used before the sputtering of metal 2 (AISi).

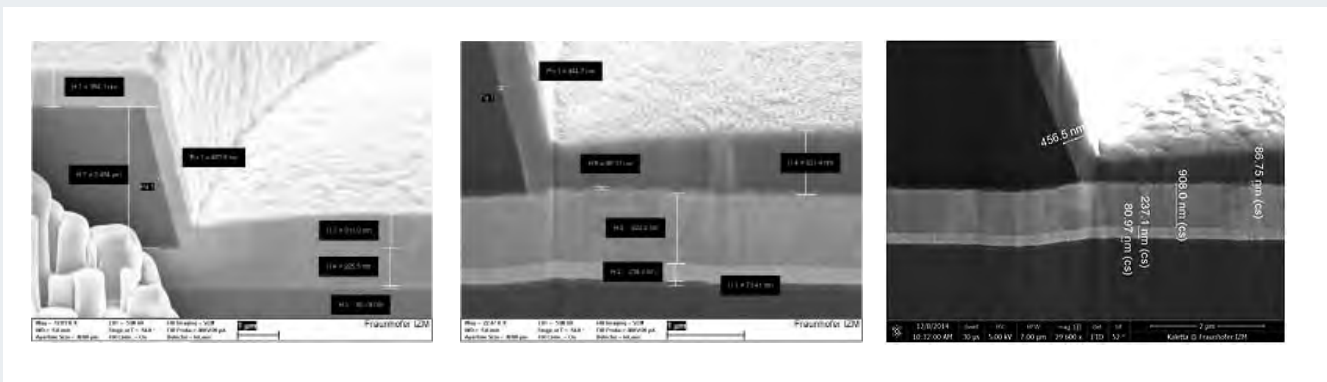


**Figure 12** Laser-ablated BCB via on AISi (left), sputtered Cu (middle) and plated Cu (right) ( $20\mu\text{m}$  mask,  $650\text{mJ}/\text{cm}^2$ ), Met 2:  $1\mu\text{m}$  AISi sputtered

## SUMMARY AND CONCLUSION: COMPARISON OF LASER ABLATION VS. PHOTO-LITHOGRAPHY

Lithography in general is a multi-step process involving developers and other wet chemicals making it increasingly unattractive. All the risks and cost associated with these chemicals, and their safe handling and disposal can be eliminated using the laser ablation process. Like every other industry, advanced packaging and interposer manufacturing is under pressure to use greener manufacturing that is less polluting and more energy efficient.

It is important to distinguish excimer ablation from laser direct imaging called LDI. Excimer laser ablation is a direct one-step subtractive process which do not need any developing agents for structuring. Only a cleaning step is required after the structuring process. LDI needs photo-sensitive material and more linked to classical photo-lithography if the process flows are compared except that a focused laser beam directly writes a pattern on a resist instead using a mask. With this new process the resolution of the BCB has been improved by a factor of around 10x (Figure 13).

This technology is currently under evaluation for other polymers like PI and PBO. First results are similar to BCB.

### Acknowledgement

Many thanks to all persons from Fraunhofer IZM and TU-Berlin involved in this work not being mentioned as co-authors.

Parts of this publication has been published at IEEE-ECTC 2015 in San Diego, USA.

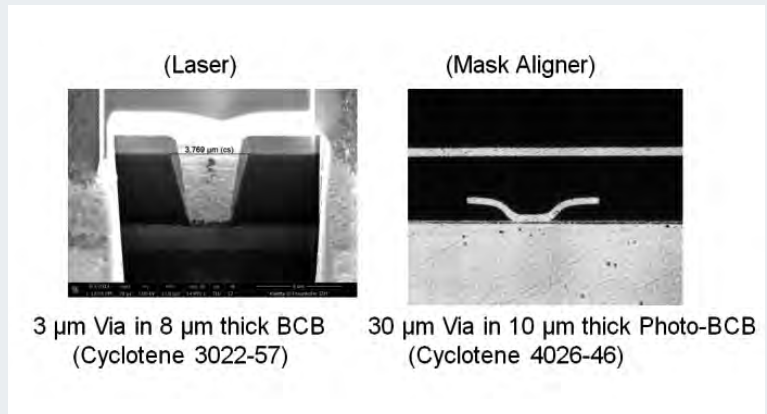


**Figure 13** Comparison of structuring BCB using laser ablation (left) and mask aligner technology (right)

*Michael Töpfer has a M.S. degree in Chemistry and a PhD in Material Science. Since 1994 he is with the Packaging Research Team at TU Berlin and Fraunhofer IZM. In 1997 he became head of a research group. In 2006 he was also a Research Associate Professor of Electrical and Computer Engineering at the University of Utah, Salt Lake City. Since 2015 he is member of the Business Development Team at Fraunhofer IZM. The focus of his work is Wafer-Level Packaging applications with a focus on materials. Michael Töpfer is Senior Member of IEEE-CPMT and has received the European Semi-Award in 2007 for WLP.*



# EVALUATION OF A NOVEL EXPOSURE CONCEPT TO ENHANCE THE CAPABILITIES OF MASK ALIGNER LITHOGRAPHY AT LARGE PROXIMITY GAPS

Frank Windrich Fraunhofer IZM-ASSID, Ringstrasse 12, 01468 Moritzburg, Germany  
Uwe Vogler SUSS MicroOptics SA, Rouges-Terres 61, Hauterive, CH 2068, Switzerland  
Marc Hennemeyer SUSS MicroTec Lithography GmbH, Schleissheimer Strasse 90, 85748 Garching, Germany

In the first instance, mask aligner lithography seems to be quite simple. A geometric pattern on a photomask is transferred into a light-sensitive photoresist by exposing both with ultraviolet light. The mask and the wafer can be in close contact or in a certain proximity gap. Contact prints deliver the best resolution down to the order of the wavelength of the illumination light. The drawback is, that contact between mask and wafer can lead to a contamination or even result in a damage of the mask or the wafer. Contamination deteriorates the best possible contact whereby small features will not be transferred sufficiently into the resist. Therefore in mass production usually a proximity gap is used, which ensures that wafer and mask will not get in contact. Depending on the process and the

substrate, for most applications the gap is between 20 and 200  $\mu\text{m}$ . As the resolution decreases with bigger gaps, the smallest mask feature size must be increased. Enhancement of the capabilities of conventional mask aligners allows cost effective lithography and will meet the strong demand to increase on-chip routing density in the field of 2.5/3D integration and advanced packaging. Here, the novel SUSS MO Exposure Optics was used in combination with diffractive mask patterns to improve the lithographic capabilities. Using Fresnel zone plates (FZP) as diffractive elements on the chromium mask in combination with the novel MO Exposure Optics allows minimizing the structure size at large exposure gaps. This enables the usage of conventional mask aligner technology to structure photosensitive materials for a wider application field, e.g.: structuring inside deep features (like fluid channels, backside through silicon vias), on high topographies or inside Taiko wafer cavities and achieve higher resolution at the same time [1, 2].

The MO Exposure Optics stabilizes the illumination and creates a defined angular spectrum at the mask plane. The optics makes it possible to design and shape this angular spectrum. The principle of the illumination optics is shown in Figure 1. It consists of two microlens-based Köhler integrators. The first integrator decouples the light source from the rest of the system. This means that the optical

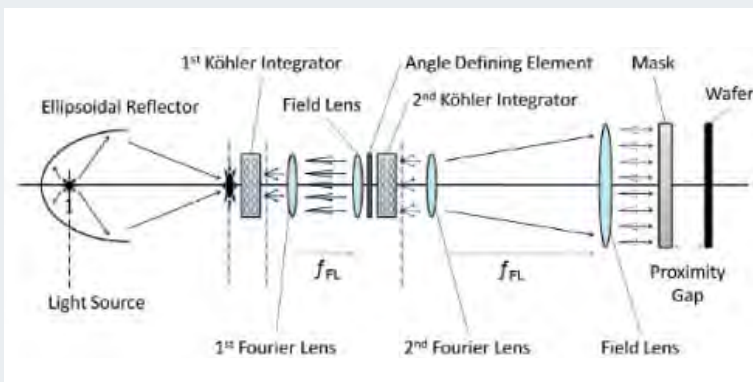
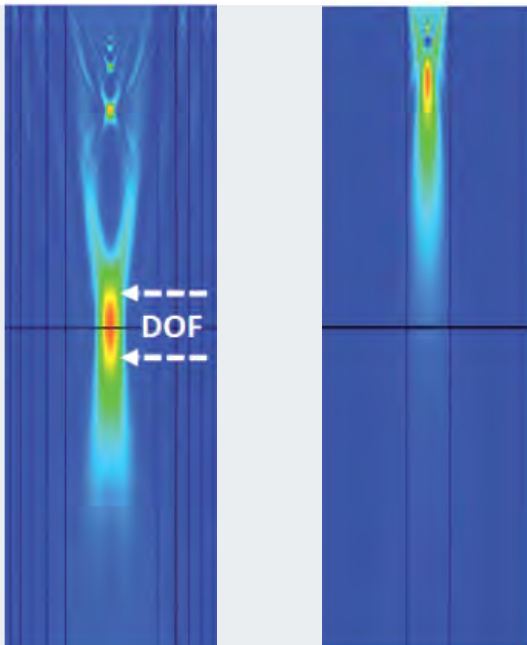


Figure 1 Simplified view of a Mask Aligner illumination system referred to as MO Exposure Optics



performance after this integrator will not be influenced by the small adjustment errors of the light source. In production, this will lead to significantly decreasing adjustment times. The second function of the first integrator is to illuminate the area of the second integrator uniformly. The second microlens integrator illuminates the mask plane. The huge amount of lenses ensures not only a uniform irradiance of radiation but also an absolute stable angular spectrum of the radiation. Because the integrator 2 is illuminated uniform by the first integrator, the radiation is also uniform within the angular spectrum. To define the angular spectrum, apertures can be placed before the integrator 2. They are referred to as Illumination Filter Plates (IFPs)/angle defining element. So it is possible to print with a mask aligner with a never seen stability and a free to design angular spectrum [3].



**Figure 2** Light distribution behind a mask with a Fresnel zone plate and a single circular element in the range of 0µm till 600µm

### DIFFRACTIVE MASK ELEMENTS

The following approach shows the design of diffractive optical elements – so called Fresnel Zone Plates – on the mask. The Fresnel zone plate (FZP) was invented by Augustin-Jean Fresnel. It focuses light at a certain focal length, similar to a refractive lens, but using diffraction. It consists of circular absorbing and transmitting zones. All zones have the same area. The most economical way to realize a FZP for mask aligner lithography is to use transparent glass and opaque chrome zones that alternate. For a certain focal length  $f$  the radii of the ring-shaped zones  $r_n$  are given by the relation

$$r_n = \sqrt{n\lambda f + \frac{n^2 \lambda^2}{4}}$$

where  $n$  is the order of the zone and  $\lambda$  is the wavelength. As can be seen from the above formula, for best results single line exposures have to be performed. Since the mask aligner has its peak intensity at the 365nm-wavelength (i-line) and also many photosensitive materials are i-line sensitive,

the following simulations and experiments were all made at i-line wavelength. In Figure 2 the difference in the mode of function between a FZP and a conventional mask structure is shown. For a conventional structure the pattern shape is casted 1 by 1 on the image plane directly under the mask. The bigger the distance of the image plane from the mask gets the more the shape gets deformed by diffraction and the more light is scattered out of the area under the opening. Caused by this the contrast gets too small to transfer the structure 1 by 1 into the resist at a certain proximity gap.

In contrast, the FZP produces a focal point like a refractive lens at a certain focal distance, whereas smaller gaps lead to images, which will be not usable. The focal distance of the FZP is defined by its geometrical layout. When keeping the number of zones and therefore the numerical aperture of the FZP constant, the focus spot size is proportional to the chosen focal distance. Identical to a refractive lens, the distance range in which the distribution of irradiance is stable, defines the

depth of focus (DOF). By increasing the number of rings, it is possible to achieve smaller resolutions at the same focal distance, but the size of the DOF will decrease. FZP are originally designed for illumination with totally collimated light. By engineering the collimation angle of the incident light it is possible to tune the size of the focus point to the desired spot size. This tuning capability is of course limited by the maximum collimation angles available in the optics.

In Figure 3, you can see the cross section through the focal plane of FZPs for certain proximity gaps. All FZPs consisted of three transparent Fresnel zones.

### EXPERIMENTAL

In order to demonstrate the lithographic performance of such FZP structures a 14" sodalime glass mask with 8 different FZP designs was created. Examples of the FZP design are shown in Figure 4.

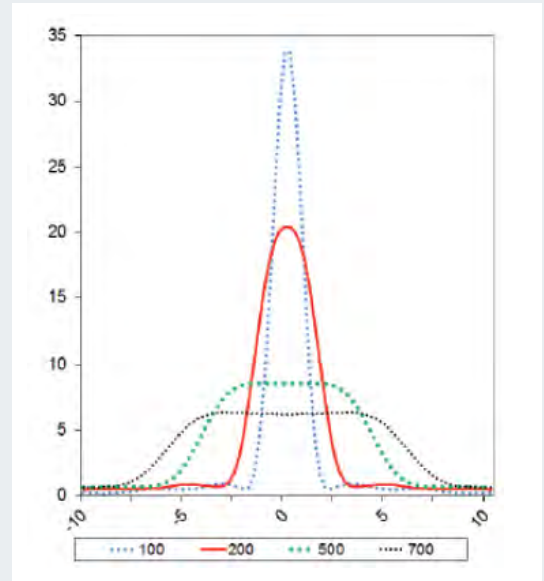


**Figure 3** The size of the focal point depends on the design of the FZP, which is defined through gap and number of rings. The graph shows the cross section of the focal point for different gaps and FZPs with 3 rings

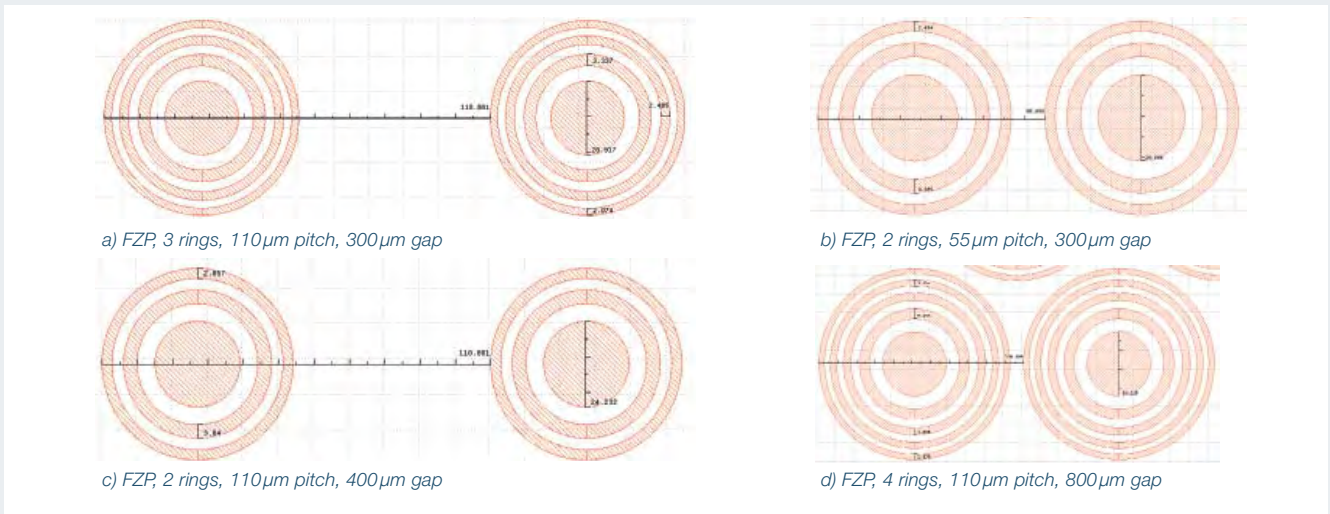


**Figure 4** Overview of 4 FZP designs with 55µm and 110µm pitch and variable ring number

Each FZP is designed with a specific number of Fresnel rings and optimized to a theoretical proximity gap, equivalent to the selected focal distance. The pitch was either 55µm or 110µm. The number

of rings is limited by the desired pitch. A higher ring number leads to partial overlapped FZP structures, when the pitch is getting too small. This will affect the focus properties of the FZP.

Table 1 gives a detailed overview of all 8 FZP designs on the test mask. The CD tolerance for generating the chromium mask requires low writing tolerances. The FZP mask was manufactured with a CD tolerance of  $\pm 0.25\mu\text{m}$ . The minimal feature size for the smallest ring was  $1.4\mu\text{m}$ . 2 testchips with  $20\times 20\text{mm}$  size were created and divided into 4 sub-dies by  $10\times 10\text{mm}$  area each. Each sub-die corresponds to one FZP design, respectively. These two testchips were alternatively repeated over the entire 14" glass mask to cover the  $300\text{mm}$  substrate.

The testmask was used to investigate the lithographic printing performance using two different photoresist materials. A standard positive tone AZ9260 resist with  $10\mu\text{m}$  film thickness was used as one material. The second material was a chemical amplified resist used usually for bumping and  $\mu\text{Pillar}$  applications. Therefore, the thick film positive tone photoresist AZ IPS528 was coated in a thickness range of  $50\mu\text{m}$ . The experiments were done at Fraunhofer IZM-ASSID on  $300\text{mm}$  silicon substrates primed with HMDS using a SUSS MA300 mask aligner. As Illumination Filter Plate (IFP) an in diameter variable circle aperture – an iris diaphragm – was used in the optics setup to adjust the UV light power and the maximum collimation angle.

Beginning with the FZP designed for  $300\mu\text{m}$  proximity gap and the  $10\mu\text{m}$  thick AZ9260 photoresist the impact of the IFP diameter was studied at constant exposure times ( $t=40\text{s}$ ). The proximity gap was adjusted to  $300\mu\text{m}$  and the IFP diameter was varied to adjust the light power between  $0.8\text{mW}/\text{cm}^2$  ( $\sim 10\text{mm}$  IFP diameter) to  $15.2\text{mW}/\text{cm}^2$  ( $\sim 70\text{mm}$  IFP diameter). The SEM X-section results are shown in Figure 5 exemplarily. It is clearly shown that the FZP gives best focus properties, when the iris was adjusted to minimal diameter. A bottom CD in the  $5\mu\text{m}$  range is achievable with an impressive steep resist profile at this rather high proximity gap. An increase in the IFP diameter (higher power) leads to bigger CD values due to an

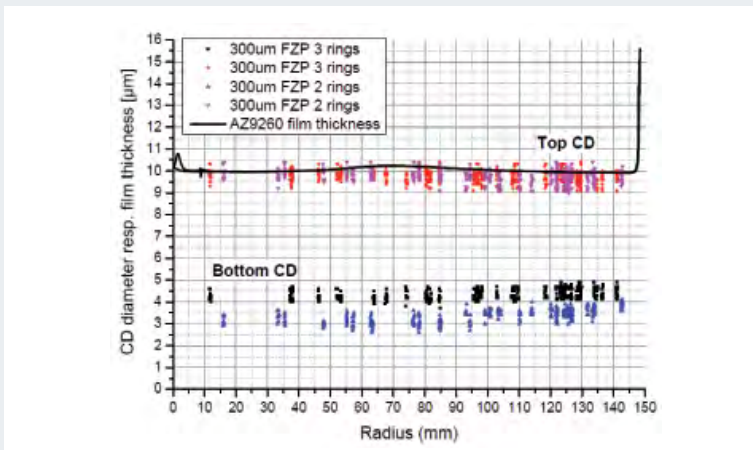
Desired proximity gap [ $\mu\text{m}$ ]	No. of rings	FZP Diameter [ $\mu\text{m}$ ]	Inner ring CD [ $\mu\text{m}$ ]	Smallest ring CD [ $\mu\text{m}$ ]	Used for test chip No.
Gap 100	2	26,76	12,09	1,42	(1) 55 $\mu\text{m}$ Pitch
Gap 200	2	37,8	17,09	2	(1) 55 $\mu\text{m}$ Pitch
Gap 300	2	46,24	20,94	2,44	(1) 55 $\mu\text{m}$ Pitch
Gap 300	3	54,76	20,94	2,04	(1) 110 $\mu\text{m}$ Pitch
Gap 400	2	53,4	24,17	2,82	(2) 110 $\mu\text{m}$ Pitch
Gap 500	4	80,08	27,02	2,3	(2) 110 $\mu\text{m}$ Pitch
Gap 800	4	101,28	34,18	2,9	(2) 110 $\mu\text{m}$ Pitch
Gap 1000	4	113,24	38,22	3,42	(2) 110 $\mu\text{m}$ Pitch

Table 1 Summary of the Fresnel zone plate design



Figure 5 SEM images for  $10\mu\text{m}$  thick AZ9260 at  $300\mu\text{m}$  proximity gap, 40s exposure time,  $300\mu\text{m}$  gap FZP design (3 rings)

increase of the spot diameter and due to higher dose. When the light power is exceeding a certain value, then the focus properties of the FZP will be affected negatively and a stronger degradation in the upper resist area is observed. The higher light power leads to an over-exposed process regime, which can be compensated by a reduction in exposure time. It means conversely, that at a constant low light power the CD parameter can be adjusted by the exposure time quite accurately within sub- $\mu\text{m}$  tolerances.



**Figure 6** Top/down microscopy CD uniformity measurements on 300mm wafer for 10 $\mu\text{m}$  AZ9260 at 300 $\mu\text{m}$  proximity gap exposed with 2 resp. 3 rings FZP (0.6mW/cm<sup>2</sup>, 40s exposure time)

To investigate the lithographic repeatability over the entire 300mm wafer substrate CD uniformity (CDU) measurements were done by optical top/down microscopy for both 300 $\mu\text{m}$  FZP designs (2 & 3 rings design). In Figure 6 the results of the top and bottom CD measurements in dependence of the wafer radius are shown. Comparing the bottom CD values for the 2 resp. 3 ring FZP design, it can be seen that the 3 rings FZP design leads to a bigger bottom CD value than 2 rings FZP design. The 3 rings FZP focus more UV energy per area and generates therefore a wider CD value. The top CD parameter is more or less independently from the number of Fresnel rings. Comparing the coating uniformity (black line) with the CD values,

it can be seen that the optics is quite insensitive to resist thickness variations. It should be noted that the measured standard deviation is in the range of 0.3 $\mu\text{m}$ , which is within the pixel accuracy of the used optical microscope. The “real” CDU should be therefore more accurate than the measured tolerances, which can be only quantified by CD-SEM metrology measurements. Therefore, it can be concluded, that this exposure concept yields to very accurate CDU tolerances. Changing the proximity gap together with the FZP design transfers the general lithographic concept to other gap ranges and other feature sizes. In Figure 7 two examples at 1000 $\mu\text{m}$  proximity gap are shown. The higher gap and the different FZP design leads to a bigger CD.



**Figure 7** SEM images for 10 $\mu\text{m}$  thick AZ9260 at 1000 $\mu\text{m}$  proximity gap, 60s exposure time, 1000 $\mu\text{m}$  gap FZP design (4 rings)

Evaluation of the exposure concept for the positive tone thick film chemical amplified photoresist AZ IPS528 with 50 $\mu\text{m}$  target thickness is discussed secondly. SEM results with 300 $\mu\text{m}$  proximity gap at a constant exposure time of 190s and variation in the UV light power are shown in Figure 8. Due to the thick resist film of  $\sim 50\mu\text{m}$  the FZP designed for 400 $\mu\text{m}$  gap gives good focus properties in this example. The resist profile and CD diameter depends significantly on the used light power and aperture diameter. With increased light power the bottom CD changes between  $\sim 14\mu\text{m} - 60\mu\text{m}$ . When the light power exceeds a certain value, then the resist is heavily degraded. A rather good profile is achieved with  $3.9\text{mW}/\text{cm}^2$ . This exposure setting can be applied for instance to a 55 $\mu\text{m}$  Cu-pillar interconnect with aspect ratio 1:1 at 110 $\mu\text{m}$  pitch inside a 300 $\mu\text{m}$  deep cavity.

To get a feeling for the impact of the proximity gap for a certain FZP design (here the 400 $\mu\text{m}$  gap, 2 ring FZP design was used) an evaluation was done with constant exposure settings (90s,  $4.1\text{mW}/\text{cm}^2$ ) and varied gap setting. The SEM results are shown in Figure 9. At low gap settings (100–200 $\mu\text{m}$ ) the FZP focus point is rather out of the resist plane. This leads to bottom CD values roughly comparable to FZP diameter ( $\sim 53\mu\text{m}$ ). At 100 $\mu\text{m}$  proximity an interesting T-shaped resist profile is generated, which can be used to electroplate T-shaped  $\mu\text{Pillar}$  interconnect structures with steep profiles. When the proximity gap is increased to 500 $\mu\text{m}$  the FZP focus more light energy to a smaller exposure area, which leads to a reduction in the bottom CD. The trade-off is that the top CD is not reduced in the same way. Therefore the resist profile is less steep. A further increase of the proximity gap to 700 $\mu\text{m}$  increases the CD values with comparable resist profiles.

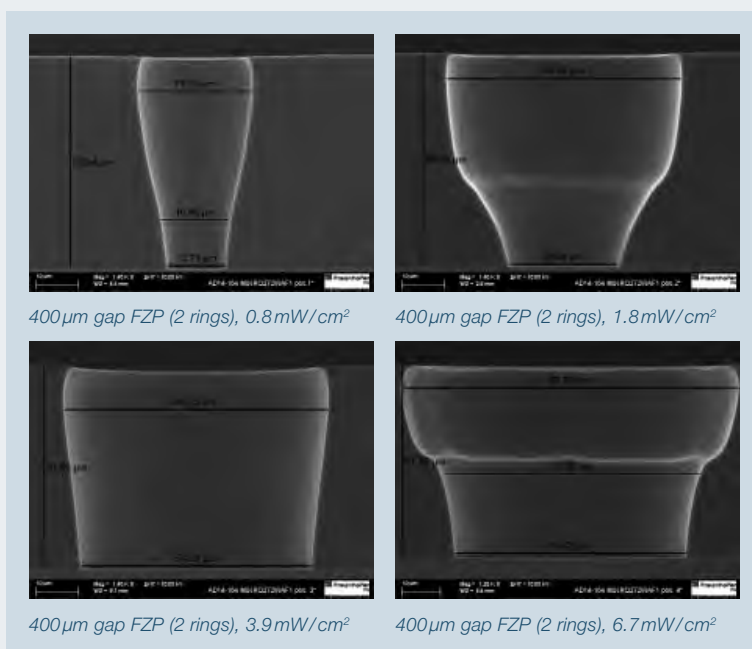


Figure 8 SEM images for 50 $\mu\text{m}$  thick AZ IPS528 at 300 $\mu\text{m}$  proximity gap, 190s exposure time, 400 $\mu\text{m}$  gap FZP design (2 rings)

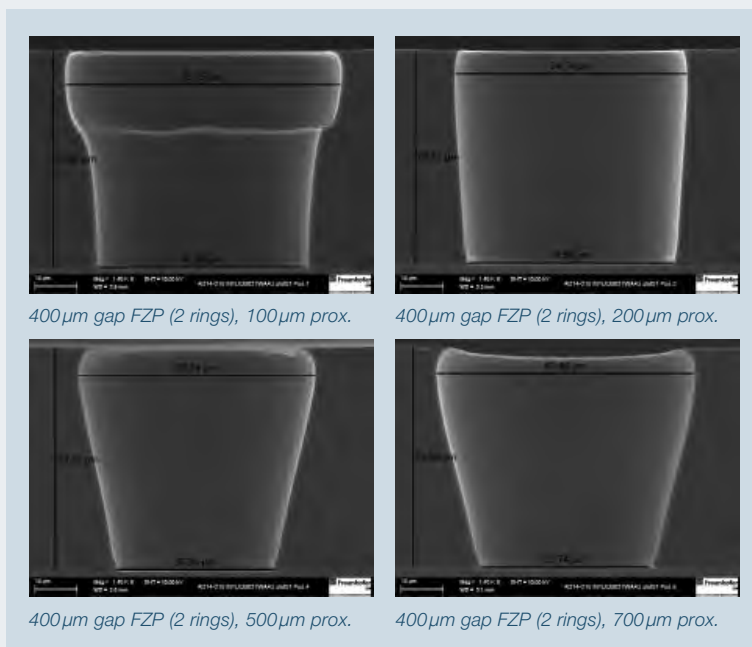


Figure 9 SEM images for 50 $\mu\text{m}$  thick AZ IPS528 at varied proximity gap between 100 to 700 $\mu\text{m}$ , 90s exposure time, power  $4.1\text{mW}/\text{cm}^2$ , 400 $\mu\text{m}$  gap FZP design (2 rings)

## CONCLUSION

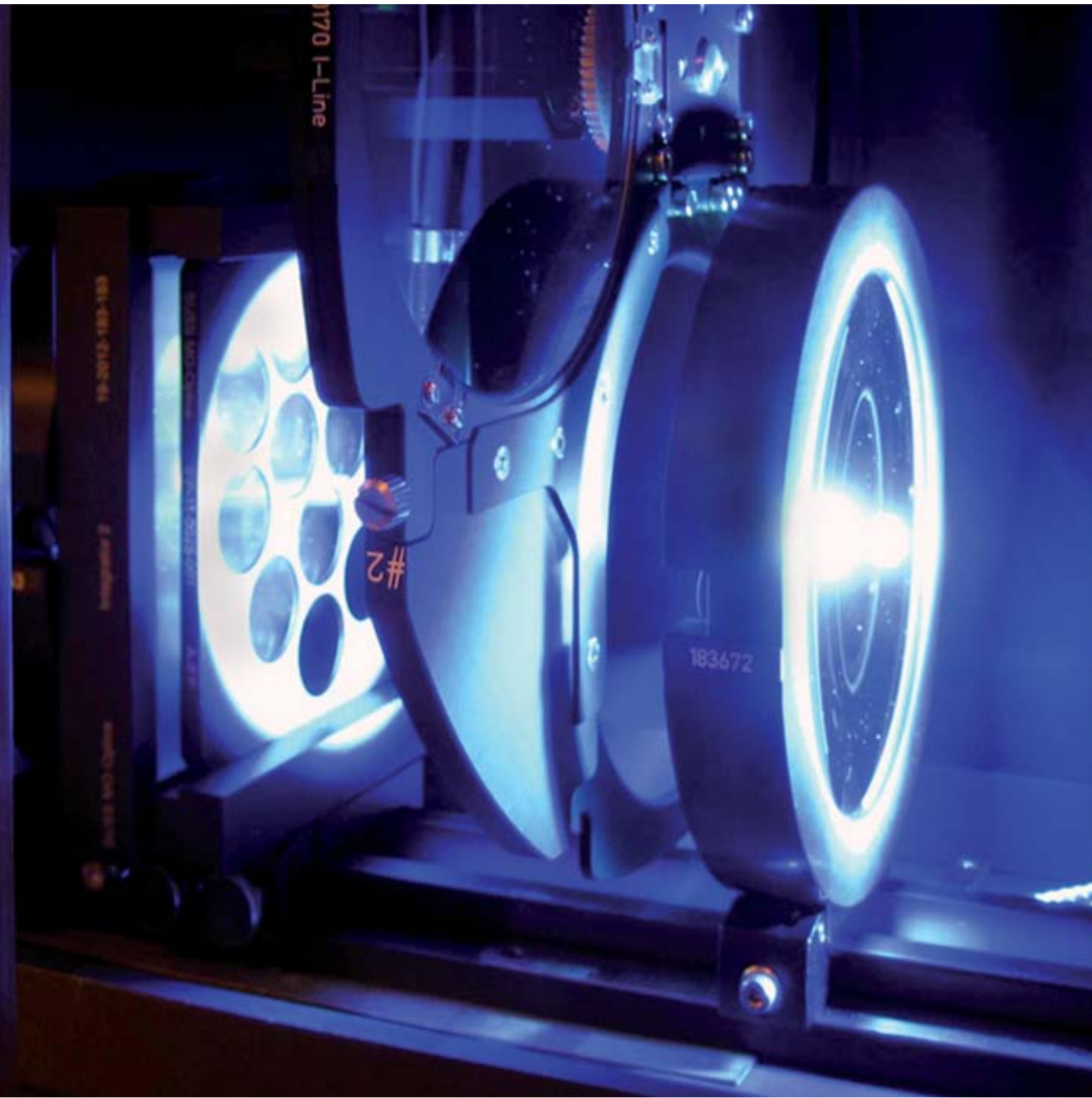
The exemplary discussed FZP concept together with the MO Exposure Optics allows to generate useful resist structures with respect to resolution and resist profile at rather high proximity gaps. This concept allows to transfer well known projection lithography principles to cost-effective mask aligner lithography. This can be applied to structure polymer or oxide openings inside deep cavities, on Taiko wafer or for MEMS applications. Together with unique chemical amplified thick film photoresist chemistry  $\mu$ Pillar interconnect structures can be formed inside deep cavities or Taiko wafers as well. Also non-conventional  $\mu$ Pillar shapes (T-shaped) can be generated with this exposure principle. This opens interesting opportunities for 3D integration packaging concepts.

## References

- <sup>[1]</sup> Vogler, U., Windrich, F., et. al., "Cost-effective lithography for TSV-structures," in *Electronic Components and Technology Conference (ECTC)*, 2011 IEEE 61st, pp.1407-1411, doi: 10.1109/ECTC.2011.5898696
- <sup>[2]</sup> Spiller, S., Hennemeyer, M., et. al., "Processing of ultrathin 300 mm wafers with carrierless technology," in *Electronic Components and Technology Conference (ECTC)*, 2011 IEEE 61st, pp.984-988, doi: 10.1109/ECTC.2011.5898629
- <sup>[3]</sup> R. Voelkel, U. Vogler, et. al., "Advanced mask aligner lithography: new illumination system," *Opt. Express* 18, 20968-20978 (2010), doi: 10.1364/OE.18.020968

*Frank Windrich graduated in Chemical Engineering from the University of Applied Science Dresden in 2003 and he holds a M. Sc. degree in Chemistry from the Technical University Dresden in 2013. He was with Fuba Printed Circuits from 2003-2009 and worked as process engineer in the PCB industry responsible for all lithography processes (inner layer, outer layer, soldermask). He joined Fraunhofer IZM-ASSID in 2010 and is working as a Scientist responsible for photoresist and polymer dielectric lithography processes in the field of Wafer-Level Packaging and 2.5D/3D Integration. Frank's current research interests are mainly focused on low-temperature cure thin film polymer dielectrics and thick-film photoresist materials for high density interconnects ( $\mu$ Pillars).*





# LOW-TEMPERATURE HERMETIC SEAL BONDING FOR WAFER-LEVEL MEMS PACKAGING USING SUB-MICRON GOLD PARTICLES WITH STENCIL PRINTING PATTERNING

**Hiroyuki Ishida** Manager, Bonder Division, SUSS MicroTec K.K., Japan  
**Toshinori Ogashiwa** Research Associate, Technology Development Section, Tanaka Kikinzoku Kogyo K.K.

## INTRODUCTION

Wafer-level hermetic packaging with electrical interconnection is necessary for the integration of MEMS and LSI devices, and low-temperature metal bonding such as AuIn, AuSn, Cu-Cu and Au-Au has been increasingly attractive [1]. Among those bonding methods, Au-Au thermo-compression bonding is a promising candidate, which has advantages of no concern of surface oxidation and simple process control [2]. In order to compensate the surface roughness after MEMS processing

which could degrade the hermetic properties, surface compliant Au-Au bonding using sub-micron Au particles has been developed combined with the patterning method using photolithography process [3]. In this study, a rim structure was adopted to define a narrow bond line width for reducing the bonding force within the range of commercial wafer bonders (e.g. the maximum force of 100kN for 200mm wafers) and conventional stencil printing was employed to lower the patterning process cost.

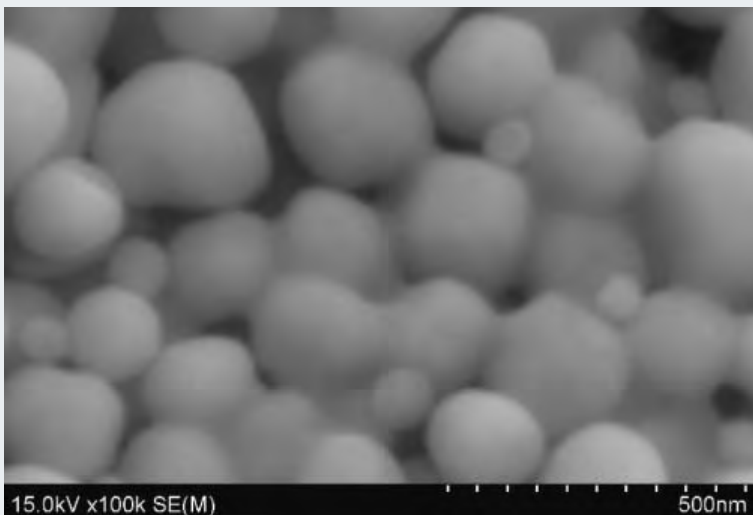


**Figure 1** SEM image of sub-micron Au particles after heating at 200 °C for 30 minutes in air

## EXPERIMENTAL PROCEDURE

### Materials preparation

99.95wt% purity, spherical sub-micron-size Au particles were prepared by a wet chemical processing method by mixing chloroauric acid solution with a reducing agent. The particle size distribution was in the range of 0.2-0.5 $\mu$ m in diameter (the mean diameter of 0.3 $\mu$ m), which could exhibit a fine size effect to activate the Au-Au interdiffusion. Figure 1 shows the sintering behavior of sub-micron Au particles being connected each other at 200 °C for 5 minutes in air without any compression force.

### Sample preparation and wafer bonding

The wafer-level hermetic sealing process using a rim structure covered with sub-micron Au particles is shown in Figure 2. A diaphragm wafer was prepared to evaluate the hermetic properties, formed by anisotropic wet etching using a TMAH (tetramethylammonium hydroxide) solution. On the other hand, to fabricate a rim wafer, 10 $\mu\text{m}$ -tall/10 $\mu\text{m}$ -wide rim structures were formed on a  $\phi 100\text{mm}$  oxidized Si wafer by Si deep-RIE (PEGASUS, SPP Co., Ltd.), and Au/Pt/Cr (0.2/0.03/0.03 $\mu\text{m}$ -thick, respectively) metal layer were deposited by sputtering (Figure 2(a)). A customized Au paste (AuRoFUSE™, Tanaka Kikinzo-ku Kogyo K.K.) was deposited to cover rims (Figure 2(b)) by conventional stencil printing method using a high-precision screen printer (LS-25TVA, Newlong Seimitsu Kogyo Co., Ltd., Figure 3) together with a suspended Ni-metal mask (Taiyo Yuden Chemical Technology Co., Ltd). After aligning the rim wafer and the metal mask on the screen printer, printing was completed within 10 seconds per wafer. As shown in Figure 4, successful wafer-level printing on 200mm wafers has already been demonstrated.

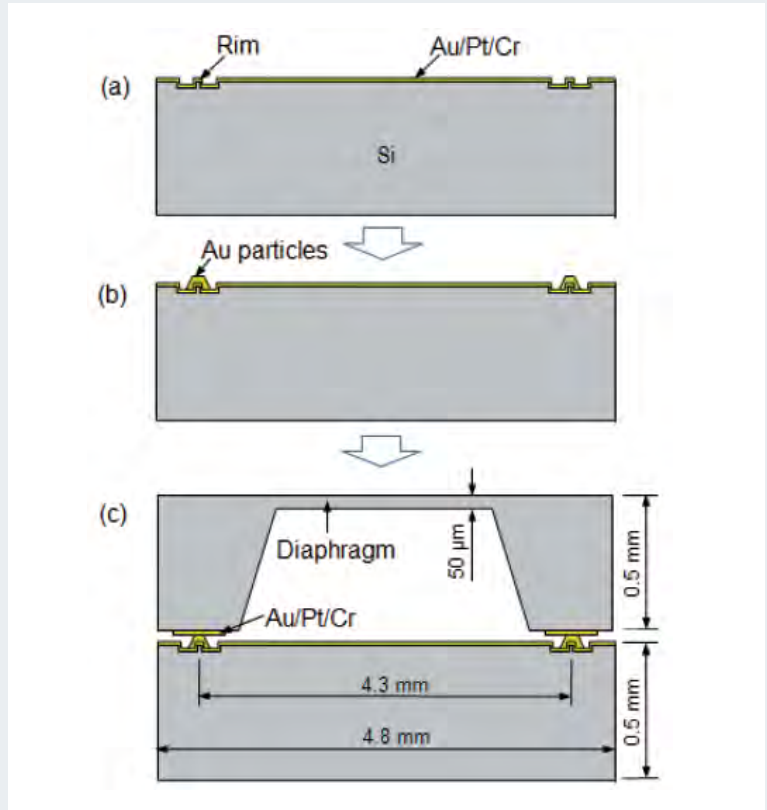


**Figure 2** Wafer-level fabrication process using sub-micron Au particles. (a) Formation of a rim structure by dry etching process and deposition of metal layers, (b) stencil printing with sub-micron Au particles (AuRoFUSE™) sintered at 200 °C, and (c) thermo-compression bonding at 200 °C

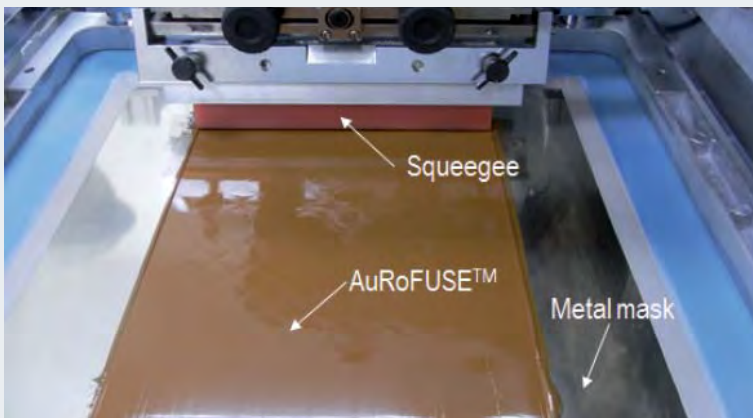


**Figure 3** Wafer-level stencil printing on a precision screen printer with AuRoFUSE™

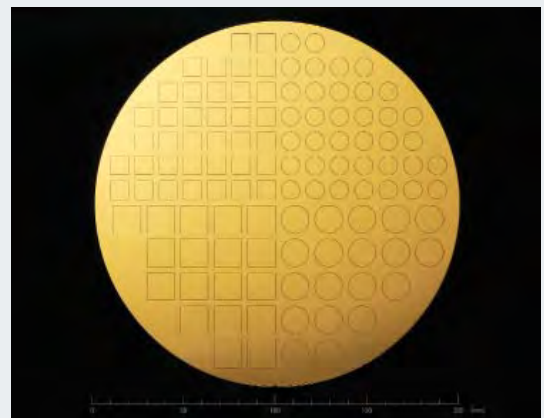


**Figure 4** An example of a 200mm wafer with test patterns of sub-micron Au particles formed by stencil printing

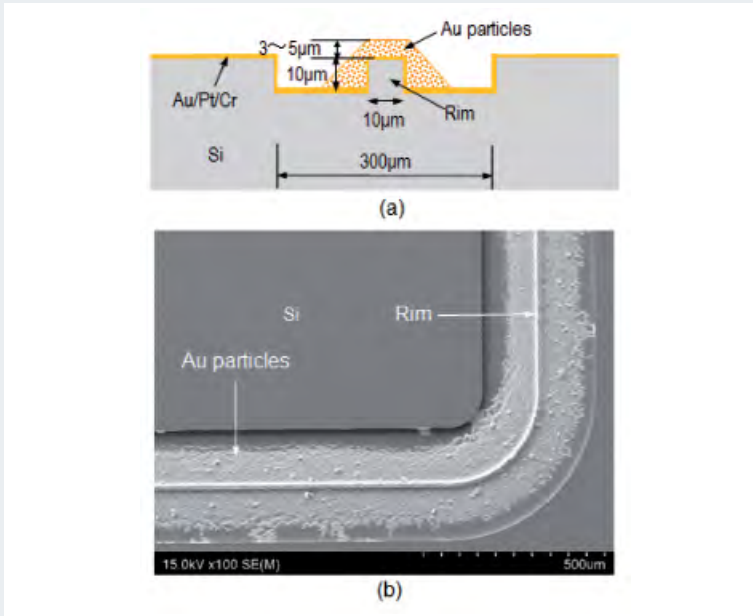


**Figure 5** (a) Schematic drawing of the cross-sectional view of the rim structure covered with sintered Au particles, and (b) SEM image of the rim on a Si wafer

Figure 5 shows (a) a schematic illustration of the cross-section rim structure and (b) a SEM image of the rim covered with sintered sub-micron Au particles. The thickness of sintered Au particles on top of the rim was in a range of 3-5µm over the entire surface of 100mm wafers. Following the annealing of the rim wafer at 200°C for 2 hours in 4% H<sub>2</sub>-Ar gas flow, precise alignment was performed between the rim wafer and the diaphragm wafer on the bond aligner (SUSS BA8). Then, the aligned wafer pair was bonded on the wafer bonder (SUSS SB8e) at a temperature of 200°C for 30 minutes with an applied pressure of 200MPa to fabricate the structure as shown in Figure 2(c). The vacuum level of the bond chamber was maintained at 10<sup>-3</sup>Pa during the thermo-compression bonding. The bonded wafer pair was diced into single chips for evaluation of the bond strength and hermetic properties.

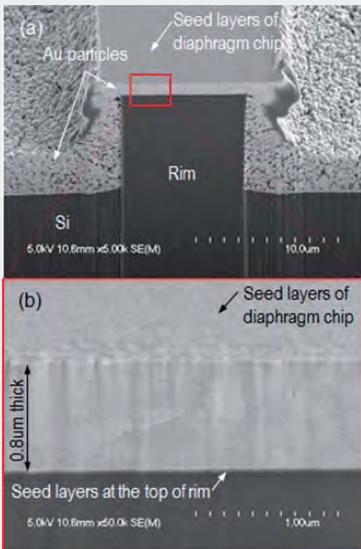


**Figure 6** Cross-sectional FIB-SEM images of the rim joint after tearing off the chip. (a) A complete picture of the rim joint, and (b) a higher magnification of the recrystallized structure of sintered Au particles and metal layers

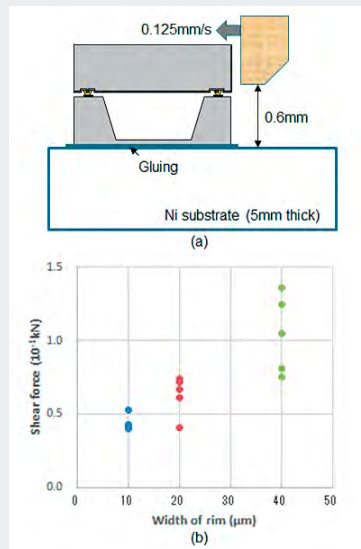


**Figure 7** (a) Schematic illustration of die shear test to measure the die shear strength of the test chip, and (b) a relationship between the die shear strength and the rim width

## RESULTS AND DISCUSSIONS

### Bonding performance

Figure 6 shows a cross-sectional FIB-SEM image of the rim joint after tearing off the bonded chip. The joint was separated at the boundary of silicon surface of the diaphragm wafer and its metal layer of Au/Pt/Cr. The metal layer of the diaphragm wafer attached closely to the densified structure of Au particles. The sintered sub-micron Au particles layer measured 3-5 µm-thick, which was compressed on the rim structure down to the thickness of 0.6µm during the bonding. The sub-micron Au particles recrystallized and densified into bulk structure to realize hermetic interface.

As shown in Figure 7, the die share strength of a singulated test chip was measured by a bond-tester (series-4000, Dage) to be an average value of 44 N.

Assuming a bond pressure of 150 MPa for achieving hermetic sealing by sub-micron Au particles bonding, Table 1 summarizes the calculated necessary bond force for each wafer/chip size with varying the seal line width. In calculation, the following parameters were assumed: edge exclusion = 5 mm, dicing street width = 0.2 mm. The bond force values were classified into three categories such as “<20kN”, “20-100kN” and “>100kN”, where 20kN and 100kN is the maximum force of SUSS SB8 Gen2 and XB8 wafer bonder, respectively. It is estimated from the table that hermetic bonding with sub-micron Au particles can be realized by commercially available wafer bonders even for 200mm wafers with a small chip size of 2 mm x 2 mm.

**Calculation of Necessary Bond Force (kN)**

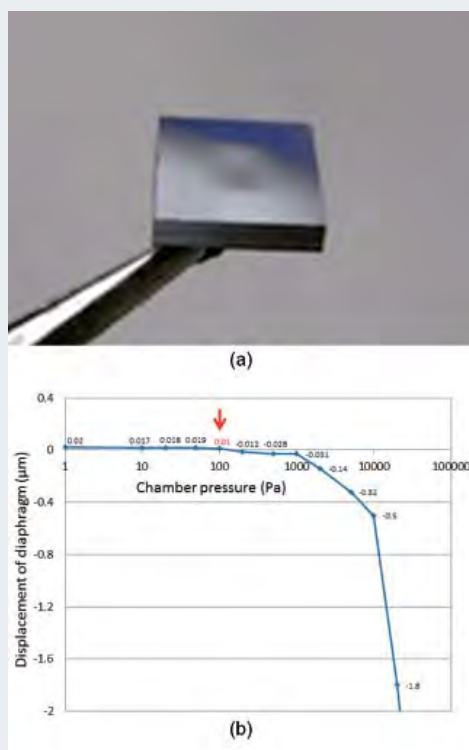
Wafer Size (mm)	Chip Size (mm-sq.)	Seal Line Width (μm)			
		10	20	30	50
100	1	30	60	88	143
	2	17	34	51	83
	3	12	24	35	58
	4	9	18	27	45
	5	7	15	22	36
150	1	73	144	213	346
	2	41	82	123	202
	3	29	57	85	141
	4	22	44	65	108
	5	18	35	53	88
200	1	134	265	393	638
	2	76	151	226	372
	3	53	105	157	260
	4	40	80	120	199
	5	33	65	97	162

< 20 kN  
 20 - 100 kN  
 > 100 kN

**Hermetic sealing performance**

Figure 8(a) shows a picture of a test chip exhibiting a concave deflection of the 50 μm-thick diaphragm under the atmospheric pressure. The deflection measured 5 μm in the ambient, indicating a vacuum encapsulation inside the sealed cavity. In order to estimate the encapsulated pressure inside the cavity, the deflection of the diaphragm in vacuum was precisely measured by an optical surface profiler (MSA-500, Polytec) with controlling the chamber pressure. The concave/convex deflection of the diaphragm against the chamber pressure is shown in Figure 8(b). From the results, the encapsulated pressure in the sealed cavity is estimated at 100Pa by seeing the chamber pressure when the diaphragm becomes flat. The hermetic performance of the sub-micron Au particles sealing was evaluated by helium fine leak test (MUH series, Fukuda Co., Ltd.). The maximum He leak rate of the test chip was estimated in the range of 10<sup>-14</sup>Pa·m<sup>3</sup>/s, which is sufficient for most of the MEMS applications.

**Table 1** The calculated necessary bond force for various wafer and chip size with varying the seal line width, with assuming the bond pressure of 150 MPa. In calculation, edge exclusion and dicing street width was assumed as 5 mm and 0.2 mm, respectively



## CONCLUSION

Low-temperature Au-Au hermetic seal bonding has been successfully demonstrated employing a rim structure on a  $\phi$ 100mm Si wafer covered with sub-micron Au particles. The sintered Au particles on the rim structure were densified by the thermo-compression bonding to realize the hermetic sealing. The summaries of this study are as follows:

- 1) The layer of sub-micron Au particles with the thickness of 3-5  $\mu\text{m}$  was deposited on the 10 $\mu\text{m}$ -tall/10 $\mu\text{m}$ -wide rim structure by a conventional stencil printing
- 2) The hermetic sealing by the sintered sub-micron Au particles on the rim structure was successfully achieved by the thermo-compression bonding with 200MPa at 200 $^{\circ}\text{C}$
- 3) An excellent vacuum hermetic sealing was confirmed; the encapsulation pressure was measured to be 100Pa, and the maximum leak rate was estimated in a range of  $10^{-14}\text{Pa}\cdot\text{m}^3/\text{s}$  (He)

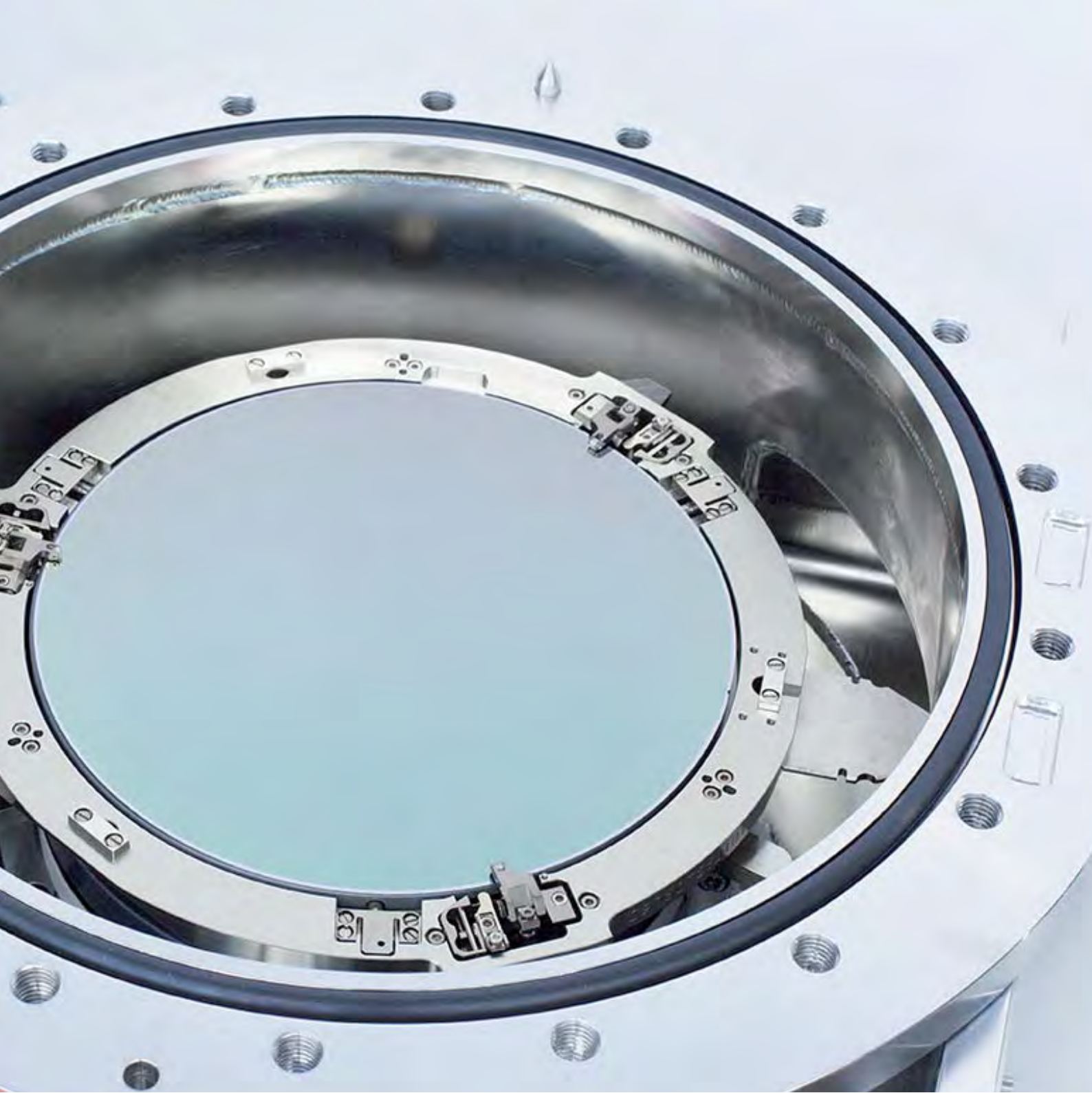
This bonding technique can be expected for further development towards production use for wafer-level hermetic sealing of MEMS packaging.

## References

- <sup>[1]</sup> C.S. Tan, J. Fan, D. F. Lim, G. Y. Chong and K. H. Li, *J. Micromech. Microeng.*, 21, p.075006 (2011)
- <sup>[2]</sup> N. Malik, H. R. Tofteberg, E. Poppe, T. G. Finstad, and K. Schjølberg-Henriksenb, "Environmental Stress Testing of Wafer-Level Au-Au Thermocompression Bonds Realized at Low Temperature Strength and Hermeticity ", *J. Solid State Sci. Technol.*, 4 (7), pp 236-241 (2015)
- <sup>[3]</sup> H. Ishida, T. Ogashiwa, T. Yazaki, T. Ikoma, T. Nishimori, H. Kusamori, and J. Mizuno, "Low-Temperature Wafer Bonding for MEMS Hermetic Packaging Using Sub-micron Au Particles," *Transactions on The Japan Institute of Electronics Packaging*, 3 (1), pp.62-67 (2010)

*Hiroyuki Ishida joined SUSS MicroTec KK in 2006 as a senior application engineer and then worked as a business development manager in Japan mainly focused on wafer bonding applications. He is now the manager of Bonder Division - Japan, being responsible in all activities related to permanent bonding and temporary bonding / debonding products. He is also taking care of the collaboration with Japanese material suppliers for temporary bonding applications. He received his B.E. and M.E. in Electronic Engineering from Tohoku University.*





# EXCIMER LASER ABLATION – A NOVEL PATTERNING SOLUTION FOR ADVANCED PACKAGING

**Ralph Zoberbier** SUSS MicroTec Lithography GmbH, Schleissheimer Str. 90, 85748 Garching, Germany  
**Habib Hichri** SUSS MicroTec Photonic Systems Inc. 220 Klug Circle, Corona, CA 92880-5409, USA

## INTRODUCTION

Photolithography has long been the key patterning technology for structuring organic materials used in advanced packaging applications like flip-chip wafer bumping, electroplated gold, solder bumps, copper pillar technologies and redistribution layers. Nowadays, proximity exposure technologies (mask aligner) or projection lithography (step and repeat or projection scanning) are the typical choices to create the features. The continuous trend of the miniaturization, increasing performance and mobility of electronic devices drive the requirements of the chip itself but also its package type. More and more, the photolithography process is becoming the limiting factor to develop cost effective and innovative package designs that meet the market requirements.

In response to this industry challenge excimer laser ablation has been adapted to the semiconductor packaging industry and is now available as a disruptive patterning technology. This complementary technology offers the promise of further reductions in manufacturing costs as well as enhancements in chip or package performance. This paper provides a comprehensive overview of the excimer laser ablation technology, and its level of maturity. It discusses the recent technology developments and corresponding debris cleaning solutions from a technical perspective.

## EXCIMER LASER ABLATION TECHNOLOGY

Excimer laser ablation is a dry patterning process, breaking a material's molecular structure and directly etching the desired circuit pattern to clearly defined depths on the substrate, with minimal heat affected zone (HAZ). This patterning technology uses the advantage of the excimer laser source to emit high energy pulses at short wavelengths. The short wavelength output on the one hand enables the imaging of small features but also supports absorption in many different materials. Depending on the material each laser pulse removes a certain amount of material. The ablation rates are in the 100nm range for polymers and dielectrics that are typically used as passivation layers in the semiconductor backend applications. The technology allows for the fine tuning of sidewall angles of the created features by adjustments of the laser fluence.

To address the latest requirements of the advanced packaging industry, such as the creation of feature sizes in the range of 2-5µm combined with an overlay accuracy of less than 1-2µm, requires a careful selection of the right equipment platform. Thus, excimer laser ablation is available on a step and repeat platform which is a very common platform for high-end lithography applications.

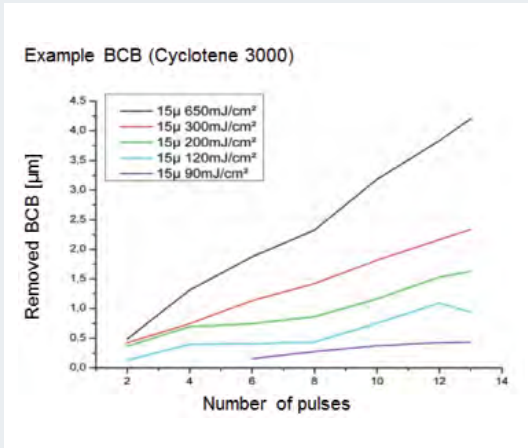


Figure 1 Overview of ablation rates in BCB (Cyclotene 3000) based on different fluence level [1]

The combination of the excimer laser source and reduction projection optics enables the capability of high resolution imaging with sufficient fluence output to pattern a large area at once to achieve the highest possible throughput. A reticle defines the pattern to be ablated, providing a high degree of pattern fidelity and placement accuracy. In addition the demagnification of the optical systems generates a high energy level on the substrate side while the illumination of the reticle itself is still in an acceptable range to avoid mask damage. Typical reticles on an excimer ablation stepper are based on chrome or aluminum on quartz or dielectric masks.

The illumination setup of the optics is typically customized based on the application requirements to ensure a match of fluence requirements based on the material to be ablated, coupled with required ablation field size that is defined by die or package sizes.

As mentioned above, the technology is similar to traditional UV steppers, however, instead of exposing a photo sensitive material, the material is etched directly without the need neither for a

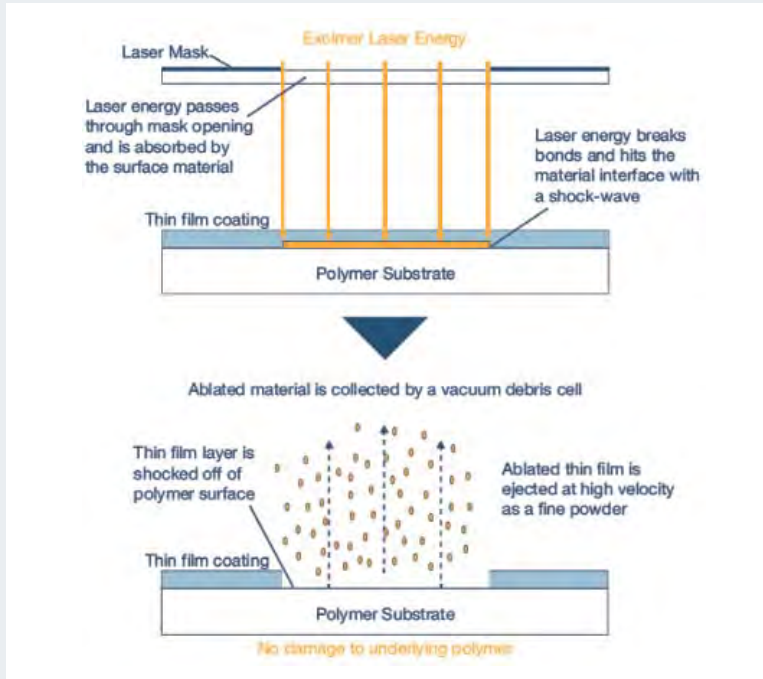


Figure 2 Schematic illustrations of excimer laser ablation of thin films from a polymer substrate in a dry one-step etch process

photoresist nor the post-develop and etch processes that accompany a photolithography process. Excimer laser ablation is suitable for ablating a wide variety of polymeric materials, thin metals (<600 nm), epoxies, EMC's, nitrides and other materials.

Excimer laser ablation technology enables the industry to use new materials that offer better mechanical properties required by the advanced semiconductor packaging industry (low CTE and residual stress, and thermally stable).

A major concern for the adoption of excimer laser ablation is effective and cost efficient debris cleaning. The laser ablation process itself creates some debris that needs to be removed. Latest developments show the availability of efficient post ablation cleaning solutions.

## ADVANCED PACKAGING APPLICATIONS AND TECHNOLOGY TRENDS

Today a wide variety of advanced packaging technologies exists to meet the requirements of the semiconductor industry. The leading advanced packages, including chip-on-chip, wafer-level packages, chip-on-chip stacking, embedded IC, all have a need to structure thin substrates, redistribution layers and other package components like high resolution vias. The consumers constant push for higher functionality on smaller and thinner end devices, like smart phones or tablets drives the need for next generation packages with finer features at increasing reliability of the package. In addition, cost considerations become more and more important to survive in the competitive landscape for all parties within the supply chain, from chip manufacturer, assembly and test to the consumer end device manufacturer. Therefore, the industry desperately strives for innovative approaches to lower manufacturing costs coupled with enabling technologies that meet the challenging technical requirements.

Specific needs in the patterning area are to overcome current resolution limitations that are caused by the today's available photopolymers. They are limited in the supported resolution and via wall angle, even though the today's imaging photolithography technologies would theoretically support even higher performance. In addition some polymers or dielectrics such as polyimides (PIs), PBOs and epoxies that are used as passivation layers remain in the package and will finally also impact the package reliability. There is a significant coefficient of thermal expansion (CTE) mismatch between these materials and the chips. Furthermore, higher density packages have bigger thermal loads, exacerbating this problem. As a result, this CTE mismatch can cause issues such as stress damage to low- $\kappa$  dielectrics and wiring layers, which are also getting thinner and, thus, are

even more sensitive to any thermomechanical stress. Different non-photo sensitive materials with a better match are available for quite some time but could not be patterned at the required resolution, required profile and at an acceptable cost level.

Finally cost pressure of the total package is typically addressed in the semiconductor industry by a transfer of technologies to a larger, next generation substrate format. While the wafer-based packages are limited to the largest wafer scale of 300mm, fan-out wafer-level package technologies offer the scalability to larger substrate sizes in a panel format.

To sum it up, a very attractive technology alternative to photolithography would be a technique that can directly structure non-photo PIs, PBOs and epoxies at high resolution combined with panel compatibility.

Excimer laser ablation technology now provides that alternative while also delivering several other advantages.

## EXCIMER LASER ABLATION IN ADVANCED PACKAGING APPLICATIONS

The most promising advanced packaging application that could benefit from the inherent technology difference using laser ablation is via drilling in polymers to create openings on top of metal pads for electrical interconnection. While the polymer is patterned by the laser energy, the relatively thick metal pad actually acts as a natural ablation stop layer. Additional key advantages are the ability to pattern a large area filled with thousands of vias enabled by the mask based patterning technology and the provided high laser energy level. 5  $\mu\text{m}$  vias or smaller can be created in both traditional photopolymers and new materials.

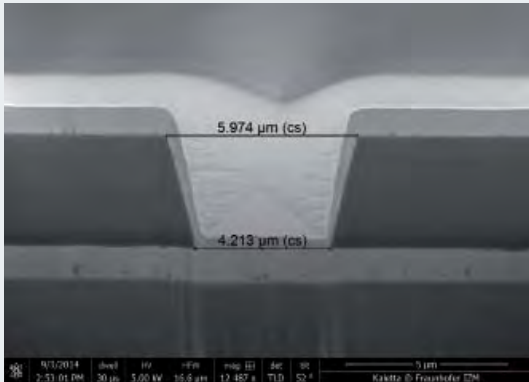


**Figure 3** SEM image of a 5µm via in BCB at 650mJ/cm<sup>2</sup>, 30 pulses [1]

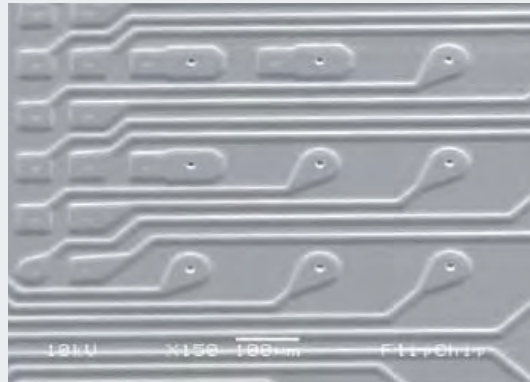


**Figure 4** SEM view of two layer PBO patterning by SUSS ELP300 [2]

A complete wafer-level package based on excimer laser ablation was completed and tested by a cooperation of SUSS MicroTec and FlipChip International. One major advantage of the excimer laser is the capability of building stacked redistributed layers of 2 and more at lower cost than photolithography tools.

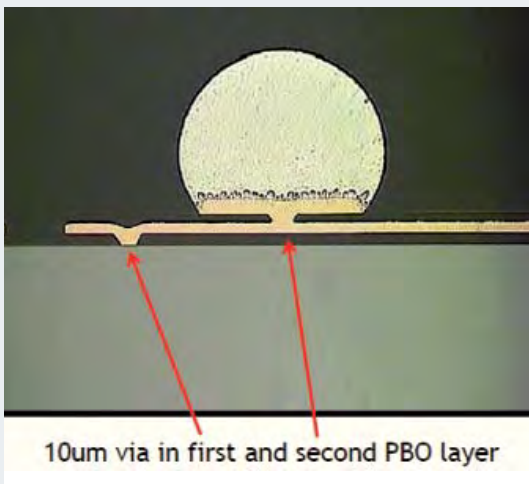


**Figure 5** Cross section of two layer PBO patterning by SUSS ELP300 with plated copper RDL and solder bump [2]

#### POST-ABLATION CLEANING

The ablation process of these photo and non-photo sensitive materials using the excimer laser usually generates debris that will need to be removed during and/or after ablation.

Excimer laser tools are always equipped with a debris cell that would remove any loose debris generated during the ablation process. Hence, in most case, one need to subject excimer processed wafer or substrates to a cleaning process depending on materials to remove any residual debris that was not removed during the ablation. Various cleaning processes exist that match the corresponding materials and ablation process. However, besides an effective cleaning process, cost efficient solutions are required by the market to allow the adoption of excimer laser ablation for cost sensitive applications in the field of advanced packaging. These cleaning technologies have been developed over the last years and promise very good efficiency that is required to introduce excimer laser ablation into high volume production. The debris formed during the ablation process must be removed after the process, using an efficiently designed debris cell. The debris cell consists of a metal confinement that surrounds the excimer laser beam during the ablation process.

This confinement is connected to a vacuum pump to pull any particles and fragments formed through the photodecomposition of dielectric material (photo and non photo polymeric materials) by the laser beam. The removal of debris during ablation is not sufficient enough to eliminate any residuals that will adhere to surface of the dielectric materials and would need other means to remove and prepare the ablated pattern to the subsequent processes such as plating or deposition of another dielectric layer or epoxy molding compounds.

Multiple approaches were suggested in the literature to clean post excimer laser ablation debris such as the use of Nd:YAG laser [3,4]. This technique is useful for specific pattern density where there is uniform distribution of thin layer of debris at dielectric surface. We have checked this technique and confirmed its validity using our picosecond DPSS laser (532 nm). Figure 1 shows the cleaning of post excimer laser ablation debris of PBO materials. We can see clearly the differences between post ablation and cleaned areas.

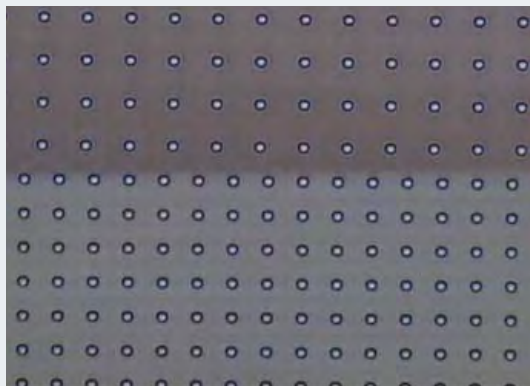


**Figure 6** Post excimer laser ablation cleaning using picosecond DPSS laser (dark area: post ablation, clear area: post debris cleaning)

Other solutions were proposed for during and post ablation debris removal such as second exposure if the same initially ablated surface of dielectric material to intermittent pulses of UV laser having alternating high and low fluences scanned in a direction away from the initial scan area [5]. CO<sub>2</sub> laser was also applied to clean black deposits formed during the excimer laser ablation of polyimide in Air [6]. The 10.6 $\mu$ m CO<sub>2</sub> radiation was strongly absorbed in the debris but only weakly absorbed in polyimide thus enabling the clean removal of the debris without any damage to the polyimide.

We have addressed the post ablation cleaning at SUSS MicroTec using other approaches that will be specific to each material since there is no “one size fits all” cleaning solutions for post ablation debris removal. Our goal is to provide alternative cleaning solutions to our customers that will either fit with their existing infrastructure and/or provide innovative techniques that add value at low cost of ownership.

## O<sub>2</sub> PLASMA CLEANING

O<sub>2</sub> plasma was well adopted in many advanced packaging fabs for patterning or resist stripping. The O<sub>2</sub> plasma was used in conjunction with either Helium (He) or Argon (Ar) gas to improve the plasma efficiency. In addition, multiple tools from different tool vendors were used to process wafers with O<sub>2</sub> plasma. We have used the O<sub>2</sub>/He or /and O<sub>2</sub>/Ar plasma to clean the post excimer laser ablation debris generated and redeposit back on the surface of the ablated dielectric material. Most of the O<sub>2</sub> plasma cleaning process will remove a thin layer of the dielectric with the debris that ranges from 200 to 600 nm that would be compensated in the initial coating process.

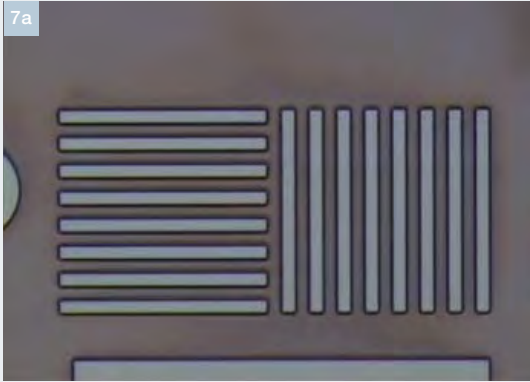


**Figure 7a** Post ablation of HD8930 showing debris around the patterned feature

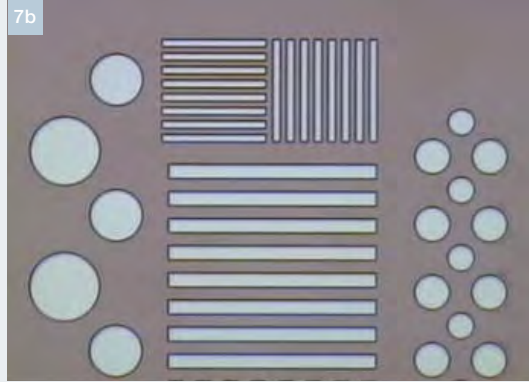


**Figure 7b** Post O2/Ar plasma cleaning of post ablation debris for HD8930

The criteria of success is high removal of debris with minimal removal of dielectric materials. Our plasma tool is supplied by Plasma Etch Inc. We processed coated wafers with PBO (HD8820 and HD8930) [7] materials through our excimer laser tool then exposed these wafers to O2/He or O2/Ar plasma process to remove the post ablation debris. The results were very impressive and we

were able of cleaning the debris with minimal material removal. Figure 7a (post ablation) and Figure 7b (post cleaning) shows the results obtained from debris removal on HD8930 using O2/Ar plasma cleaning process. Figure 8a (post ablation) and Figure 8b (post cleaning) shows the efficient removal of post ablation debris from HD8820 using O2/He plasma cleaning process.

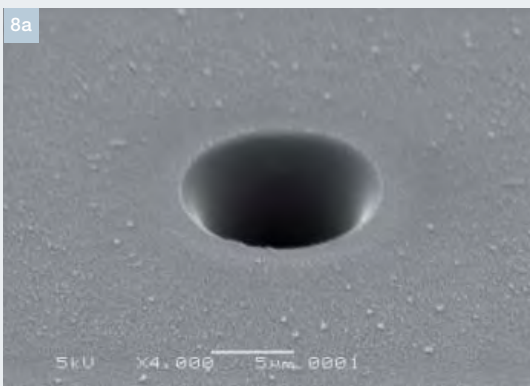


**Figure 8a** SEM view of post via ablation of HD8820 showing debris around the patterned feature

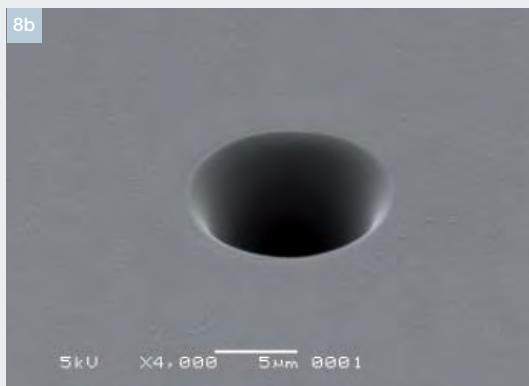


**Figure 8b** SEM view of post O2/He plasma cleaning of post ablation debris for HD8820

### SACRIFICIAL LAYER

The search for a cost effective solution to remove the post ablation debris leads us to look into formulating a sacrificial thin water soluble film that is capable of absorbing the UV light during scan ablation. This sacrificial layer would be easily removed with water spray after the ablation process. The removal of the sacrificial layer will carry with it all the debris redeposits during ablation on top of it. The literature indicated the existence of other sacrificial layers that were used for the solid state or CO<sub>2</sub> laser where only one feature at a time was ablated [8,9] (Emulsitone EMS4611 or HogoMax from Disco). Hence some of these materials were not able to withstand the excimer laser scan process where a full die was scanned in one time.

To solve this issue, we have formulated our own thin sacrificial layer using water soluble UV absorbent polymer to be able to be ablated with the dielectric. Figure 9a shows the amount of debris post ablation surrounding the vias and trenches patterned into HD4104 [7]. Figure 9b shows pattern cleaned after the removal of the thin sacrificial layer with the debris redeposits using water spray.

### CO<sub>2</sub> SNOW CLEANING

Another post ablation cleaning solution was also developed using the CO<sub>2</sub> snow [10]. It consists of exposing the surface of the ablated dielectric to CO<sub>2</sub> snow spray to remove the debris redeposit during ablation. This technique was used to remove post seed layer removal and also post via and redistributed layer ablation using excimer laser. Figure 10a shows the surface of the dielectric post seed layer removal ablation process. Figure 10b shows the surface of the dielectric materials post CO<sub>2</sub> snow spray where most of the post ablation debris was removed.

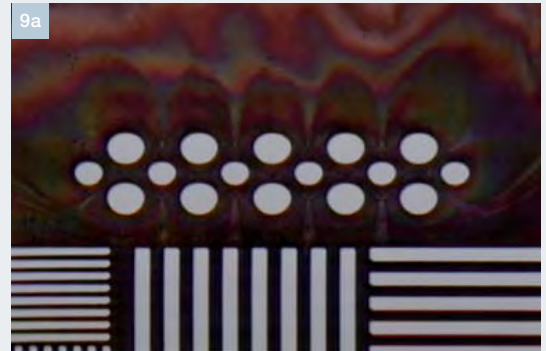


Figure 9a Post ablation of HD4104 showing debris around the patterned feature redeposit on top of the sacrificial layer

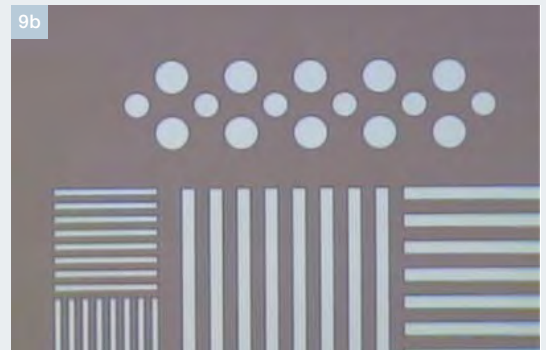


Figure 9b Post water spray cleaning showing removal of the sacrificial layer with the post ablation debris that was on top

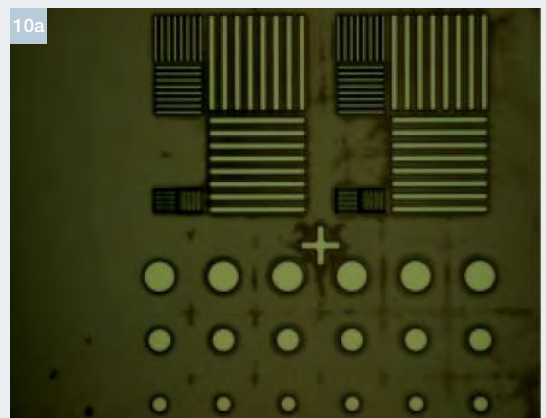
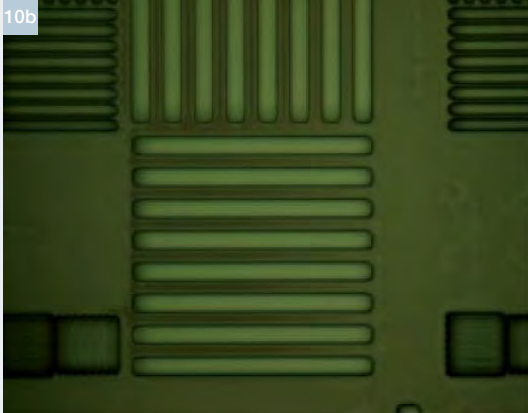


Figure 10a Post ablation of HD8820 showing debris redeposit around the patterned feature



**Figure 10b** Post CO<sub>2</sub> snow spray cleaning showing significant removal of the post ablation debris

The post ablation cleaning solutions proposed above are only few to address specific materials and process conditions. To achieve higher efficiency of cleaning, it would be recommended to either use O<sub>2</sub> plasma, sacrificial layer, DPSS, or to combine two solutions when infrastructure and cost allow such as CO<sub>2</sub> snow followed by O<sub>2</sub> plasma or CO<sub>2</sub> ionized water spray followed by O<sub>2</sub> plasma.

## SUMMARY

Excimer laser ablation was demonstrated to be a high potential patterning technology that meets today's but also the future requirements for advanced packaging platforms in patterning of polymers and dielectrics. In addition to the patterning technology and material qualifications, efficient cleaning methods have been developed to support the introduction and adoption of the technology in high end manufacturing technologies. Further developments will continue to open up new application areas to support the ever increasing requirements of industrial and consumer electronics.

## References

- [1] Michael Töpfer, Karin Hauck, Lukas Weituschat, Mario Schima, "Laser Ablation of Thin-Film Polymers for a Sub-5 μm Via Technology" SUSS Technology Forum Semicon Europa 2014
- [2] Jim Zaccardi, Guy Burgess, Theodore Tessier, Matt Souter, "Dielectric Laser Via Drilling for Next Generation Wafer Level Processing" IMAPS Device Packaging Conference, March 2014
- [3] Jianhui Gu, Puay Khim Lim, and Pean Lim, "Method for Cleaning Debris off UV laser Ablated Polymer, Method for Producing a Polymer Nozzle Member Using the Same and Nozzle Member Produced Thereby" US Patent application US2003/0052101 A1, March 20, 2003
- [4] Jianhui Gu, Puay Khim Lim, and Pean Lim, "Nd: YAG Laser Cleaning of Ablation Debris From Excimer-Laser-Ablated Polyimide", Proceeding SPIE 4595, Photonic Systems and Applications, 293 (October 29, 2001)
- [5] Kevin j. McIntyre, "Method of Cleaning Laser Ablation Debris", US Patent 5,257,706, November 2, 1993
- [6] J. Koren, and J.J. Donelon, "CO<sub>2</sub> Laser Cleaning of Black Deposits Formed During The Excimer Laser Etching of Polyimide in Air", Applied Physics B, Vol. 45, Issue 1, pp45-46, January, 1988
- [7] HD Microsystems, [www.hdmicrosystems.com](http://www.hdmicrosystems.com)
- [8] Emulsitone Chemicals LLC, [www.emulsitone.com](http://www.emulsitone.com)
- [9] Disco Corporation, [www.Disco.co.jp](http://www.Disco.co.jp)
- [10] Eco-Snow Systems, [www.Eco-snow.com](http://www.Eco-snow.com)

Ralph Zoberbier graduated in Precision Engineering and Microsystems Technology from the University of Applied Sciences in Nuremberg. He joined SUSS MicroTec in 2001 as R&D Project Manager. In 2005 he became International Product Manager Aligner. From 2010 – 2014, he led the Aligner Product Management team as Director Product Management. With the acquisition of Tamarack Scientific Inc. his responsibility was extended by complementary projection lithography and laser process technology. In 2014 he was appointed to General Manager Exposure and Laser Processing. Ralph gained his MBA degree in Entrepreneurship at Louisville University, Kentucky.



# SEQUENCE 1

## AUTO-ALIGNMENT INSIGHTS

Dr. Marc Hennemeyer, Dr. Thomas Hülsmann SUSS MicroTec Lithography GmbH, Schleissheimer Str. 90, 85748 Garching, Germany

**This article is the first part of a short series of articles focusing on pattern recognition and alignment in SUSS mask aligners. It is meant as a guideline especially for beginners in the field of pattern recognition, but even more experienced users might find one or the other aspect about pattern recognition which is new to him or her.**

Almost all production steps in the manufacturing of semiconductor and MEMS devices need some sort of alignment of the new features to structures already placed on the substrate earlier. This is especially true for back end of line processes which are the main field of application of SUSS mask aligners.

Since according to Moore's law also backend processes are targeting ever smaller feature sizes the requirement on alignment accuracy saw a constant tightening in the last years. Nowadays, required alignment accuracies of 1  $\mu\text{m}$  or even smaller are common, where it used to be several micrometers just a couple of years ago. While measurement of the pattern position with sub-micron accuracy in principle is not an issue for modern pattern recognition systems – they are capable to find positions of structures with accuracies far smaller than the pixel resolution of the image capturing system, down to several tens of nanometers – as often the devil is in the details. While alignment systems in the front end processing rely on fixed target geometries, in backend processing target variation is a lot bigger and the target quality often much worse. This can be caused by countless reasons, substrate surface

condition and covering by insufficiently transmitting materials just being two examples.

The following overview will try to give some insight into the complexity of the task of creating reliable and accurate alignment pattern models under varying surface and surrounding conditions. It can be used as a quick guideline when starting alignment target training. However, for more complex challenges in target model training the reader is pointed to the extensive trainings offered by the SUSS training center and which are noted at the end of this article.

The first part of the series will cover general information about the pattern recognition system used in SUSS mask aligners and how changing the conditions of the grabbed image is influencing the pattern recognition process. The following parts will focus on rules and processes how to setup and optimize pattern in order to achieve good accuracy and reliability in the alignment process as well as on some application examples more detailed.

### COGNEX PATMAX® VERSUS CNL

The alignment system in SUSS MicroTec mask aligners is based on the standard solution in the semiconductor market: the PatMax® geometric pattern recognition algorithm of Cognex.

In contrast to cross-correlation methods like CNL which directly compare the grey levels of the acquired images, the PatMax® system extracts geometrical information from the images to create edge models of the structures found in

the image. Although grey values are also used for the identification of the edges inside of the image, geometrical pattern matching has several advantages over correlation matching.

1. Due to the restriction of the used information on geometrical data, the system is less sensitive to changes in brightness and contrast between the trained model and the actual scene presented to the system during a pattern search.
2. It is up to the user to decide which edges carry the position information and which edges are ignored.
3. Furthermore, flexible transformations of geometrical data, like scaling and rotation allow automatic or manual adaption to changing process conditions.
4. The model's edges are displayed giving the user feedback on the model and the position and quality of its match with the targets.

#### THE MODEL OR PATTERN AND ITS MATCH WITH THE TARGET

Pattern matching algorithms operate with a target "model" or "pattern". The most common way to define target models is the model creation from a part of an image of the real world target. In case of PatMax®, the model is an "edge model", some matches of such a model with an image are shown in the title figure on page 10. The match in the center is supposed to deliver the highest score. Mismatches are represented with red lines indicating missing edges.

It is obvious, that especially during the target model training a high expertise has to be put into selecting well suited real world structures. A bad choice of the structure used for training e.g. a very small area will result in a trained target model which gives multiple and thus unreliable recognition results.

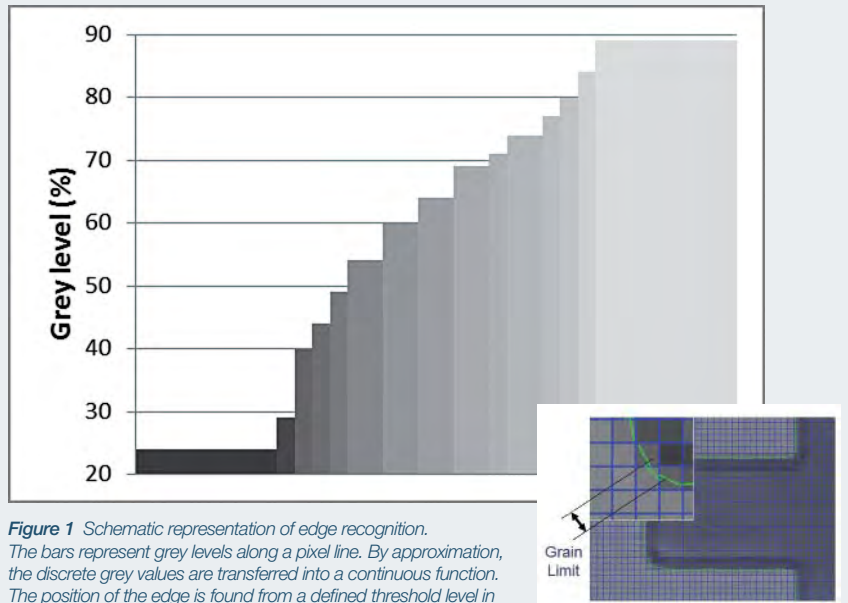


**Figure 1** Schematic representation of edge recognition. The bars represent grey levels along a pixel line. By approximation, the discrete grey values are transferred into a continuous function. The position of the edge is found from a defined threshold level in the continuous data (here 50% of spanned grey range). Inlet: image of edges found in typical mask aligner target

#### WHAT IS AN EDGE?

The extraction of geometries from the pixel images is performed by analyzing grey scale levels. If the grey level changes in a certain area surpass the limit "edge threshold" for the slope and "contrast threshold" for the height, then we have found an edge segment. For a schematic drawing see figure 1. The size of this vicinity is appointed by the grain limit control in the PatMax® software.

As the lateral position of the edge is determined from the approximated continuous data, it can be located with sub pixel accuracy. The direction of the edge segment is found using the grey levels of its neighborhood. This edge detection is performed on each scene during the actual pattern recognition, but also in case of pattern training from real world data.

### SUB-PIXEL ACCURACY

In tests we proved a sub-pixel accuracy of below 1/40 pixel. That can be explained: A target which measures 50  $\mu\text{m}$  yields 200 edge segments, whose positions and directions are averaged.

The advantage is that low power objectives can be used.

Example: A 5x objective and a camera may result in 1  $\mu\text{m}$ /pixel magnification. But although the objective has only a 2  $\mu\text{m}$  L/S resolution, the systems yields a 25 nm position resolution. Besides granting a large field of view low power objectives contribute to machine stability with their high depth of focus.

### ILLUMINATION: KEY TO SUCCESS

The art in setting up reliable pattern recognition and therefore reliable alignment processes lies in balancing the need for flexibility to recognize varying targets with the need for uniqueness to reduce the amount of wrong findings.

The most important parameter to improve the reliability of pattern recognition is a proper definition of the illumination conditions. The illumination of the scene should fulfill a whole set of requirements:

1. It must be bright enough to keep any detector noise at a low level and to insure that even in the darkest areas real features are still discernible.
2. On the other hand the illumination should be low enough not to overexpose bright image areas and crossfade important details.
3. It must not create artifacts.
4. The contrast between edge and environment must be high enough to distinguish them from each other.
5. Avoid exposure of the photo resist.

That can be seen exemplarily on the SiO<sub>2</sub>-substrate in figure 2. Here, changing the illumination setup created anything from hardly discernible substrate

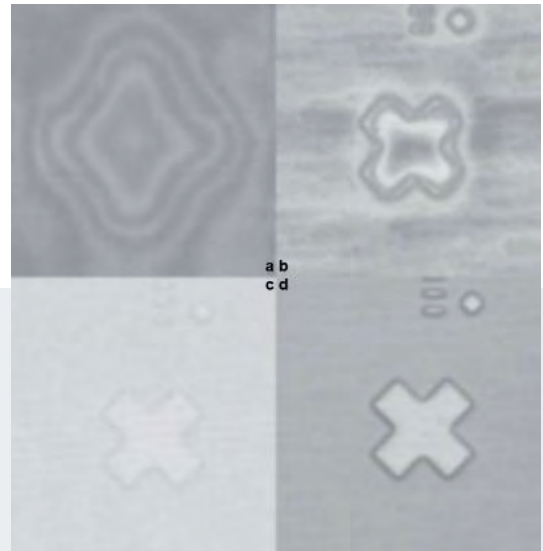


**Figure 2** Influence of illumination on target visibility. Microscopic images acquired with different illumination settings. a) undefined customer illumination, b) red LED, c) yellow filtered white LED (6000K), d) yellow filtered white light halogen (3200K)

structures over strong shadow artifacts and very weak contrasts to crispy images with very good structure representation. Parameters that can be varied for this adjustment in the SUSS mask aligners are the illumination method (reflected or transmitted light), light sources (halogen/LED), color filtering and collimation angles of the incident light (ring illumination).

It is easy enough to understand, that having sufficient contrast in the images to be analyzed by the pattern recognition is of crucial importance. This is especially true if the image is used as a template for creating the target model, as lower contrast always increases the risk to train features in the scene that are actually not part of the real target.

However, as the images in figure 2a) and 2b) demonstrate, illumination can also create virtual edges within the scene that can heavily interfere with the pattern recognition and consequently with the complete alignment process. Common reasons for such ghost edges or artifacts are reflections from the substrate surface interfering with geometries on the mask, which can be suppressed or at least greatly reduced by choosing larger imaging gaps. A second reason is the presence of interference artifacts within transparent layers on top of the structures on the substrate. Figure 2a) is a good example of the effect these interference artifacts can have on the observed images.

## PROCESS VARIATIONS

The second serious influence on the reliability of the pattern recognition is, of course, the repeatability of the structures presented in the individual scenes. Due to process fluctuations, the target structures on the wafer can drastically vary from wafer to wafer. Figure 3 presents examples of structure variation between wafers caused by preceding process steps. The top row shows an example of back ground wafers. Here, due to the different degree of scrub marks, contrast and even polarity of the marks changes together with a varying level of clutter in the scenes. Also the bottom row, which shows targets on epilayers, presents a severe degree of variation. These variations are based on the varying reflectivity caused by the surface roughness. As can be seen in the image this even leads to reasonable changes in the identifiable edges.

As can be understood from these examples, the choice of suited scenes for the target training is of crucial importance. Selection of bad targets for the training (scenes with untypical information, bad contrast, untypical polarity and so on) will severely deteriorate the reliability of the pattern recognition process.

The next parts of the articles will therefore introduce guidelines on how to select good scenes for target training and procedures for testing and optimizing the trained target models.

Meanwhile, we would like to remind the reader of the extensive trainings that are offered by the SUSS MicroTec training department covering this subject. For information on trainings please be referred to the respective SUSS webpage:

<http://www.suss.com/en/customer-service/training.html>

and the contact information therein.

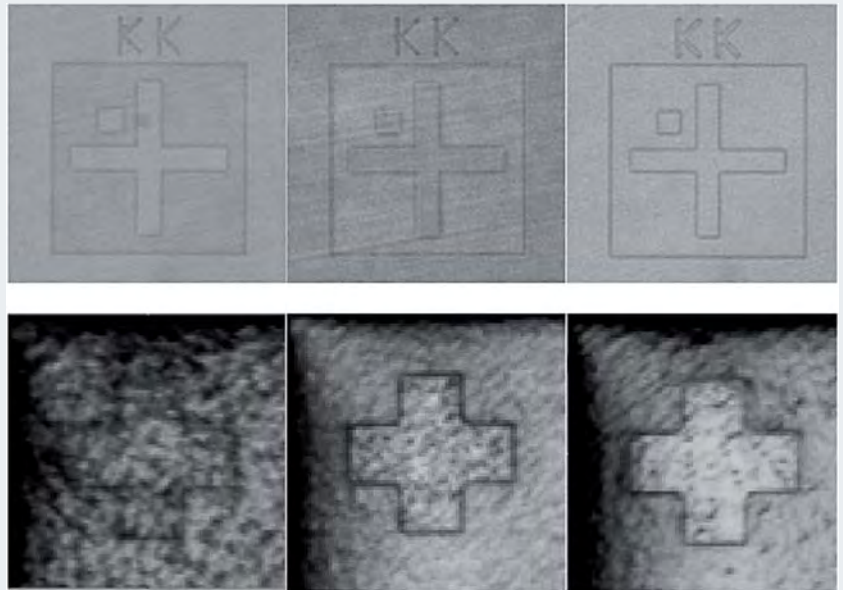


**Figure 3** Two examples of screen shots of target variation in different scenes. Scrub marks (top row) and epilayers (bottom row) can introduce clutter and change contrast

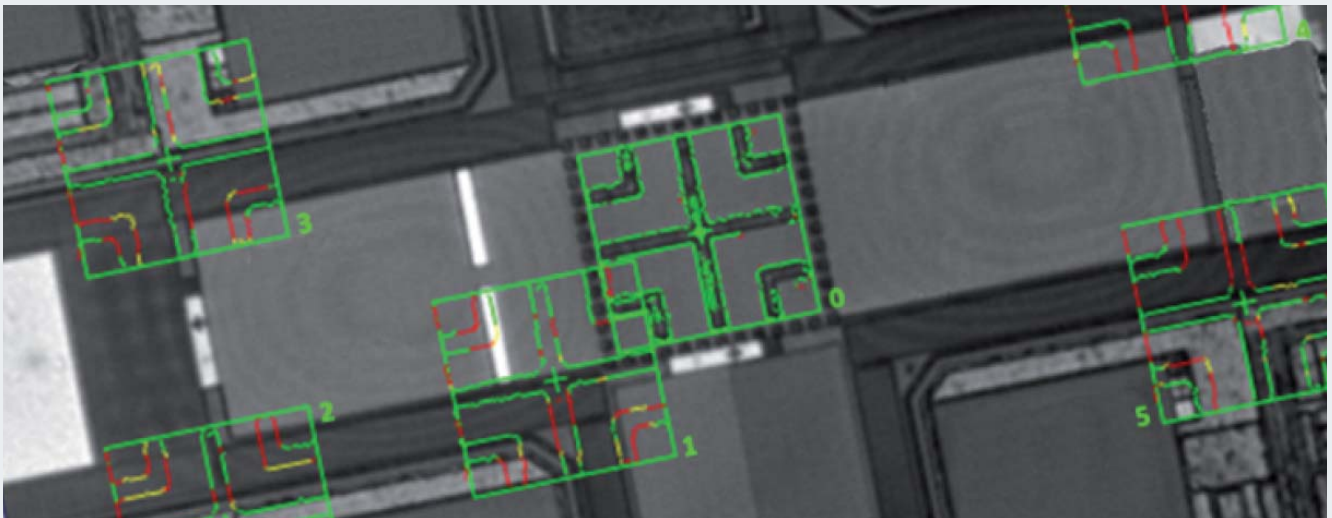
*Dr. Marc Hennemeyer is Product Manager at SUSS MicroTec Lithography. He is responsible for the automatic mask aligner product group. After his graduation in Physics at University of Munich where he also received his PhD working on micro fluidic systems for biological applications he joined SUSS MicroTec in the Application Department before he proceeded to his current job. He authored and coauthored several papers on various topics, including micro imprinting and lithography.*



# SEQUENCE 2

## AUTO-ALIGNMENT INSIGHTS – PART 2: CASE STUDIES

Dr. Marc Hennemeyer SUSS MicroTec Lithography GmbH, Schleissheimer Str. 90, 85748 Garching, Germany



### INTRODUCTION

This article is the second part of the short series of articles which started in issue 01/2013 of this magazine. The series focuses on pattern recognition and alignment in SUSS mask aligners. It is meant as a guideline especially for beginners in the field of pattern recognition, but even more experienced users might find one or the other aspect about pattern recognition which is new to him or her. This second part of the series highlights the most common alignment reliability issues using case studies. Based on the analysis of the cases promising measures to improve the alignment reliability in such cases are suggested.

As discussed in the first part of this alignment guide a proper definition of the illumination conditions is one of the most critical steps to achieve a reliable autoalignment. But even under perfect illumination conditions many scenes contain too little significant information or too much disturbing noise. In such cases a smart target design, a clever selection of fields of view and an adept creation of the model can make the difference for you between a stable alignment process and the need of frequent operator intervention.

To quantify the quality of the pattern training and to understand the root causes of alignment errors it is important to understand the error type causing the alignment mistake.

Leaving unsuccessful alignment due to missing targets out of consideration the two typical statistical error types remain. Errors of type 1, so called false negatives, occur if a target which is present in the current scene is not recognized by the pattern recognition. Errors of type 2, also called false positives, occur if the system detects the trained pattern at positions in the scene where no real target is present. Many parameters of the pattern recognition influence both types of errors – unfortunately inversely. While changing one of these parameters may reduce the errors of type 1, in the same time it will increase the errors of type 2. Typical examples for such parameters are score threshold, contrast threshold, degrees of freedom, score using clutter, scaling and polarity restrictions. To achieve reliable target recognition, careful balancing of the two error types is needed and for an efficient improvement of the alignment stability, it is essential to understand which error type is dominant in the observed errors.

The following paragraphs will highlight typical challenges an engineer will need to confront while setting up alignment processes and will exemplarily sort them into the respective error types. From each case study universally valid recommendations for better alignment stability are derived.

#### CASE 1: REDUNDANT INFORMATION

The first case is a typical example for error type 2. Figure 1a presents a typical pattern as trained with the standard training method from a life scene and found in a respective life pattern. Almost any life scene contains both relevant and irrelevant pattern information. In Figure 1a additional shadows are visible besides the true target edges (the darker areas around the bright target). These shadows are recognized during pattern training as additional edge information and generate the outer yellow lines in the image. Only the innermost line represents the actual edge information of the real life target. This additional information heavily increases the risk to find the target at wrong positions, especially when further degrees of freedom need to be used, e.g. ignoring polarity. Figure 1b) shows an example of such a wrong detection. Polarity is ignored in this example. All green lines match edges in the life scene. Red lines are pattern features that are not matching to any structure in the life scene. The matching score for such a detection would still be  $> 0.5$ . Since the trained pattern contains information that is not part of the real structure on the substrate but is caused by shadow artifacts, matching scores of 0.5 can also occur with perfect matches, if the shadow is not

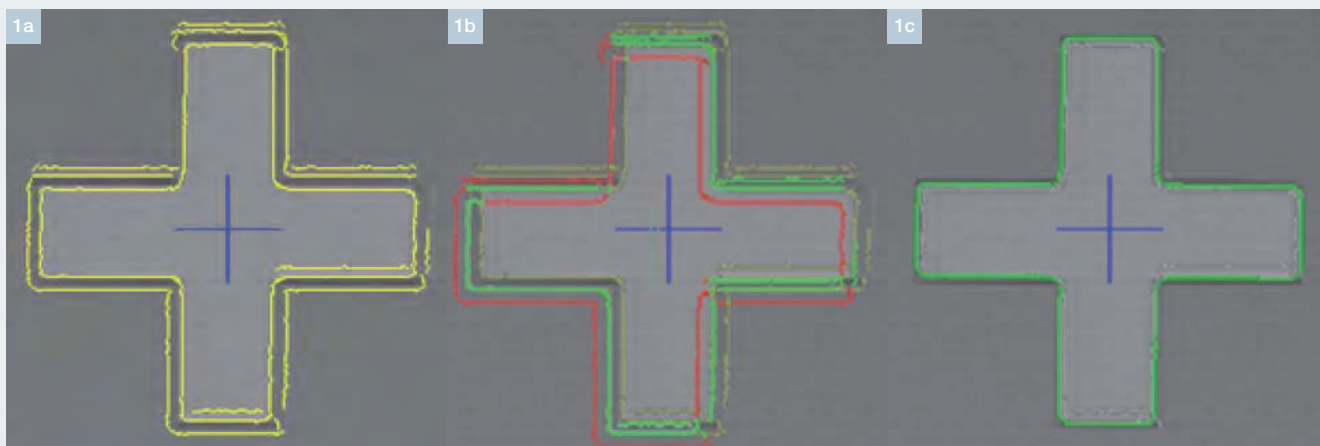


**Figure 1** a) alignment pattern as trained from a (less than perfect) real scene and b) respective matching information of an error analysis for the same scene. Matching score in b) still would be  $> 0.50$  if polarity is ignored (green lines vs. red lines). c) shows how an improved target would look like: no redundant information is present in the target

visible in some of the process targets. Therefore the risk of misalignment is significant and must be reduced by optimizing the trained pattern and the setting of recognition parameters.

Already taking the polarity into account would severely improve the situation on this example, but might not always be feasible due to polarity changes of the targets in general due to variations in preceding process steps.

A second, even more promising way to improve would be restriction of the trained pattern on real edges of the target. Figure 1c) shows the match of an accordingly altered pattern in the life scene. Even if polarity is ignored, an offset match of the *model* would result in very low matching scores.

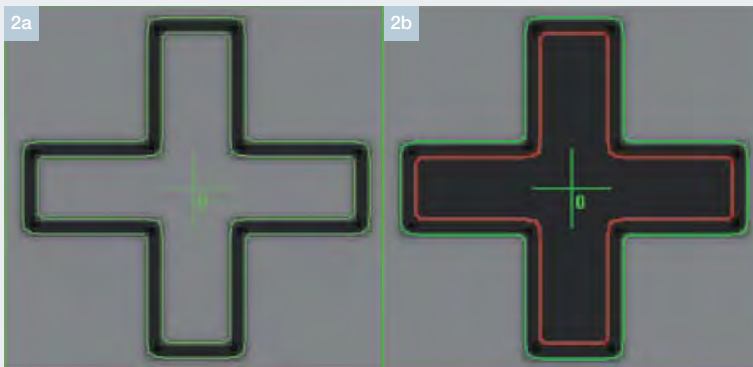


**Figure 2** Example of reduced matching scores due to changes of the target appearance from wafer-to-wafer. Both targets are real targets from the same production process. While in **a)** the target shows a distinct double edge, which was also trained in the pattern, **b)** shows a target with overall darker appearance, that does contains a double edge. Matching score on **b)** is as low as  $-0.5$

## CASE 2: CONFUSION

A second case of errors of type 2 is confusion of the real target with similar features in the field of view. An example of this can be seen in the title image. The image shows the result of a mistake test, i.e. a test in which the system present all recognized target positions to allow for a quick check

about the uniqueness of the alignment feature inside of the field of view. As can be clearly understood of the image in the presented case several additional recognitions occur besides the true pattern recognition in the center of the image. Matching scores for the wrong positives were  $> 0.7$  for some of the recognitions.

In such cases there are basically only two possibilities to improve the alignment.

First and most rigorous would be a redesign of the general layout of the field of view on substrate and mask. Of course, the most straight forward way would be to provide a clearfield around the alignment features which is free of any confusing structures. This would give safety to no longer getting wrong positives. Where this is not possible due to process (or business) restrictions, a redesign of the alignment targets itself is advised. As a general rule targets should always be defined with a geometry that has no resemblance with structures present in the field of view. The predominant structure orientation in the title picture is orthogonal, placed in the image under an angle of about 11 deg. The main features of the alignment pattern are oriented parallel to these predominant structures. Although the human eye does not recognize an obvious similarity, the depicted false positive recognitions prove the high level of confusion risk in this scene. Since the pattern recognition system gives the user full flexibility of the pattern definition, using mainly edges diagonal to the predominant structures or using circular pattern would clearly reduce the risk of confusion.

However, since the scene shown in the title image includes some diagonal structures and even circular noise pattern, such a redesign would most likely not reach the same level of reliability as the design of a clearfield as suggested before.

Where even a redesign of the alignment targets is impossible, e.g. due to customer specifications,

a combination of changed model design and improved parameter setting can still be helpful. However, such approach typically cannot provide the same level of reliability as the strategies described before.

A more thorough analysis of the title image reveals that the adjustment of several parameters could be improved in order to reduce the amount of false positives.

- **Polarity:** when defining the alignment recipe, polarity was switched to “ignore”, as can be understood e.g. from match 4, where an edge is recognized along a polarity change. With regarded polarity several of the false positives would drop underneath the defined threshold and not being recognized anymore.
- **Score using clutter:** Also score using clutter was switched to off. This parameter controls, whether information which are additionally contained in the life scene, but not in the trained model are recognized as feature edges. This parameter can be a mighty tool to reduce errors of type 2. All additional matches in the title image present a significant level of additional information, which would reduce their matching score and can push it underneath the threshold. However, this parameter has to be used careful and its influence on the recognition process must be kept in mind when preceding processes introduce a relevant level of noise into the life scenes. When scoring with clutter regarded, this noise can also reduce the matching score of the true target considerably. If noise is present, it should therefore be carefully checked, whether using clutter compels a lower scoring threshold and hence counters the benefit in the exclusion of false positives.

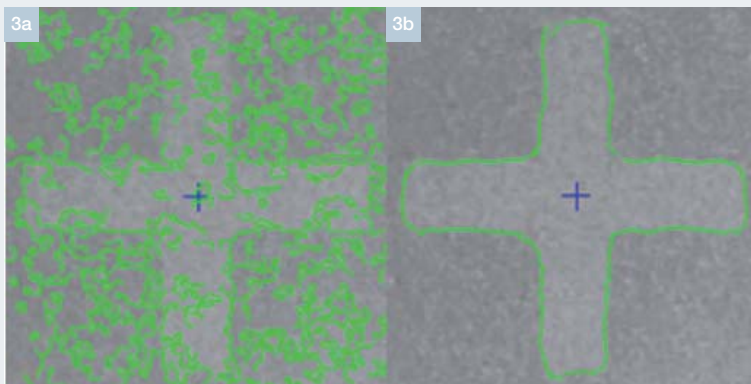


**Figure 3** Alignment models as used in the alignment of wafers with unpolished surfaces. **a)** shows the original model as created by the customer based on edge recognition from a life target **b)** an optimized model cleaned off the noise

### CASE 3: NOISY MODEL

Also caused by noise, but causing errors of type 1 instead of type 2 is the case presented in figure 3. Due to the high level of noise in the original model, which the customer created from a life scene, obviously no reliable pattern recognition was possible. Several methods can be used to improve the model. Using a synthetic target, created from life images in an image editor program or by importing CAD data is the most rigorous and successful approach for images with similar noise level. However, also adjustments of the edge threshold, image processing like contrast and brightness adjustments as well as masking irrelevant structures in the image can be helpful and can be accessed from the advanced alignment editor at the machine. Figure 3b) presents the result of the model training after several of these optimizations were applied to the training image. Using this target model a stable and reliable alignment was possible.

## GENERAL RULES

From the presented cases a couple of general rules can be given to support the setup of reliable alignment models and recipes and to speed up the optimization process of the recipes.

As a starting point, the target and its model

- Should be located in a reasonable clearfield
- Should have a different predominant structure orientation than the neighborhood
- Should contain all relevant feature edges of the target
- Should not contain any irrelevant edges of noise or other structures
- Should not contain edges that are in close neighborhood to each other (redundancy)
- Should take the polarity into account
- Should use clutter information for scoring

Since in general errors of type 1 have a smaller impact on the customers product (a pure error type 1 would stop the machine, but would not damage customer material), it is sensible to start the alignment recipe optimization with the strictest parameter set possible, i.e. besides the parameters mentioned in the list above also high matching score thresholds and deactivated degrees of freedom.

If this recipe is producing errors of type 1 too frequently an error analysis similar to the presented case studies will guide the user which parameters have to be relaxed to allow for a stable and reliable pattern recognition.

At this point we would like to remind the reader of the extensive trainings that are offered by the SUSS training department covering this subject. For information on trainings please be referred to the respective SUSS webpage: <http://www.suss.com/en/customer-service/training.html> and the contact information therein.

*Dr. Marc Hennemeyer is Product Manager at SUSS MicroTec Lithography. He is responsible for the automatic mask aligner product group. After his graduation in Physics at University of Munich where he also received his PhD working on micro fluidic systems for biological applications he joined SUSS MicroTec in the Application Department before he proceeded to his current job. He authored and coauthored several papers on various topics, including micro imprinting and lithography.*





# EXCIMER LASER DEBONDER FOR 2.5D AND 3D INTEGRATION

Dr. Tim Griesbach SUSS MicroTec Lithography GmbH, Ferdinand-von-Steinbeis Ring 10, 75447 Sternefeld, Germany

SUSS MicroTec has recently introduced an Excimer Laser based Debonding module (ELD300), which allows the stress free separation of a glass carrier wafer that was bonded to a device wafer by means of an adhesive layer in order to support the device wafer during thinning or backside processing steps. Temporary bonding of device wafers to a carrier is typically used for supporting the device wafer during various critical process steps such as thinning and backside processing in area of 3D integration, 2.5D interposers, MEMS or power devices. The laser debonder can be used as a stand-alone, semi-automated system or as an integrated process module in SUSS MicroTec's XBC300 Gen2 platform. The debonding method used in the ELD300 system is based on a 308nm excimer laser which is used to separate the glass carrier from the tape mounted, thinned device wafer. The ultraviolet (UV) light of the pulsed laser beam is absorbed in the adhesive or in an optional UV absorption layer within a few hundred nanometers. The absorbed laser energy breaks the chemical bonds in the adhesive or absorption layer without generating thermal stress on the thinned device wafer. After the actual laser debonding process the glass carrier wafer can easily be lifted off with close to zero mechanical lift-off force.

## INTRODUCTION

In the last decades the semiconductor industry has witnessed two major developments: On the one hand the constant decrease of feature sizes, coinciding with Moore's Law and leading to almost a doubling of integrated circuits per wafer every one to two years. On the other hand production processes are being transferred to increasingly larger wafers to save cost by being able to produce more dies per wafer. Additionally, in the last years a third market trend has emerged: Similar or different devices are placed next to each other on a carrier, a so-called interposer (2.5D technology) or stacked three-dimensionally (3D technology). The target is to create the shortest possible signal lines while at the same time increasing the number of input and output lines between the single devices in order to increase the signal bandwidth while reducing power consumption and heat dissipation. Instead of using classical wire bonding technologies this new technology uses photolithographic patterning of signal lines, through-silicon via (TSV) connections and contact pads with far smaller feature size in order to allow higher integration densities. High density through-silicon via fabrication typically requires the device wafers to be thinned to a final thickness in the range of 50–100µm.

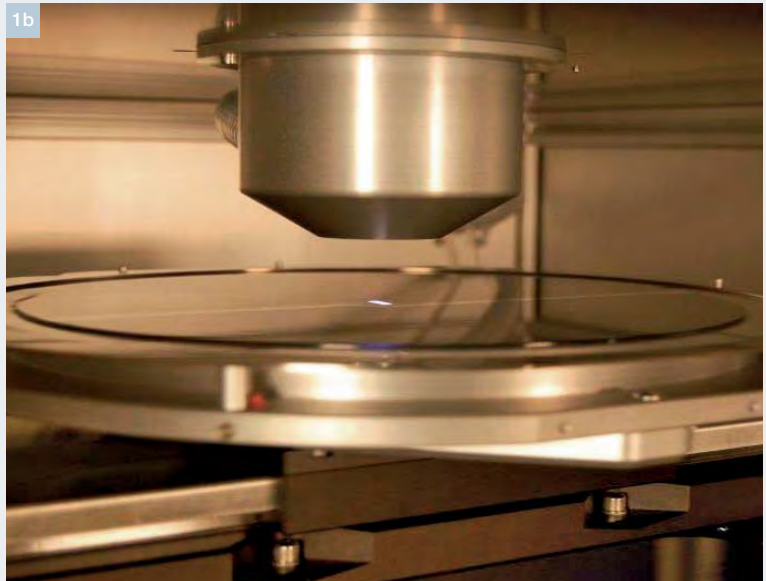


**Figure 1** Excimer Laser Debonder ELD300: (a) Overall view of the process chamber; (b) inside view of the process chamber during laser debonding process of a wafer

In order to allow the processing of such thin wafers with commonly used production equipment the wafers are temporarily glued or bonded to another silicon or glass carrier wafer prior to thinning. After backgrinding and performing all necessary backside processes, the thinned device wafer is mounted on a dicing tape which is held in a metal or plastic frame. For further processing the temporarily fixed carrier needs to be removed (debonded) to allow the separation of the thinned device wafer into individual chips using a wafer saw. The debond process of the carrier from the device wafer can be effected mechanically or through a laser procedure. For the laser-based debonding process of wafers excimer laser tools with a wavelength of 248nm or 308nm have been proved particularly successful. During the laser debonding process a laser beam is directed over the glass carrier to open the bond interface between the carrier and the adhesive material. The excimer laser produces a very high energy density. Due to the short pulse length of only a few nano-seconds, hardly any

thermal energy is distributed on the surface of or within the device wafer. In July 2014, the first semi-automatic laser debonding module was produced and qualified by SUSS MicroTec. Figure 1a shows a picture of this Excimer Laser Debonding (ELD300) module. The scan table with an on a tape frame mounted wafer is shown in Figure 1b during the excimer laser debonding process. SUSS MicroTec has developed special chucks for tape frames for this module, guaranteeing that the bonded wafer pairs can be safely held during the laser debonding process even at high scanning speeds of the x-y table. After debonding with the excimer laser, the glass carrier can easily be removed from the device wafer with a vacuum gripper. The thinned device wafer remains mounted on the dicing frame. Besides a stand-alone version, the excimer laser debond module is also available as a process module for the XBC300 Gen2 platform, allowing a fully automated process with a throughput of 40 wafers/hour, including all, wafer and tape frame handling as well as carrier lift-off.

### PRINCIPLE OF EXCIMER LASER DEBONDING

The debonding method used in the ELD300 module based on a 308nm excimer laser to separate the glass carrier from a tape mounted thinned device wafer. The UV light of the pulsed laser beam is absorbed in the adhesive or in an optional UV absorption layer within a few hundred nanometers. The absorbed energy breaks the chemical bonds in the adhesive or absorption layer without generating thermal stress on the thin device wafer so that the glass carrier wafer can easily be lifted off after the debonding process. For this procedure a laser beam is directed over the glass carrier to remove the bond interface between the carrier wafer and the adhesive material. Figure 2 shows the principle of the laser debonding process.

The excimer laser works with an extremely high energy density in pulse operation mode. One pulse period lasts only a few nanoseconds, producing hardly any thermal energy to distribute on the surface of or within the device carrying wafer. Additionally, the excimer laser offers a very homogeneous energy distribution leading to a low penetration of UV radiation in the absorbing material (Figure 3).

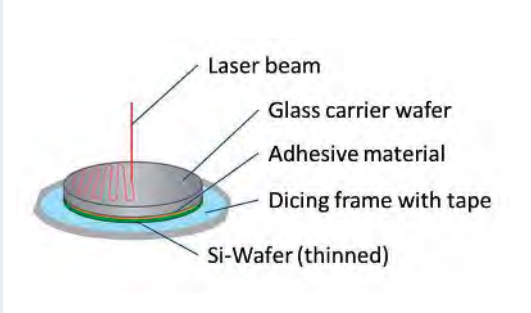


Figure 2 Principle of the laser debonding process

### OPTIMIZATION OF THE LASER ENERGY

For the excimer laser debonding process of a specific temporary adhesive material two process parameters have to be optimized. The first parameter is the focus point of the excimer laser. The excimer laser offers sufficient depth of focus so that variations in adhesive or device wafer thickness typically do not require any re-adjustments. The second process parameter is the laser energy. The laser energy needs to be optimized for the specific absorption properties of the adhesive or UV absorption layer. Figure 4 shows the effect of single laser pulses with different energy levels in five different areas of a test wafer.

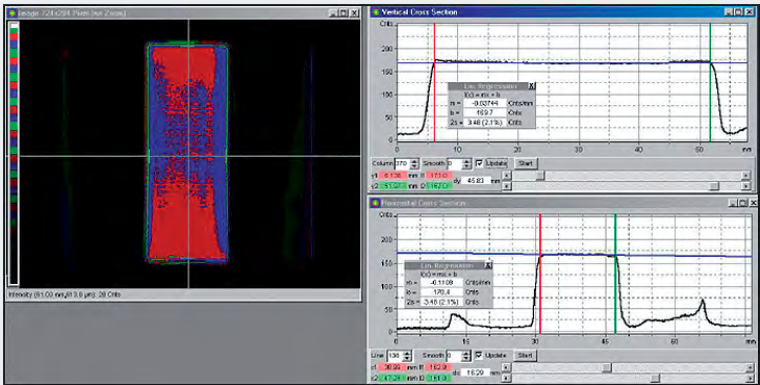


Figure 3 Energy distribution and beam profile of an 308nm excimer laser

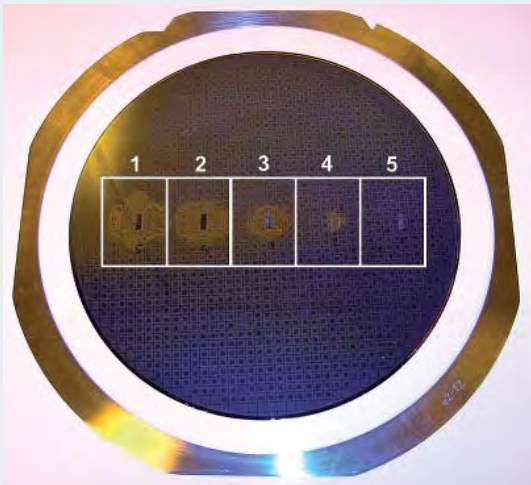


Figure 4 Optimization of the laser energy density

Zone	Laser energy density [mJ/cm <sup>2</sup> ]
1	270
2	230
3	180
4	140
5	90

**Table 1** Investigation of the optimal laser energy density for the debonding process

A summary of the different laser energy levels is shown in Table 1. The laser energy was decreased from 270mJ/cm<sup>2</sup> (area 1) to 90mJ/cm<sup>2</sup> (area 5). The higher the laser energy the larger the delaminated area. By reducing the laser energy density to 90mJ/cm<sup>2</sup> the delaminated area is decreasing considerably. On the other hand, higher fluence may result in a stronger degradation of the UV absorbing material or more ablation residues. Cleaning or recycling of the glass carrier wafer will be more difficult with a larger amount of residues present. For the material example shown in this experiment the optimum laser energy was found to be 140mJ/cm<sup>2</sup> (zone 4). That energy level did produce sufficient delamination while the residue level on the glass carrier was very low.

### EXCIMER LASER DEBONDING PROCESS

For the ELD300 module the maximum available laser energy density that can be applied is 400mJ/cm<sup>2</sup>. The pulse frequency is programmable up to 50Hz. During the debonding process the laser is directed over the glass carrier to open the bond interface between the carrier wafer and the adhesive material. In collaboration with material makers like Brewer Science, a large number of new materials were qualified to prove the reliability of the excimer laser debonding procedure. Using Brewer Science's new materials in combination with the ELD300 System, the laser debonding process of a 200mm wafer takes less than 30 seconds on average. For a 300mm wafer the excimer laser-based debonding process takes less than 60 seconds. Figure 5 shows a device wafer before (Figure 5a) and after (Figure 5b) the excimer laser release and glass carrier lift-off process.

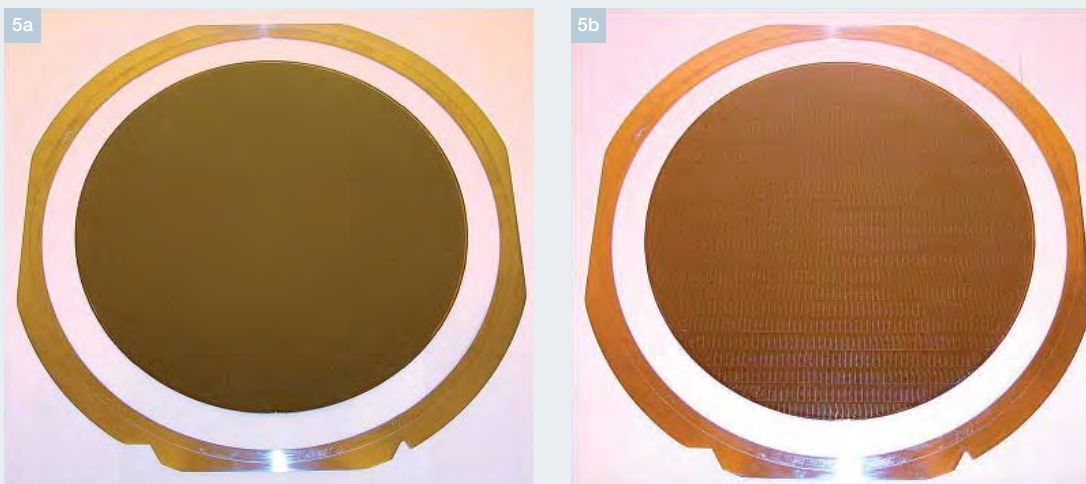


**Figure 5** Laser debonding sample: (a) before and (b) after laser debonding process

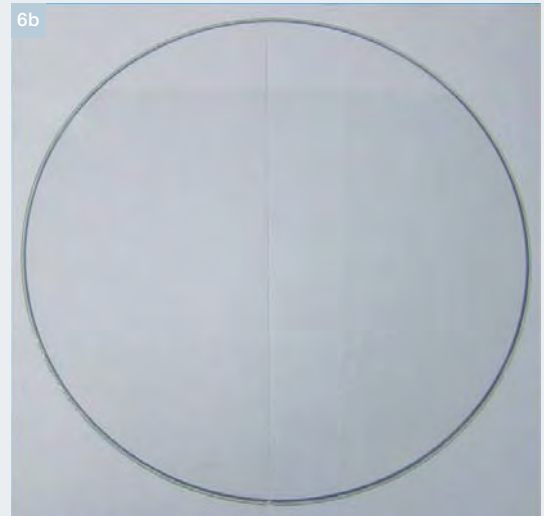
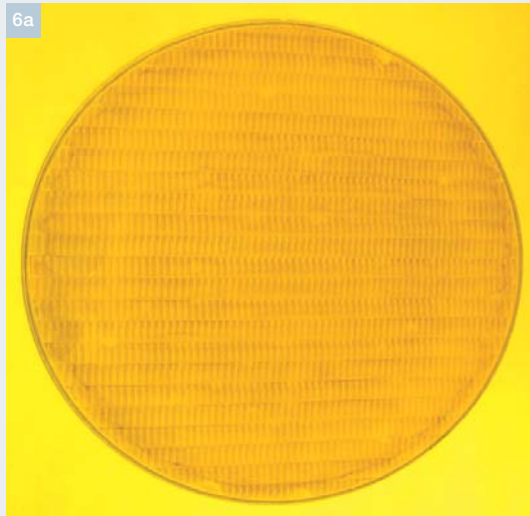


**Figure 6** Glass carrier wafer: (a) debonded glass carrier with UV release layer residue; (b) after oxygen plasma cleaning process

The corresponding glass carrier wafer is shown in Figure 6. Residues of the UV release layer can be observed on the surface of the debonded glass carrier wafer (Figure 6a). These residues can be easily removed by an oxygen plasma cleaning process, which offers the possibility of the reuse of this wafer for new temporary bonding applications. The glass carrier wafer is shown in Figure 6b after an oxygen plasma cleaning step.

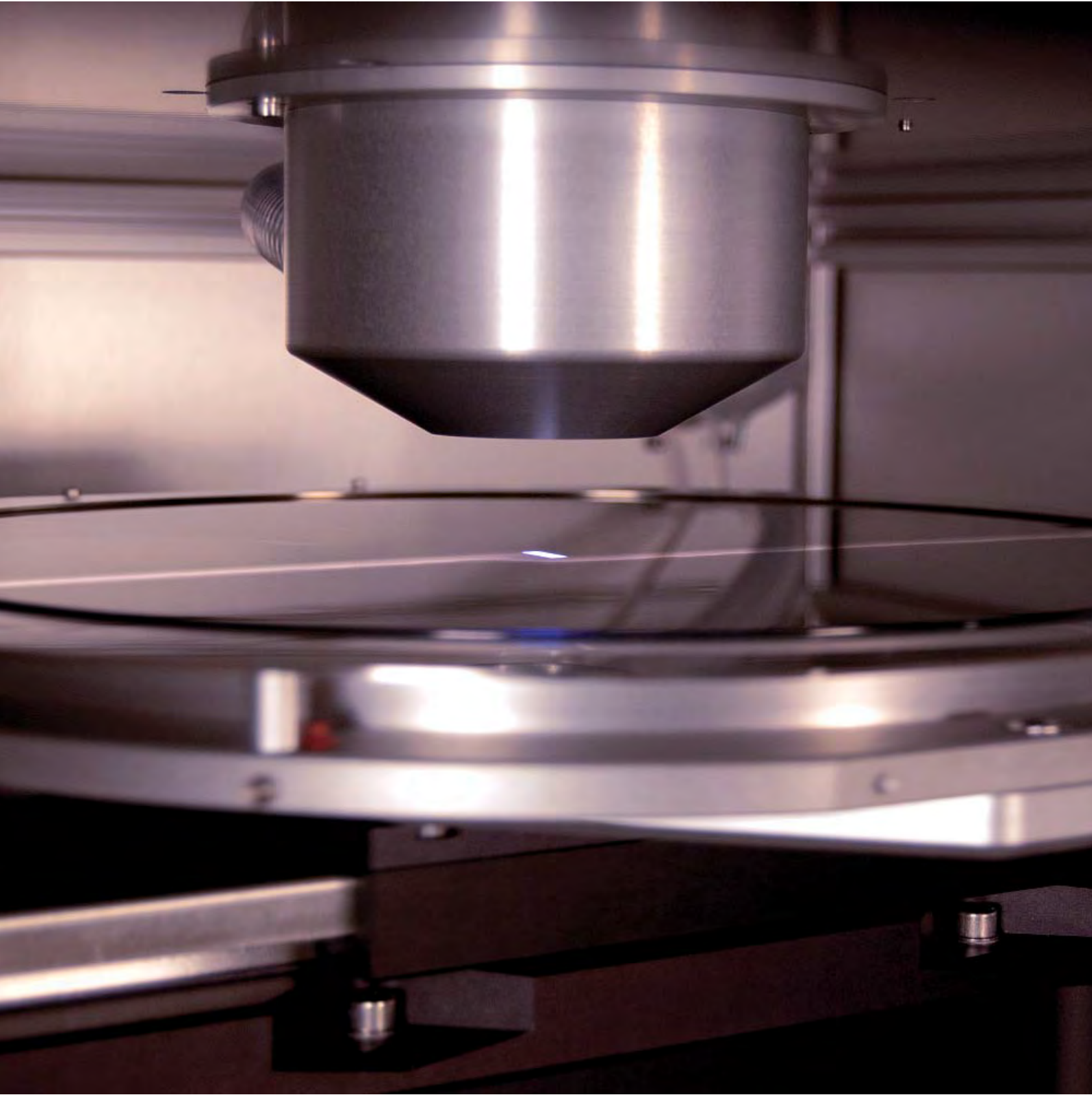
### SUMMARY

For the stress free debonding of 200mm and 300mm wafers SUSS MicroTec is offering an Excimer Laser Debonding module ELD300, which can be used as a stand-alone, semi-automated system or as an integrated process module in SUSS MicroTec's XBC300 Gen2 platform. For the debonding process a 308 nm excimer laser is used to separate the glass carrier from a tape mounted thin device wafer. The absorbed energy breaks the chemical bonds in the adhesive or absorption layer without generating thermal stress on the thinned device wafer. At the end of the laser debonding process the glass carrier wafer can easily be lifted off. In collaboration with material makers like

Brewer Science, a number of new materials were qualified to demonstrate the reliability of the excimer laser debonding procedure. Using Brewer Science's new materials in combination with the ELD300 system, the laser debonding process of a 200mm wafer takes less than 30 seconds on average. For a 300mm wafer the excimer laser-based debonding process takes less than 60 seconds.

*Dr. Tim Griesbach studied Mechanical Engineering specializing in Micromechanics and Bio-Medicine Technology at the Leibniz University Hannover, Germany. After his studies he was working as a research assistant at the Institute of Microproduction Technology and earned a PhD degree from the Leibniz University Hannover for his research work on the development of a new manufacturing technology for the fabrication of micro sensors on flexible substrate materials. Dr. Tim Griesbach joined SUSS MicroTec as Application Scientist for permanent and temporary wafer-to-wafer bonding processes in September 2012.*





# SUSS SMILE TECHNOLOGY – LARGE AREA IMPRINT A SOLUTION FOR PATTERNING OF MICRO AND NANO FEATURES

Dr. Eleonora Storace | SUSS MicroTec Lithography GmbH, Schleissheimerstr. 90, 85748 Garching, Germany

## INTRODUCTION

Due to the constant growth of the market for wafer-level-cameras and for image sensors, the request for implementing the manufacturing of optical devices such as microlenses in the very well established semiconductor technology is also steadily increasing.

In order to address this opportunity, in the previous years SUSS MicroTec released SMILE (**SUSS MicroTec Imprint Lithography Equipment**) and had been constantly improving it ever since.

The most critical process specifications typically coming from the microlens market are the accuracy and the uniformity of the thickness of the polymer constituting the optical device, directly affecting the optical properties of the end product. It is then clear that the extremely high degree of control that the SMILE technology allows in the imprinting process presents a strong advantage for customers in this field.

In the present article, the current status of the SMILE technology will therefore be reviewed, with particular focus on its flexibility in performing different types of processes.

## CONTROL OF BASELINE THICKNESS AND UNIFORMITY

The final thickness of the polymer employed in an imprint process in a Mask Aligner is controlled by the Wedge Error Compensation (WEC) process. The base SUSS MA/BA8 Gen3 mask aligner is equipped with a WEC head system that allows reaching the parallelism between substrate and mask (or, as in this case, stamp) with a micrometric precision over a 200mm surface.

After loading substrate and stamp and before starting the imprint process, the wedge error compensation is performed as follows:

1. The WEC head system moves upwards, until it reaches a physical contact with the mask / stamp loaded onto the mask/stamp holder. Alternatively, three proximity spacers can be swung inwards to keep the contact at a minimum. The upper part of the WEC head, at this moment, is free to move and tilt. When pushed by the Z-axis motor against the stamp, the upper part of the WEC head will tilt until reaching full contact over the whole substrate surface.

2. Once the WEC sensor has detected the contact, the position is set as reference for the Z-axis and from this moment onwards, the process gap is calculated referring to the number of rotation of the Z-axis spindle. Therefore there is no other direct measurement of the distance between substrate and stamp during the process.
3. After setting the “reference” position, the whole stage moves back downwards.

Even though such a design allows for the highest precision when processing hard substrates coated with incompressible resists and hard masks as for standard optical lithography processes, for an imprint process additional considerations have also to be made. The compressibility of the typical materials employed in those processes plays in fact a crucial role. In this case then, the force acting on the whole WEC system becomes a very important parameter: when moving the Z-axis upwards, the viscosity of the process material offers an initial resistance against the Z-axis movement. After this first contact, though, the imprint resist squeezed between the substrate and the stamp spreads towards the edge of the stack, decreasing the resistance sensed by the WEC head, until reaching an equilibrium position.

Furthermore, the standard MA/BA8 Gen3 WEC head can hold a pressure up to 250N, after which the pneumatic breaks holding its position start to lose their grip and the whole WEC head starts sliding downwards, leading to a mismatch between the actual process gap and the one as shown by the MA8 Gen3 software.

In order to overcome this issue and allow for a higher degree of control of the actual process gap even in the case of processes employing compressible

materials, the so-called “Active WEC” technology has been developed by SUSS MicroTec. Here, the base MA/BA8 Gen3 WEC head is additionally equipped with three piezo-actuators and the mask aligner is also equipped with an independent option to measure the actual gap between stamp and substrate, either mechanically (with a set of Heidenhain sensors) or optically (with a spectrometer sensor set). The read-out of those sensors is fed into the controller unit regulating the piezo-actuators and in this way they can automatically bring and/or hold the WEC head to the target position.

A second major advantage of the Active WEC design is the possibility to re-adjust the relative orientation of the substrate with respect of the stamp even during the recipe flow, whereas the standard WEC design does not allow such a balancing motion.

Finally, each piezo-actuator can sustain a pressure up to 1 kN, allowing the WEC head assembly to hold its position without sliding downwards up to a total of 3 kN. Even though, on one side, such a specification permits to squeeze the process polymers to very thin layers, on the other side the operator has also to consider the effect of such a strain applied to the whole stack.

#### **MA/BA8 GEN3 SMILE TOOLING AND PROCESS OPTIONS**

Depending on the type of process, either a 9” x 9” soda lime glass, typically 3mm thick, or a flexible (0.2mm thick) AF32 glass is used as stamp carrier. The first allows for a stiffer and more robust support for both the imprint and the general material handling, while the latter for a more controlled contact sequence during the imprint and for the use of readily-coated substrates.

Depending on the chosen process, two different stamp holders are available:

**1. An open version:** The stamp is held by vacuum only at the outer edges and additionally secured by external mechanical clamps. This stamp holder is used for processes employing thick stamp carriers. As described in Figure 1, the imprint process flow is as follow:

- 1a** The viscous polymer is dispensed as a puddle onto the top of the substrate; the surface tension will give it a curved shape, with the highest point in the centre.
- 1b** By moving the substrate chuck upwards, the resist will have its first point contact where the resist is thickest and then it will be spread outwards, sandwiched by the stamp on top and the substrate in the bottom.
- 1c** The chuck will keep moving upwards until reaching the targeted resist thickness.
- 1d** The lamp house moves forward and expose the photosensitive resist to cure it, and
- 1e** the stamp can then be detached from the imprinted resist on the substrate.

Typical processes carried out using such a tooling are those ones that involve rather thick polymer layers (from 50µm upwards, depending on the various viscosities) and/or materials with known issues concerning coating results (such as poor adhesion or too large edge bead). A most used application, for example, is the imprint of microlenses for the wafer-level camera and for the image sensor markets.

**2. The closed version** of the stamp holder:

A 9mm thick glass plate is placed in its centre and additional vacuum grooves allow fixing the substrate both at its edge and at its centre.

This stamp holder can be used with both, thick and thin stamp carriers, provided that the thick ones are still within the depth of focus of the

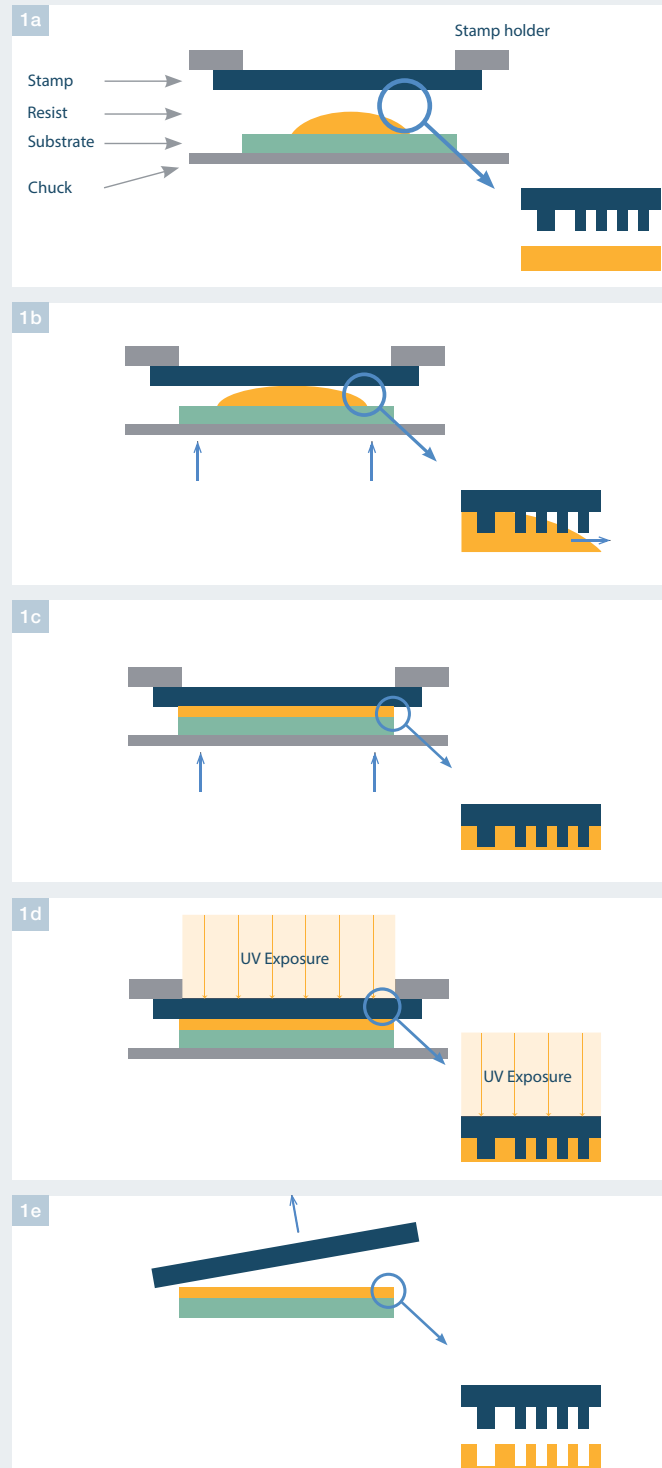


Figure 1 Imprint process via the puddle dispense method

Mask aligner microscopes and that the whole stamp and substrate stack still fit in the tool. When using thin stamp carriers, the main advantage of this design is the possibility to bend the stamp during the imprint sequence, allowing the use of pre-coated substrates, as described in Figure 2:

- 2a** The stamp is held by the stamp holder via both inner and outer vacuum and the coated wafer is placed on the chuck.
- 2b** The inner vacuum is released, while a tuneable pressure is applied to the inner region to bend the thin stamp downwards; the stamp is still held at its edge by the outer vacuum grooves.
- 2c** The chuck and the substrates are moved upwards, until the stamp contacts the coated resist locally in the substrate centre. The chuck moves further up, extending the contact front across the desired active area.
- 2d** The chuck is then moved towards the stamp holder so that the stamp and the substrate are in contact over the whole surface. At this point, the operator can decide whether to apply a defined pressure to the back side of the stamp to push it in the polymer or to adopt a pressure free process, where the polymer is attracted in the stamp structure purely by capillary forces.
- 2e** After curing the imprint resist via UV exposure,
- 2f** the stamp-substrate stack can be removed from the SMILE tooling and the stamp peeled off.

This method should be employed especially when targeting resist thicknesses below the micrometric range, that the puddle dispense method would not easily achieve. Typical applications are therefore optoelectronics devices such as PSS wafers or optical gratings.

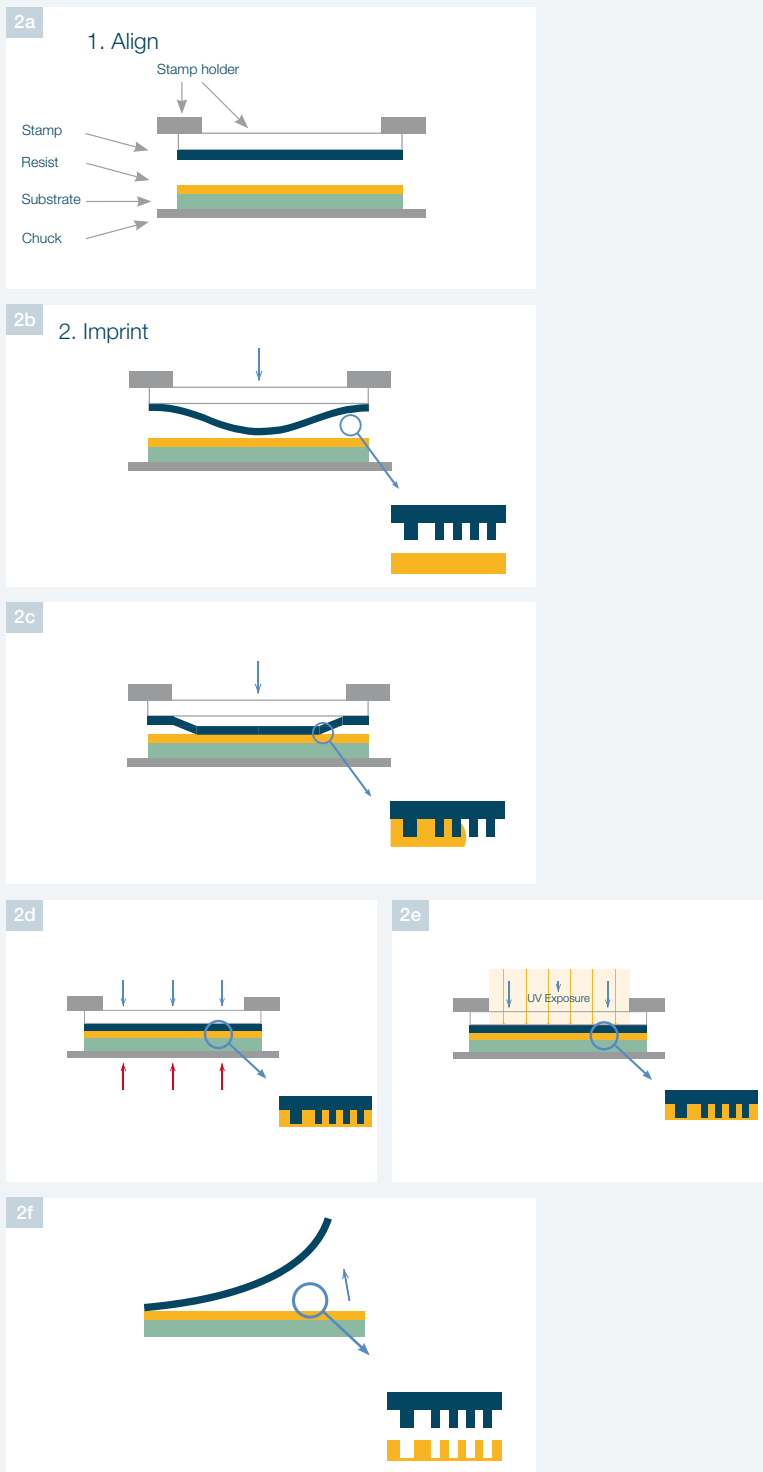


Figure 2 Imprint process via the coated substrate method

Also thick stamp carriers can be used in combination with the closed stamp holder design. In this case, although, the stamp itself cannot be bent and therefore the process flow is based on the puddle dispense method (Figure 1) rather than the one for coated wafers. The main advantage of using a closed holder is, in this specific case, the additional support against stamp warpages.

### STAMP PREPARATION

The stamps used for the imprints can be produced using the SMILE technology as well. Either the open or the closed stamp holder can be employed, depending on the stamp carrier thickness and on the process specifications. The stamp moulding process is analogous to the imprint with the puddle dispense method:

- a The blank stamp carrier is loaded in the stamp holder, while the master mould on the chuck. Typically, the master mould is treated with an anti-adhesion layer and the stamp carrier with an adhesion promoter.
- b The high Young modulus stamp material (silicone or acrylate, for example), still in its liquid form, is dispensed in the centre of the master mould and then spread outwards.
- c The stamp material is then cured, either by UV exposure or by time.
- d Finally, the stack is unloaded and separated, where now the pattern from the master mould is replicated into the stamp material glued to the carrier.

### CONCLUSION

Recently, SMILE has demonstrated to be an extremely versatile and flexible technology, able to address many different processes from a single platform.

A careful matching of tool hardware, stamp type and process chemistry allows large area imprinting of nano- and microdevices, offering a valuable equipment for many diverse markets.

*Dr Eleonora Storace is Product Manager Aligners at SUSS MicroTec Lithography in Garching, Germany, with her focus on SUSS various Imprint Technologies. After her graduation in Solid State Physics at the Università degli Studi dell'Insubria (Como, Italy), she completed her PhD at the Max Planck Institute for Solid State Research (Stuttgart, Germany). In October 2010 she joined SUSS MicroTec as Application Scientist first and Lead Technologist afterwards, and she is based in Garching, Germany*





NORTH AMERICA

EUROPE

ASIA



- Headquarters
- Production
- Sales

[www.SUSS.com](http://www.SUSS.com)

**Imprint**

Publisher:  
 SUSS MicroTec AG  
 Schleissheimer Str. 90  
 85748 Garching, Germany  
 info@suss.com

Register Court Munich  
 HRB Nr. 121347

Value added tax identification number:  
 DE192123619

Executive Board:  
 Dr. Per-Ove Hansson (CEO)  
 Michael Knopp (CFO)  
 Walter Braun (COO)

Chairman:  
 Dr. Stefan Reineck

Contact:  
 Hosgör Sarioglu, Director Corporate Marketing

© 2015 SÜSS MicroTec AG

While every attempt has been made to ensure that the information contained within this publication is accurate, the publisher accepts no liability for information published in error, or for views expressed. All rights for **sussreport** are reserved. Reproduction in whole or in part without prior written permission from the publisher is strictly prohibited.